# COMPUTATIONAL MODELS FOR PREDICTING SHOE FRICTION AND WEAR

by

**Seyed Reza Mirhassani Moghaddam**

BS Mechanical Engineering, Sharif University of Technology, 2008

MS Biomedical Engineering, Iran University of Science and Technology, 2011

MS Industrial and Manufacturing Engineering, University of Wisconsin-Milwaukee, 2013

Submitted to the Graduate Faculty of

Swanson School of Engineering in partial fulfillment

of the requirements for the degree of

Doctor of Philosophy

University of Pittsburgh

2018

UNIVERSITY OF PITTSBURGH

SWANSON SCHOOL OF ENGINEERING

This dissertation was presented

by

Seyed Reza Mirhassani Moghaddam

It was defended on

March 22, 2018

and approved by

Steven D. Abramowitch, Ph.D., Associate Professor, Department of Bioengineering

Rakié C. Cham, Ph.D., Associate Professor, Department of Bioengineering

Tevis D. Jacobs, Ph.D., Assistant Professor, Department of Mechanical Engineering and Materials Science

Mark S. Redfern, Ph.D., William Kepler Whiteford Professor, Department of Bioengineering

Dissertation Director: Kurt E. Beschorner, Ph.D., Associate Professor, Department of Bioengineering

**COMPUTATIONAL MODELS FOR PREDICTING SHOE FRICTION AND WEAR**

Seyed Reza Mirhassani Moghaddam, Ph.D.

University of Pittsburgh, 2018

Slips and falls are a serious occupational and health problem. Insufficient friction between a shoe and flooring, quantified by the coefficient of friction (COF), increases the likelihood of slips and falls. Moreover, shoe's slip-resistant properties change over its lifetime due to wear. This dissertation applies physics-based computational finite element modeling techniques to predict shoe-floor-contaminant friction. Computational models that simulate COF due to hysteresis are developed using multiscale methods. These models are used to assess the effects of shoe design factors and biomechanical parameters of human gait on the predicted COF. To address a gap in the literature regarding models that simulate shoe wear progression, this dissertation develops and validates an innovative finite element modeling process utilizing Archard's law that predicts shoe wear. Models introduced in this dissertation not only increase the understanding of slips and falls but also offer a valuable tool that can be used in designing slip-resistant and durable shoes in order to achieve the ultimate goal of reducing slip and fall injuries.

## TABLE OF CONTENTS

## LIST OF TABLES

## LIST OF FIGURES

# PREFACE

I would like to express my utmost thanks to the great people in my life. I want to start by thanking my PhD advisor, Kurt Beschorner who has been an inspiring mentor; He has pushed me to grow in academic and professional directions by simultaneously challenging and supporting me. I want to also thank Kurt for putting up with me during this scientific journey where I have been constantly learning. I want to thank the other members of my dissertation committee, Steven Abramowitch, Rakié Cham, Tevis Jacobs, and Mark Redfern who have significantly contributed to improving this work and my modest academic success by giving me their intelligent feedback that could only come from the eyes of brilliant scholars, and by teaching me complex concepts that are essential to this work. I want to thank my co-workers at the Human Movement and Balance Laboratory for making the lab a friendly place for me and a pleasant environment for research. I want to thank all the friends in Pittsburgh and elsewhere who made this journey an enjoyable experience and inspired me to become a better person. I would also like to thank my parents, Narges and Hojjat, and my siblings, Sahar and Peyman who have been supportive of me personally and have always been encouraging me to pursue higher education and mature academically. Finally, I want to thank my best friend and partner, Kelly, who has been there for me throughout this, calmed me down and kept me upbeat in difficult times.

## NOMENCLATURE

$A$ Contact area

$A_c$ Real contact area

$ACOF$ Available coefficient of friction (experimental)

$A_{Micro}$ Nominal area in microscopic models

$b$ Exponent describing the relationship between contact area and normal load

$\beta$ Exponential decay constant for microscopic coefficient of friction

$COF$ Coefficient of friction

$COF_{Adhesion}$ Coefficient of friction due to adhesion

$COF_H$ Coefficient of friction in high normal loads

$COF_{Hysteresis}$ Coefficient of friction due to hysteresis

$COF_\infty$ Microscopic coefficient of friction asymptote in high contact pressures

$COF_L$ Coefficient of friction asymptote in high normal loads

$COF_{Model}$ Coefficient of friction predicted by multiscale model

$COF_0$ Microscopic coefficient of friction in low contact pressures

$\Delta h$ Wear depth

$\Delta_q$ Root mean square slope of surface profiles

$E$ Elastic modulus

$E(t)$ Variation of compressive modulus with respect to time

$F_{Adhesion}$ Friction force due to adhesion

$F_{Fluid}$ Fluid force due to hydrodynamic pressures

$F_{Friction}$ Friction force

$F_{Hysteresis}$ Friction force due to hysteresis

$F_N$ Loading force normal to the surface

$F_{Normal}$ Normal load in macroscopic models

$f(p)$ Piecewise polynomial describing frictional shear stress due to hysteresis as a function of contact pressure

$\gamma$ Exponential decay constant for shear modulus

$G_\infty$ Short-term shear modulus

$G(t)$ Variation of shear modulus with respect to time

$G_0$ Long-term shear modulus

$h$ Fluid film thickness

$k$ Wear constant

$l$ Length of the untreaded area

$\lambda$ Exponential decay constant for coefficient of friction with respect to normal load

$\mu$ Fluid viscosity

$v$ Poisson's ratio

$p$ Contact pressure

$RCOF$ Required coefficient of friction

$R_z$ Average peak-to-valley distance of surface profiles

$s$ Sliding distance

$\sigma_f$ Frictional shear stress due to hysteresis

$\boldsymbol{\sigma_s}$ Interfacial true shearing stress required to break the contact junctions

$\boldsymbol{\tau}$ Time constant of exponential decay in material properties

$\boldsymbol{v}$ Sliding velocity

# 1.0 SPECIFIC AIMS

Slips and falls are routinely among the leading causes of serious work-related injuries. Inadequate friction between shoes and flooring, quantified by coefficient of friction (COF), is the main parameter that contributes to an increased probability of slips and falls. Shoe design can impact the COF. Physics-based computational modeling may offer potential in predicting shoe-floor COF and guiding shoe tread designs with higher COFs. Previous studies have demonstrated that a shoe's slip-resistance properties change over its lifetime due to wear. However, there is a lack of computational models in the shoe-floor friction literature that are capable of simulating shoe-floor friction and shoe wear progression. The dissertation develops and validates innovative models that predict shoe friction and wear. The long-term goal of this project is to utilize computational modeling to guide tread designs in order to reduce slip and fall injuries in the workplace. The objective of this proposed research is to develop computational models that predict shoe-floor COF and wear and apply these models to shoe-floor designs. The proposed research consists of four aims that are outlined in this chapter.

## 1.1 SIGNIFICANCE

Slips and falls are among the primary causes of occupational accidents. In 2015, slip, trip, and fall incidences contributed to 27% of non-fatal occupational injuries [1]. In 2016, 16.5% of

fatal occupational injuries were related to slips, trips and falls [2]. According to the Centers for Disease Control and Prevention, falls occurring in a single year account for a total cost of $170 billion in the United States [3]. Between the years of 1998 and 2010, workers' compensation costs due to same level falls had the fastest growth among all the main injury causes [4]. Approximately 50% of occupational falls are initiated by slips [5].

Amongst different environmental and biomechanical factors that affect slips and falls, frictional characteristics of the shoe-floor interface has a significant importance. Statistical models have indicated that the probability of slips and falls can be determined by the difference between the friction present between shoe and flooring, quantified by the available coefficient of friction (ACOF) and the minimum friction required in order to sustain normal walking, that is quantified by the required of coefficient of friction (RCOF) [6, 7]. Evaluative methods that utilize slip-testers are typically employed by researchers to measure the available COF [6-9]. Different slip-testers have been reported to yield inconsistent results in predicting the risk of slips and falls [9] and repeatability of some of the slip-tester results has been questioned in the literature [10]. Furthermore, these methods have mostly emphasized on examining different floorings rather than shoes [9, 11]. Another set of studies have investigated the effects of tread design properties such as hardness, tread depth, width, and orientation on shoe-floor friction [12-15], but there is no consensus on the effects and contributions from different shoe design parameters. Effects of some parameters such as tread orientation and groove width are not completely understood and are inconsistent across different studies [12-14]. Models of shoe-floor friction, on the other hand, can help simulate the contributing mechanisms to shoe-floor friction. Therefore, this approach can identify the relative contributions of shoe design parameters, their interactions and guide design improvements. Previous research has demonstrated the promise of

tribological models in predicting the available COF and identifying the fundamental tribological mechanisms relevant to the shoe-floor-contaminant friction complex [16-19]. The proposed research will present an existing line of investigation on developing physics-based models of shoe-floor-contaminant friction that are capable of predicting COF and aiding in design for slip-resistance.

Wear of shoes is another important factor that affects their frictional properties and therefore their slip-resistance potential [20-27]. Worn down shoes decrease COF [23, 26] and have been reported to increase slipping risk in occupational settings [20, 21, 27]. Specifically, a crossover study conducted in the limited-service industry revealed a 55% reduction in slip risk by replacing worn slip-resistant shoes with new ones [27]. A previous study in a laboratory setting, has also demonstrated an increased slip severity in subjects walking in worn shoes [22]. While it is known that shoe and flooring design affects shoe wear progression rate, there are no published results on the underlying mechanisms and the most important shoe and flooring design parameters that influence shoe wear. Rubber material properties, the counterpart's surface characteristics and the contact pressure between the interacting surfaces have shown to affect wear of the elastomers [28]. Research on computational modeling of rubber wear, similar to models that have been developed for tires and seals [29, 30], has the potential to increase understanding of the shoe wear mechanisms and identify effects of shoe design and material properties on shoe wear. The proposed research will apply computational techniques of modeling elastomers to the shoe outsole in an effort to predict safe life of shoes and aid in design for durable slip-resistance.

The proposed research will produce an improved understanding of the shoe-floor interface friction and wear phenomena. Through the computational models that will be

introduced in this dissertation it will become possible to deploy finite element methods in the shoe design process. The outcomes will not only advance the field of shoe-floor friction research but will also have broad impacts on improving quality of life by reducing the number of slip and fall accidents caused by insufficient shoe-floor friction and/or worn shoes.

## 1.2 INNOVATION AND RESEARCH OUTCOMES

This dissertation implements two important innovations: 1. It is expected to develop and perform validation analyses for a novel computational methodology that predicts shoe-floor COF based on shoe and flooring microscopic and macroscopic features. Such a multiscale modeling approach has been introduced for modeling frictional behavior of rubber [31, 32] but has not been used in shoe-floor friction research or applied to predict slipping risk. 2. It will develop a computational model that predicts shoe wear. Physics-based models for wear of elastomers have been around for other tribological modeling purposes [29, 30] but have not been developed for shoes or used for predicting shoe's slip-resistant life. The research proposed in this dissertation deviates from the currently used methods for shoe-floor friction in that it is predictive rather than evaluative [6-9, 33, 34].

The research plan introduced in this dissertation will have the following impacts: 1) It will identify critical footwear characteristics for slip-resistance and will lead to a smart selection of footwear to reduce slip and fall accidents. 2) It will provide an engineering tool to evaluate and design slip- and wear-resistant footwear. 3) It will provide *a priori* predictions of shoe's frictional behavior and allow for optimizing shoe tread design to achieve superior slip-resistance. The framework presented in this dissertation lays the foundation for future efforts to package the

modeling efforts introduced in this dissertation into a software. Such a software package will allow for these methods to be widely used for designing shoe treads.

## 1.3 SPECIFIC AIMS

### 1.3.1 Specific aim 1

**Develop and validate a predictive computational model of shoe-floor-contaminant interface friction at the microscopic level.**

The computational model includes measurable properties such as surface topography, material properties, shoe-floor interface contact pressure, and sliding velocity and predicts hysteresis and adhesion COF at shoe-floor interface. The model's predictions are compared to the experimentally-measured tribological COF values obtained from a pin-on-disk tribometer. Experimental tribological techniques are used to separate hysteresis friction from adhesion friction.

### 1.3.2 Specific aim 2

**Develop and validate a predictive multiscale computational model of shoe-floor-contaminant friction.**

The multiscale computational model combines the microscopic COF predictions from aim 1 with the contact pressure distribution over the macroscopic surface of the outsole (i.e. tread) to predict the whole shoe-floor COF. The model also predicts shoe-floor interface contact

area. The model's predictions are compared to shoe-floor interface's experimentally-measured COFs (via a robotic slip-tester) and the experimentally-measured shoe contact areas (via ink imprints of the shoe outsole on the flooring).

### 1.3.3 Specific aim 3

**Apply the computational model of shoe-floor-contaminant friction (Specific aim 2) to interfaces with different shoe design parameters and biomechanical parameters of human gait.**

The computational model of shoe-floor friction is utilized to explain the effects of shoe design parameters such as shoe material properties, shoe's geometrical curvature and kinetic and kinematic parameters of gait such as normal loading and shoe-floor contact angle on shoe-floor COF.

### 1.3.4 Specific aim 4

**Develop and validate a computational model of shoe wear progression.**

The computational model simulates the contact pressures between the shoe and flooring to predict shoe wear. The model's predictions are compared to a custom-developed experimental setup (shoe wear simulator apparatus).

## 1.4 DISSERTATION STRUCTURE

This dissertation is structured in seven chapters:

1. Chapter 1.0 represents the specific aims, significance and the innovative aspects of the research that is presented in this dissertation.
2. Chapter 2.0 provides the reader with the background and theory that is required for the research that is presented in this dissertation.
3. Chapter 3.0 represents the microscopic computational model of shoe-floor-contaminant friction (Specific aim 1).
4. Chapter 4.0 represents the multiscale model of shoe-floor-contaminant friction (Specific aim 2).
5. Chapter 5.0 represents the applications of the multiscale model of shoe-floor-contaminant friction to human factors and shoe design (Specific aim 3).
6. Chapter 6.0 represents the computational model of shoe wear progression (Specific aim 4)
7. Chapter 7.0 summarizes the findings of the research that is presented in this dissertation and provides recommendations for continuing this line of research.

# 2.0 BACKGROUND AND THEORY

The purpose of this chapter is to provide the reader with the necessary background information and relevant theory to the research that is presented in the following chapters of this dissertation. Specifically, this chapter presents a brief review of the epidemiology of slip and fall accidents, biomechanics of slips as it relates to shoe-floor friction, and tribology mechanisms relevant to shoe-floor interface.

## 2.1 EPIDEMIOLOGY

Slips and falls are a serious health and financial problem. Falls occurring in a year lead to a lifetime cost of $180 billion in the United states [3]. According to the Liberty Mutual Workplace Safety index, falls account for 28% of the cost of work-related injuries (Figure 2-1) [4] and workers' compensation costs due to slips and falls is approximately 18.5 billion [35]. During the past few years, the costs associated with slips and falls in the workplace have been persistently increasing while a decrease in the costs associated with other workplace hazards such as overexertion have been occurring [4] perhaps because of the ergonomic interventions that have been developed in those areas. The increase in costs and size of slip and fall accident problem necessitates the development of preventive measures to reduce slip and falls accidents.

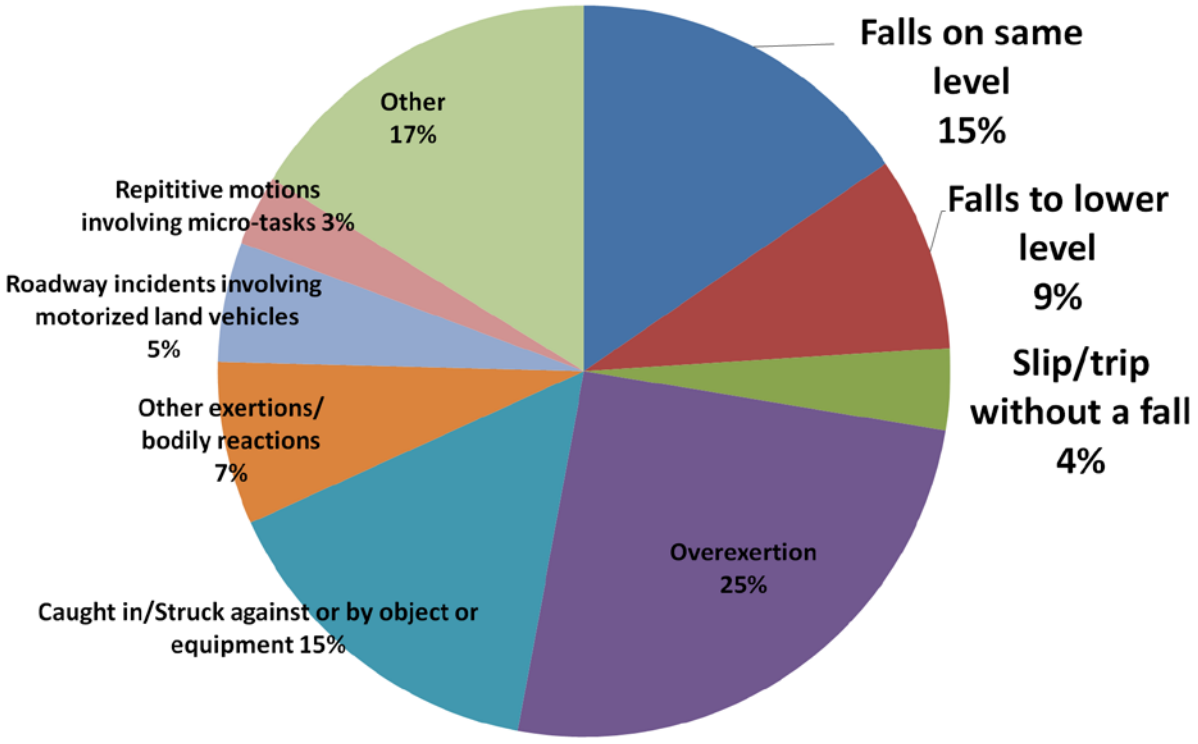


**Figure 2-1.** Major causes of work-related injuries.

Slipping is the preceding event to more than a half of injurious falling incidents [5]. Frictional properties of the shoe are a critical factor in determining the propensity of slips and falls. Increasing the available friction between the shoe and walkways has been demonstrated to be an effective method for preventing slips and falls [7, 9, 34, 36]. The available friction of shoes changes across the shoe's life as the tread material wears. Severely worn shoes are associated with a reduction in friction which in turn increases the risk of slips and falls [22, 23, 26, 27]. Enhancing the shoe-floor friction by developing superior slip-resistance and durable shoe and floor designs focuses on fitting the environment to the individual. Thus, it is an effective approach to reducing slip and fall accidents.

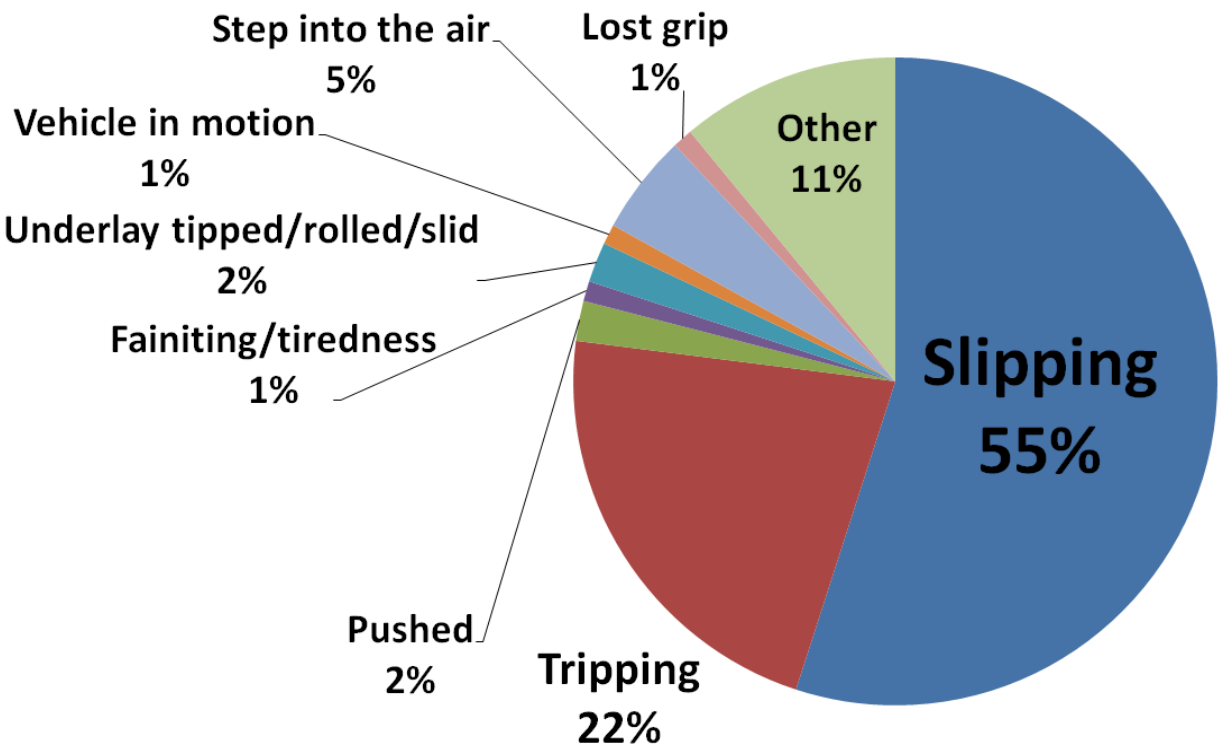


**Figure 2-2.** Major triggering events to falling accidents.

## 2.2 BIOMECHANICS OF SLIPS AS IT RELATES TO SHOE-FLOOR FRICTION

This section provides a brief review of the methods used in the literature to connect shoe friction to the risk of slips and falls. Furthermore, it reviews the under-shoe dynamic conditions during walking, human gait parameters relevant to slipping and their influences on the chance of slips and falls.

### 2.2.1 Available coefficient of friction/Required coefficient of friction

Previous research has demonstrated that the probability of slips and falls can be effectively estimated using the available friction between the shoe and flooring, quantified by the available coefficient of friction (ACOF) and the minimum amount of friction required to maintain normal walking, quantified by the required coefficient of friction (RCOF).

ACOF is measured using a tribometer or a slip-tester (Figure 2-3). Typically, a normal force, shoe angle and sliding speed is specified and shear force is measured. ACOF is then calculated as the ratio of shear to normal force. Shoe design parameters such as tread depth, width, orientation and presence of a contaminant at the interface affect ACOF [13, 14]. Computational models developed in chapter 4.0 of this dissertation simulate ACOF.

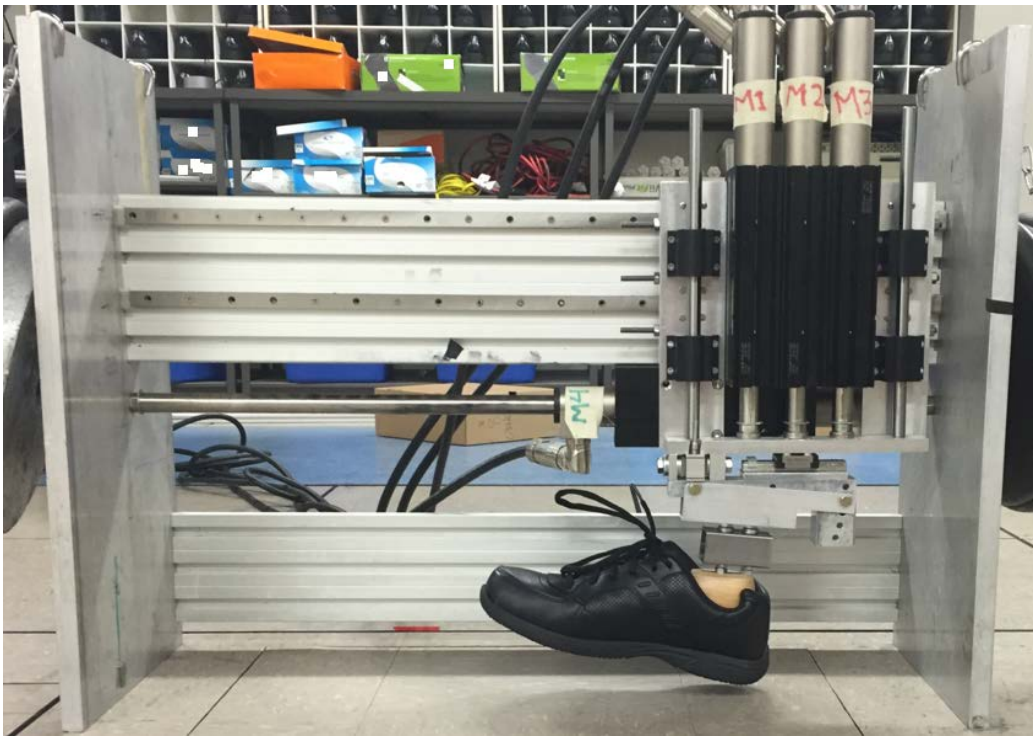


**Figure 2-3.** A robotic slip tester that measures the whole-shoe ACOF (Courtesy of Human Movement and Balance Laboratory, University of Pittsburgh).

RCOF is influenced by the biomechanics of gait and therefore it is measured on dry surfaces in a gait laboratory using force plates and human subjects [7, 37, 38]. Instantaneous RCOF is calculated by dividing the resultant friction force by the normal force during the gait cycle [39]. Peak RCOF is then typically extracted from the time-series of the instantaneous RCOF when several criteria are met [38] and is used as a measure of the required friction.

Once ACOF and RCOF are measured, logistic regression models can be developed that are able to predict the probability of slips and falls as a function of the difference between ACOF and RCOF [7, 9, 33, 34, 36, 37, 40]. Slips can be prevented through the increase of ACOF or a decrease of RCOF.

### 2.2.2 Under-shoe dynamic conditions during gait/slipping

Previous research on under-shoe dynamic conditions during slipping has identified the kinematic and kinetic parameters that are relevant to slipping. These conditions sometimes are referred to as ‘biofidelic’ testing conditions. In 2001, a group of researchers introduced a range of biofidelic testing conditions [41]. Biofidelic recommendations suggest that slip-testing should be conducted at sliding velocities within the range of 0-1 m/s and at normal loads that simulate contact pressures within the range of 0-1 MPa [37, 41, 42]. Shoe-floor angles within the range 0-20 degrees are also reported as biofidelic [10, 12, 33, 37, 43]. These parameters provide some of the inputs to the computational models introduced in chapters 3.0 to 6.0 of this dissertation.

### 2.2.3 Influence of human factors on under-shoe conditions

Human gait parameters are known to influence the under-shoe dynamic conditions. Higher gait speeds have been associated with higher risk of slips and falls [44]. Human gait speed influences the heel contact velocity [45, 46]. Heel contact velocity can be simply interpreted as sliding velocity in friction testing experiments. Therefore, the effect of sliding velocity on COF is investigated in chapter 3.0 of this dissertation via computational modeling. Another gait factor that influences slip and fall risk is step length. Larger step lengths will lead to higher shoe-floor angles which are also associated with higher slip rates in human subject studies [46]. A person's body weight which determines the magnitude of the normal load that is applied during gait also affects the risk of slips and falls. Obese and overweight people have been demonstrated to have a higher risk of slips and falls [47-49]. Thus, the effect of shoe-floor angle and normal load on COF is investigated in chapter 5.0 of this dissertation.

## 2.3 TRIBOLOGY MECHANISMS REALTED TO SHOE-FLOOR INTERFACE

This section provides the reader with an overview of the tribology mechanisms relevant to the shoe-floor interface. Specifically, lubrication, friction and wear mechanisms are reviewed. A brief description of the computational approaches for modeling friction and wear is also provided.

### 2.3.1 Overview of lubrication mechanisms

The Stribeck curve (Figure 2-4) describes the relationship between dynamic conditions of the interface (i.e. normal loading and sliding velocity) and the contaminant (i.e. viscosity) with the COF and fluid film thickness [50-52]. According to this theory, three distinct lubrication regimes can are predicted: 1. Boundary lubrication in which there is minimal presence of a fluid film and therefore COF is relatively high. 2. Mixed lubrication, in which the surfaces begin to separate from each other as a fluid film begins to develop; this phenomenon results in a drop in COF as the fluid film thickness increases. 3. Hydrodynamic lubrication regime, in which both the COF and fluid film thickness begin to increase as a result of further separation of the surfaces due to the relatively high fluid shear stresses and fluid pressures, respectively.

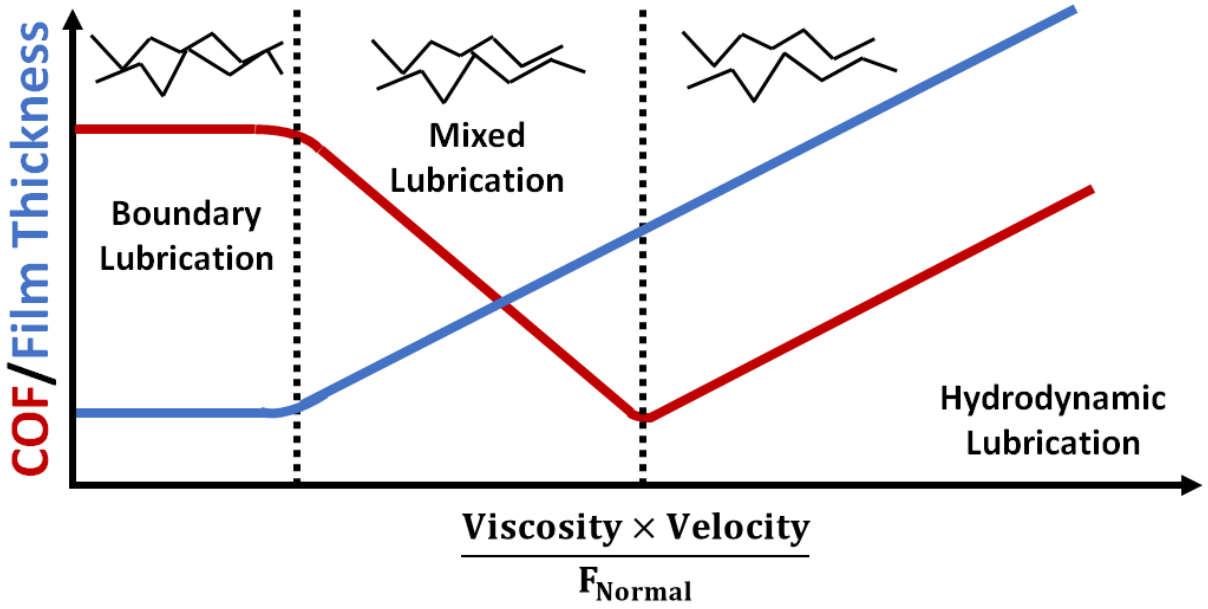


**Figure 2-4.** Typical representation of the Stribeck curve. Asperities at the top of each lubrication regime represent the amount of separation that the surfaces experience.

Recent research has emphasized the importance of boundary lubrication in treaded shoes and in presence of a contaminant [18, 19, 53] and its relevance to slipping accidents. These effects are further explained in section 2.3.3 of this dissertation and friction mechanisms in boundary lubrication are discussed in section 2.3.2. The models introduced in chapters 3.0 and 4.0 investigate the available friction in boundary lubrication.

### 2.3.2 Overview of friction mechanisms relevant to elastomers

Shoe outsoles are typically made of rubber (i.e. elastomers). Previous research on friction in elastomers have identified hysteresis and adhesion as the two major friction mechanisms [41, 54-56]. According to the theory, while both mechanisms originate from the microscopic interactions at the interface, they are different in nature. Hysteresis is due to the material deformation and adhesion is due to the force occurring between the materials. These differences are depicted in Figure 2-5, discussed in the following subsections and further analyzed via computational modeling in chapter 3.0 of this dissertation.

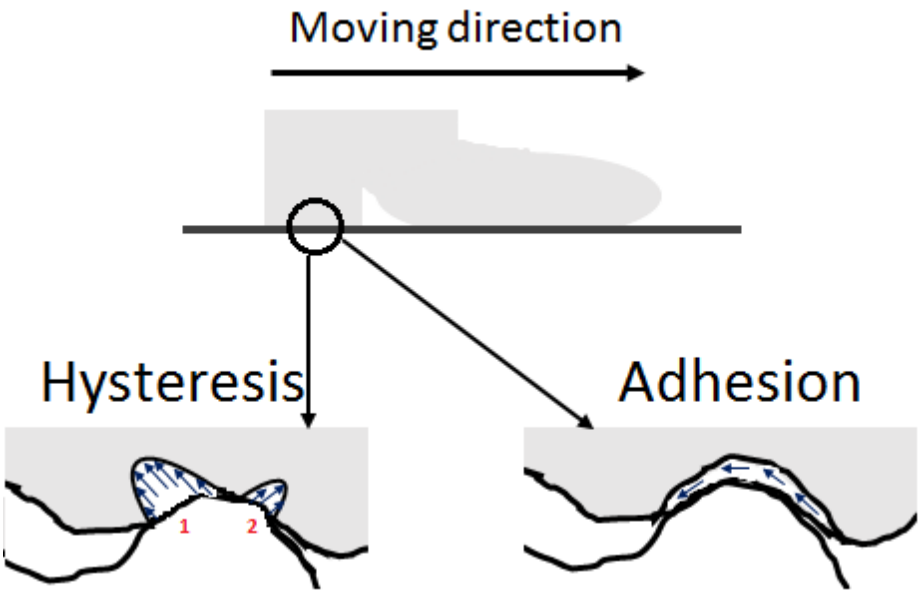


**Figure 2-5.** Schematic of the origins of hysteresis and adhesion friction as they apply to shoe-floor interface.

#### 2.3.2.1 Hysteresis

Hysteresis friction originates from the deformations occurring in a viscoelastic material due to asperity interactions at the microscopic scale of the two contacting surfaces. When asperities of a viscoelastic material (such as shoe) engage in contact with a harder surface (such as flooring), differences in pressures developed in trailing and leading edges of those asperities are typically observed [56-58]. This is due to the stress relaxation in the viscoelastic material and the time it takes for the material to recover to its original state because of its viscoelastic nature (Figure 2-5. Bottom left). This difference in pressures will lead to the development of a net force (Equation 2-1.) that causes hysteresis friction.

$$F_{Hysteresis} = \int p_1 dA_1 - \int p_2 dA_2 \qquad \text{Equation 2-1.}$$

#### 2.3.2.2 Adhesion

Adhesion friction also has its origins at the microscopic scale. Adhesion friction occurs at the surface level and it is due to the intermolecular adhesive bonds and attractive forces [59-61] that generate when the surfaces come into contact (Figure 2-5. Bottom right). Therefore, adhesion force is dependent on the true interfacial shearing stress ($\sigma_s$) that is required to break those adhesive junctions at the contact interface and the real area of contact ($A_c$) (Equation 2-2.). The interfacial shear stress and the real area of contact are influenced by on the material properties, surface roughness and contact pressure [55, 60, 62].

$$F_{Adhesion} = \sigma_s A_c \qquad \text{Equation 2-2.}$$

### 2.3.3 Tribology of shoe-floor-contaminant complex

Tribology research have identified that both friction components (i.e. hysteresis and adhesion) are relevant to the shoe-floor-contaminant system [18, 19, 22, 41] (Figure 2-6). However, recent literature suggests that hysteresis friction is the dominant and unaffected mechanism in the presence of a liquid contaminant (i.e. presence of a contaminant results in a drop in adhesion friction) [19, 53]. Analyzing both of these friction mechanisms at the microscopic scale using computational modeling is conducted in chapter 3.0 of this dissertation. Afterwards in chapter 4.0 , this dissertation focuses on models for hysteresis friction which seems to be the reliable friction in treaded shoes and in presence of fluid contaminants (Figure 2-6).

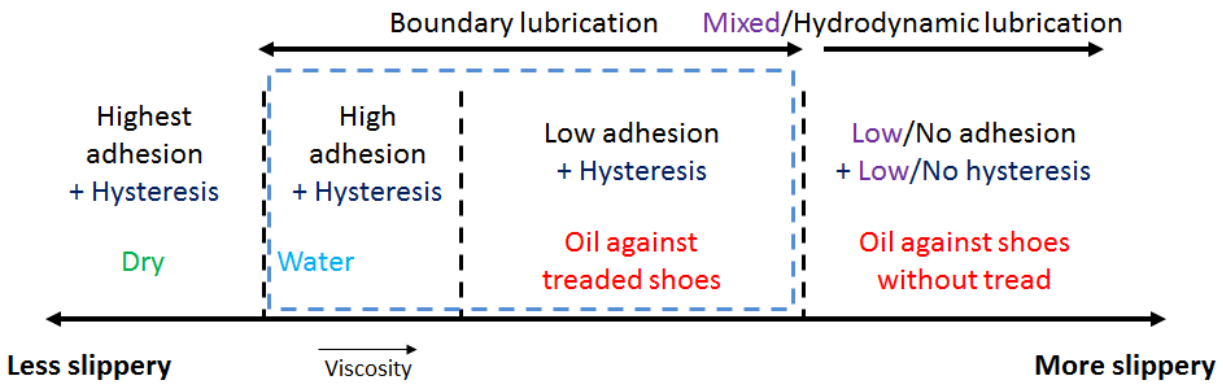


**Figure 2-6.** Spectrum of the friction and lubrication mechanisms relevant to the shoe-floor-contaminant complex.

#### 2.3.3.1 Relevant friction models in other applications

Finite element modeling has been demonstrated to be effective in modeling the contact between elastomers and rigid surfaces. Specifically, computational models have been developed that investigate the contact between rubber and hard surfaces at the microscopic asperity (i.e. µm) scale [57, 63] and utilize multiscale modeling schemes (i.e. utilizing the information provided by modeling in one scale by models operating in another scale) to investigate the contact interface at the macroscopic (i.e. mm) scale [31, 32, 64]. In these models, a response surface is created that describes the COF as a function of surface characteristics, material properties and contact pressure at the microscopic scale. The macroscopic model will then use response surface from the microscopic scale along with the results of the model at the macroscopic scale to calculate COF at the macroscopic scale. However, these modeling techniques have yet to be applied to shoe-floor-contaminant interface. This dissertation aims to fill the knowledge gap in modeling shoe-floor friction by applying some of the concepts from the above-mentioned techniques to the interface. To this end, the microscopic contact modeling

method using LS-Dyna® similar to one in [63] and a multiscale modeling scheme similar to one in [32] are used in chapters 3.0 and 4.0 of this dissertation, respectively.

### 2.3.4 Wear mechanisms relevant to shoe-floor interface

Previous research on wear of the shoes has identified abrasive and adhesive wear as the major wear mechanisms relevant to shoe-floor interface [24, 25, 65]. Abrasive wear occurs when the asperities of the hard material (flooring) penetrate into the soft rubber (shoe) material and cause material removal. Therefore, abrasive wear is more prevalent on rough surfaces. Adhesive wear typically takes place on relatively smooth surfaces. It occurs when the relative motion of the soft rubber (shoe) with respect to the relatively rigid counter-surface (floor) results in breakage of the adhesive junctions at the contact interface [65]. Both of the above-mentioned mechanisms seem to be relevant to the shoe-floor interface given the wide variability in the roughness of the walkway surfaces.

#### 2.3.4.1 Archard's law

Classic equation developed by Archard [28] is still widely used to predict the abrasive and adhesive wear in elastomers [29, 30, 66-68]. Archard's law (Equation 2-3.) states that wear depth ($\Delta h$) is proportional to contact pressure ($p$) at the interface and sliding distance ($s$). In Equation 2-3., $k$ is interpreted as wear constant that can be measured experimentally. Contact pressure in Equation 2-3. can be estimated using computational modeling techniques (Chapter 4.0 ). Chapter 6.0 of this dissertation utilizes contact modeling methods introduced in chapter 4.0 along with Equation 2-3. to develop a computational model of shoe wear progression.

$$\Delta h = kps$$ Equation 2-3.

#### 2.3.4.2 Wear modeling

Finite element modeling techniques along with Archard's law have been demonstrated to be successful in predicting wear in several applications such as tires, seals, and disc brakes [29, 30, 66-69]. Typically, wear models employ finite element method to predict contact pressure distribution at the contact interface and utilize Archard's law to predict the resulting wear. These models use an iterative approach to update the geometry and contact pressures as the material wears away. Updating the geometry due to wear can be accomplished by either moving the contact nodes at the interface or destroying the elements at the contact [66]. In either case, the wear geometry will need to be re-meshed (i.e. global remeshing) due to the distorted elements or geometrical irregularities that are likely to occur [29]. Methods of moving nodes and global remeshing are used in chapter 6.0 of this dissertation for modeling shoe wear progression.

# 3.0 A MICROSCOPIC FINITE ELEMENT MODEL OF SHOE-FLOOR HYSTERESIS AND ADHESION FRICTION

## 3.1 ABSTRACT

Few efforts have attempted to model the tribological interaction of shoe-floor contacting surfaces despite the high prevalence of slipping accidents. Hysteresis and adhesion are the two main contributing mechanisms in shoe-floor friction at the microscopic asperity level. This study developed a three-dimensional microscopic finite element model of shoe-floor surfaces to quantify the effect of surface topography, shoe material properties and sliding speed on hysteresis and adhesion friction. The validity of the model was assessed by comparing model predictions to pin-on-disk experimental data. The model predicts that hysteresis friction increases for harder shoe materials, rougher shoe surfaces and rougher floor surfaces, while adhesion increases for smoother shoe surfaces, smoother floor surfaces and decreasing sliding speed. The effects of shoe material and floor roughness on the predicted hysteresis friction values were consistent with the experimental data. The effects of sliding speed on adhesion friction were moderately consistent with the experimental data. In addition, the predicted hysteresis magnitudes were consistent with experimental data. This model is a significant step towards development of a comprehensive shoe-floor friction model.

**Keywords:** Shoe-floor friction; Finite element model; Hysteresis; Adhesion; Biotribology; Elastomers

## 3.2 INTRODUCTION

Increasing friction between shoe soles and floor surfaces is a critical strategy for improving public and occupational safety. According to the US Bureau of Labor Statistics, 23% of non-fatal occupational accidents occur due to a fall [70] and about half of those falls are due to slips. According to Liberty Mutual Workplace Safety Index, fall accidents had the highest percentage of cost growth trends among the most disabling workplace injuries between 1998 and 2010 [4]. Previous research has reported an increase in the probability of slips and falls when the available coefficient of friction between shoe and floor becomes less than the required coefficient of friction [6, 7]. Improving friction through enhanced slip-resistant shoes and flooring designs is an effective strategy for reducing slip and fall injuries.

Previous studies have developed empirical relationships between coefficient of friction and sliding speed [50, 71], vertical force [36, 50, 72], shoe material and tread [13, 14, 19, 23], and floor surface roughness [36, 72, 73]. However, each of these studies used a limited set of testing conditions and the findings cannot be easily generalized or integrated given the complex interactions among the factors affecting friction [19]. Developing a physics-based computational model of shoe-floor friction may have potential for efficiently considering these multiple factors including shoe/floor roughness, shoe material properties and sliding velocity. Once a comprehensive model of shoe-floor friction is developed, different parameters can be easily

changed to assess their effects on the friction phenomenon. Additionally, such a predictive model would be capable of optimizing shoe and floor design parameters to maximize friction.

Over thirty-six computational models of shoes have been developed and implemented in order to reduce high pressure regions for improving shoe comfort or athletic performance [74]. Yet few studies have developed models for improving the safety of shoe outsoles and examining shoe-floor friction [17, 75]. This study will address this paucity of knowledge by developing a finite element model for investigating the components of shoe-floor friction at the microscopic level.

The proposed computational model is based upon relevant tribological theory. Shoe soles are typically made of elastomers and the two dominant friction mechanisms in elastomer contacts are adhesion and hysteresis [55, 61, 76]. Adhesion occurs when contacting asperities form an adhesional bond at the molecular level [61]. The adhesion force is proportional to the real contact area and real contact area is a function of the topographic parameters such as asperity geometry and roughness of the two contacting materials [61, 76]. Hysteresis is the result of viscoelastic energy loss during deformation of the soft elastomer caused by its interactions with the asperities of the hard contacting surface [61]. Moreover, boundary lubrication [18, 19] and hydrodynamic lubrication [16, 18, 50] are reported as the two different lubrication mechanisms relevant to shoe-floor-contaminant friction. In the boundary lubrication regime, the fluid reduces the adhesion component but does not have a significant effect on hysteresis [19]. Thus, hysteresis friction is important for maintaining adequate friction in boundary lubricated regime. Simulating the microscopic interactions of shoe-floor asperities is a critical first step towards developing a comprehensive friction model since microscopic features play a major role in adhesion, hysteresis and overall friction [51, 54, 55, 60, 61, 76-78].

Finite element analysis is an effective approach for modeling the friction between elastomer and hard surfaces. For example, computational models have been successfully used to model the friction and wear in contact between rubber and other surfaces [57, 63, 79-81]. Yet these models are typically applied to tire mechanics and rubber-metal contacts. Research by Tokura demonstrated the ability of explicit finite element modeling to simulate the microscopic contact of rubber against hard surfaces [63]. Applying similar methods with multiple asperities to shoe and flooring may provide opportunities to improve shoe-floor-contaminant friction much like previous models have been used to investigate elastomer friction in other applications.

In this study, a three-dimensional finite element microscopic model is developed to simulate the frictional interactions between shoe and floor surfaces in boundary lubrication. The model calculates the real contact area between the surfaces, which is known to be proportional to the adhesion friction, and the shear force due to hysteresis. The finite element analysis is conducted with dynamic conditions relevant to slipping (i.e. normal interface pressure, slipping speeds, genuine shoe sole material properties, and roughness levels for actual shoe and floor surfaces). Model results are compared with experimental data to assess its validity in predicting the effects of surface roughness, material properties and sliding speed on adhesion and hysteresis friction. This model represents a first step towards developing a full multi-scale model of shoe-floor friction.

## 3.3 METHODS

### 3.3.1 Finite element model

Three-dimensional shoe and floor models were created using eight-node solid hexahedral elements in explicit finite element analysis software (LS-Dyna®, Livermore Software Technology Corporation, Livermore, California, USA). This type of element is efficient and accurate in contact simulations and when exposed to severe deformations [82]. The model was created based on the topography and material properties of two shoe materials and three ceramic tiles with different roughness levels, which were physically measured to ensure that the model inputs were relevant to the actual shoe and floor samples (Section 3.3.2). Finite element models of contact of rough surfaces at microscopic scale typically utilize simplifying assumptions to simulate the effects of surface roughness parameters [83]. Within this context, various geometric shapes including but not limited to probabilistic distribution of hemispherical asperities, half cylinders, saw tooth and sine waves have been examined [83-85]. For this work, a sawtooth pattern was chosen to represent the surface asperity distribution because it simply allows for including surface roughness and slope parameters that are strongly correlated to lubricated friction at shoe-floor interface [86, 87]. Roughness was applied to the interface side of the shoe and floor surfaces by raising and lowering nodes to achieve a sawtooth pattern (Figure 3-1). Asperity peaks and valleys were displaced from the mean line of the surface by half of the desired average peak to valley distance roughness ($R_z$) and the spacing between asperities was selected such that the slope of the asperities was consistent with the measured root mean square slope ($\Delta_q$). The microscopic shoe sample models were 0.415 mm in length, 0.28 mm in width, and 0.275 mm in height. The floor models were 1 mm in length, 0.6 mm in width, and 0.06 mm

in height. Mesh sizes for shoe samples elements ranged from 5 to 62.5 µm while mesh size for floor elements was 29 µm (Figure 3-1). In the preliminary modeling efforts, mesh refinement in the floor did not significantly impact the von mises stresses developed in the shoe, so all the simulations were performed without mesh refinement of the floor elements. Shoe samples were meshed with a finer mesh for regions near the contact area. Mesh size for the shoe samples was determined based on the convergence in the ratio of real contact area to normal force (Equation 3-5.)

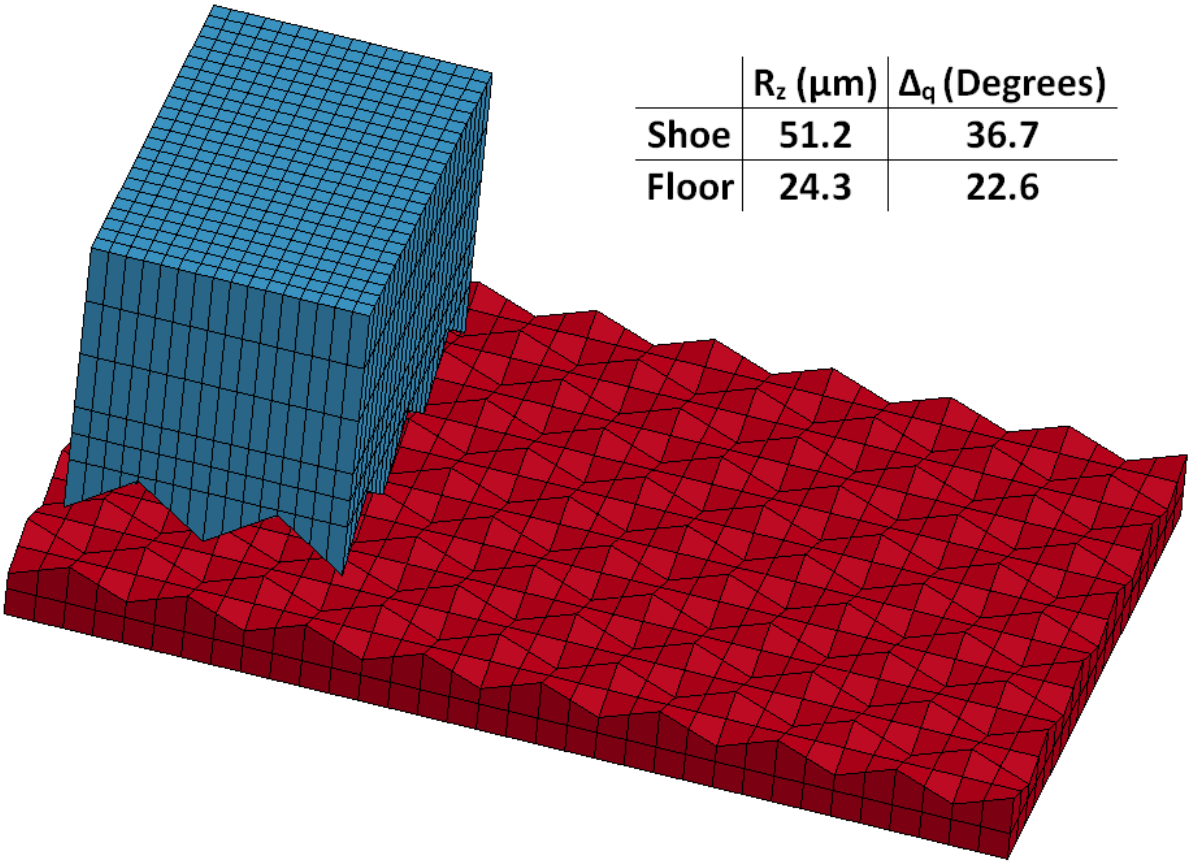


**Figure 3-1.** Shoe and floor surfaces with microscopic asperities created in finite element software. (High shoe roughness and medium floor roughness)

A viscoelastic material model was applied to the shoe elements (See section 3.3.2 for material properties) while a rigid material model was applied to the floor elements. A rigid material model was used for the floor because the modulus of ceramic floor material model was orders of magnitude larger than the shoe materials' moduli. The viscoelastic material used for the shoe was chosen because time-dependent material properties are needed for simulating adhesion and hysteresis friction since both components are related to the viscoelastic properties of the rubber [54]. The viscoelastic model describes shear stress relaxation of the material using a multi-term exponentially decaying function [88], (Equation 3-1.).

$$G(t) = \sum_{m=1}^{5} G_m e^{-t/\tau_m}, \tau_m = 10^{-(m-1)}\tau_1 \qquad \text{Equation 3-1.}$$

Boundary conditions were set to achieve pressure and sliding speeds relevant to walking and slipping. The contact pressure was controlled using the vertical displacement of the nodes on the top surface of the shoe. This downward movement occurred until an average normal contact pressure of 160 kPa was achieved. The contact pressure was set to this value to match the experimental conditions that were used in the validation (Section 3.3.2). This pressure is of the same order of magnitude of under-shoe contact pressures during walking [89]. The second loading step moved the nodes on the top surface of the shoe in the shear direction at the desired speed. Sliding speeds between 0.1 and 1 m/s were simulated to maintain consistency with the experimental validation research and because these speeds are relevant to slipping [41]. In all of the simulations, floor elements were constrained from both translation and rotation.

A segment based automatic surface to surface contact was used in the modeling efforts to overcome the instabilities in simulating contact of rubber with rigid surfaces [63]. During model

development, this contact algorithm was the only method capable of handling the large deformations of the soft rubber material and avoiding 'hourglassing' and 'checkerboarding' problems. The shoe sample was considered the slave material since it is softer and the floor sample was considered the master since it is harder.

Hysteresis coefficient of friction ($COF_{Hysteresis}$) was calculated by dividing the average shear force due to hysteresis by the average normal force between the two surfaces (Equation 3-2.). $COF_{Hysteresis}$ was averaged across the second loading step time period during sliding (Figure 3-2).

$$COF_{Hysteresis} = \frac{F_{Hysteresis}}{F_N} \qquad \text{Equation 3-2.}$$

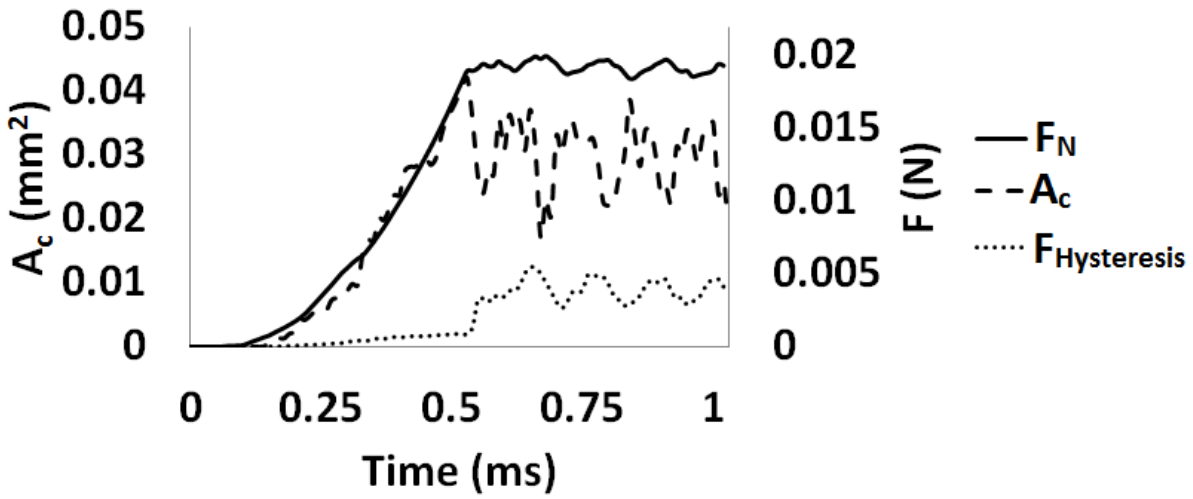


**Figure 3-2.** Representative plot of real contact area ($A_c$), normal force ($F_N$) and shear force due to hysteresis ($F_{Hysteresis}$) generated between shoe and floor model with respect to time (rubber material, medium floor roughness, high shoe roughness, sliding speed of 1 m/s).

The ratio of real contact area to normal force was used as a measure of the adhesion coefficient of friction. Adhesion frictional force, $F_{Adhesion}$, is commonly calculated as the product of the real contact area, $A_c$, and the interfacial true shearing stress required to break the contact junctions, $\sigma_s$ (Equation 3-3.) [59, 60, 90]. The interfacial shear stress is estimated by fitting Equation 3-3. to the experimental data [60] and is dependent on the elastomer material, substrate surface and liquid contaminant [55, 60, 62]. Since the adhesion coefficient of friction ($COF_{Adhesion}$) is the ratio of adhesion friction force and the normal force (Equation 3-4.), the ratio of real contact area to normal force ($A_c/F_N$) should be proportional to the adhesion coefficient of friction (Equation 3-5.). The $A_c/F_N$ was averaged across the second loading step (Figure 3-2). This approach for quantifying adhesion friction is inappropriate for comparing adhesion across different materials since the interfacial shearing strength, $\sigma_s$, and the real contact area, $A_c$, vary across material properties. Therefore, this ratio was only used to assess the effects of sliding speed, shoe roughness and floor roughness on adhesion friction within each shoe material.

$$F_{Adhesion} = \sigma_s A_c \qquad \text{Equation 3-3.}$$

$$COF_{Adhesion} = \frac{F_{Adhesion}}{F_N} \qquad \text{Equation 3-4.}$$

$$COF_{Adhesion} \propto \frac{A_c}{F_N} \qquad \text{Equation 3-5.}$$

### 3.3.2 Experimental validation

Two shoe materials (Neolite and nitrile rubber) were modeled and tested experimentally. Neolite had a Shore A hardness of 95 and it is considered a standard raw material in shoe-floor friction research [72]. The nitrile rubber sample (Referred to as “rubber” in this chapter), removed from an intact work shoe, had a Shore A hardness value of 50. Test samples included cylindrical untreaded specimens of the materials (Diameter of 13.5 mm and height of 5.7 mm) [53]. Roughness parameters were measured using a stylus profilometer. Eight roughness measurements were collected at different locations and orientations for each shoe and floor surface using a scan length of 12.5 mm and a cutoff length of 0.80 mm. The roughness was described with the average peak-to-valley distance ($R_z$) and root mean square slope of the profile ($\Delta_q$) averaged across the scans (Table 3-1). These parameters have been reported to have a strong positive correlation with shoe-floor-contaminant coefficient of friction [86, 87]. Therefore, these parameters were chosen as the parameters for surface description. Because the materials that were used in this study had different material properties and different roughness levels, simulations were conducted using both shoe roughness levels and both shoe material properties in order to isolate roughness versus material effects.

**Table 3-1.** Surface roughness parameters for shoe and floor surfaces.

| Shoe/Floor | Material/Roughness level | $R_z$ (μm) | $\Delta_q$ (Degrees) |
|---|---|---|---|
| Shoe | **Neolite (Low)** | 6.7 | 28 |
| | **Rubber (High)** | 51.2 | 36.7 |
| Floor | **Low** | 16.6 | 15.9 |
| | **Medium** | 24.3 | 22.6 |
| | **High** | 35.1 | 26.3 |

Material parameters were primarily determined experimentally. Density of the shoe samples was measured based on the volume and mass of the samples. The shear relaxation and the exponential decay constants (Equation 3-1.) were measured with compression stress relaxation tests (MTS Systems Corporation, Eden Prairie, Minnesota, USA) [91]. Two rectangular blocks of Neolite (Average thickness of 5.5 mm, average area of 612 $mm^2$) and rubber (Average thickness of 6.1 mm, average area of 552 $mm^2$) with approximately equal and uniform thickness were adhered to aluminum plates. The compression test was repeated three times and the results were averaged for each shoe material. The testing method compresses the materials by 10% of the total thickness of elastomers (10% strain), then applies this constant displacement level for 240 seconds (Figure 3-3) and finally unloads the samples.

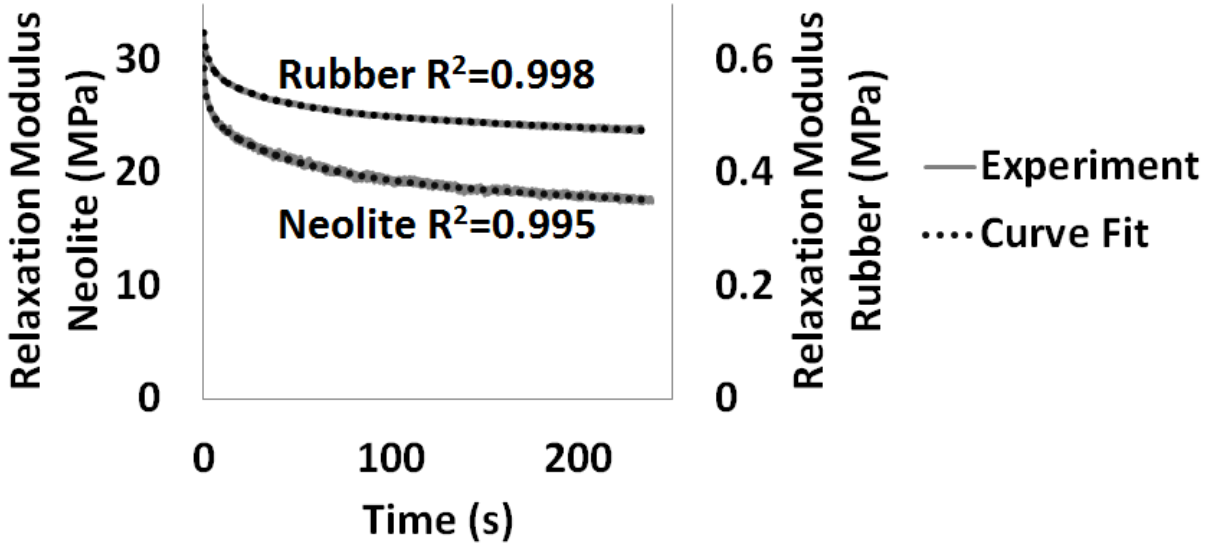


**Figure 3-3.** Relaxation modulus versus time during the stress relaxation test for the Neolite and rubber material and the corresponding curve fits.

Poisson's ratio was set to 0.499 for the shoe sample since rubber is typically categorized as a nearly incompressible material and is reported to have a Poisson's ratio of 0.49-0.499 [92]. Equation 3-6. governs the relationship between shear modulus, compressive modulus, and Poisson's ratio [92] and was used to find shear modulus as a function of time where compressive modulus was calculated as the ratio of the applied force to area divided by the applied strain (10%). In order to find the required coefficients in Equation 3-1. from stress-relaxation tests, an exponential curve fitting (Figure 3-3) was done using the curve fitting toolbox in MATLAB® (Mathworks, Natick, Massachusetts, USA). The values obtained for viscoelastic material parameters of Neolite and rubber are summarized in Table 3-2.

$$G(t) = \frac{E(t)}{2(1+\upsilon)} \qquad \text{Equation 3-6.}$$

**Table 3-2.** Viscoelastic material parameters used for modeling Neolite and rubber

| | $G_m$(MPa) | | | | | |
|---|---|---|---|---|---|---|
| **Material** | $G_1$ | $G_2$ | $G_3$ | $G_4$ | $G_5$ | $\tau_1$(s) |
| **Neolite** | 16.36 | 3.47 | 5.028 | 2.638 | 3.093 | 4703.7 |
| **Rubber** | 0.5044 | 0.007879 | 0.06938 | 0.05364 | 0.01377 | 3546.1 |

Model output was compared with experimental data collected with a pin-on-disk tribometer (Figure 3-4) on 300 mm x 300 mm square ceramic tiles with three different roughness levels for both shoe materials (Neolite and rubber) at six sliding speeds [53]. The three surface roughness levels for the ceramic tiles were achieved using a sandblasting process that used aluminum oxide as the abrasive. The simulated speeds included 0.1, 0.25, 0.5, 0.75, and 1 m/s to match the speeds used in the experimental study. The experimental study quantified hysteresis using a lubricant (SAE 75W140) that dramatically reduces adhesion [19]. The study also quantified fluid lubricated adhesion friction at each of the speeds by subtracting the hysteresis friction (measured with SAE 75W140) from the wet friction. Dry adhesion from the experimental study (at speed of 0.01 m/s) was compared with lowest simulated speed (0.1 m/s) to assess validity of the model in simulating the effects of shoe and floor roughness on dry adhesion because the experimental study did not measure dry adhesion for higher speeds. To examine the effects of speed on adhesion, the wet adhesion data from the lowest viscosity fluid, 25% glycerol/75% water lubricant, was compared with the model output as part of the validation for the effects of speed on adhesion.

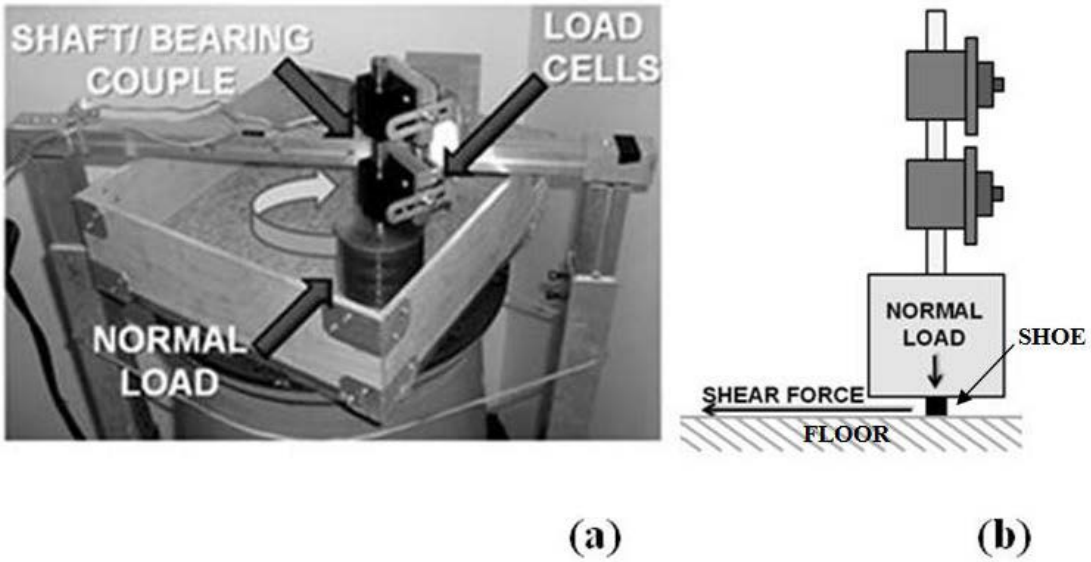


**Figure 3-4.** (a) Custom pin-on-disk tribometer used for collecting friction data (Courtesy of Human Movement and Balance Laboratory, University of Pittsburgh). (b) schematic of the shoe (Pin) and floor (Disk) material and shear and normal forces. Picture from [19] (Permission obtained.)

## 3.4 RESULTS

### 3.4.1 Hysteresis

Increased shoe and floor roughness in the model generated large increases in $COF_{Hysteresis}$ for both materials (Figure 3-5). The mean increase in hysteresis coefficient of friction was 160% (range of 56 to 200%) with increasing shoe roughness for the Neolite material and a mean increase of 20% (range of 15 to 22%) with increasing shoe roughness for the rubber material. Increasing floor roughness caused a mean increase of 21% (range of -28 to 50%) in hysteresis

coefficient of friction for the Neolite material and a mean increase of 34% (range of 17 to 52%) for the rubber material. Thus, the Neolite shoe material was more sensitive to shoe roughness, while the rubber material was more sensitive to floor roughness.

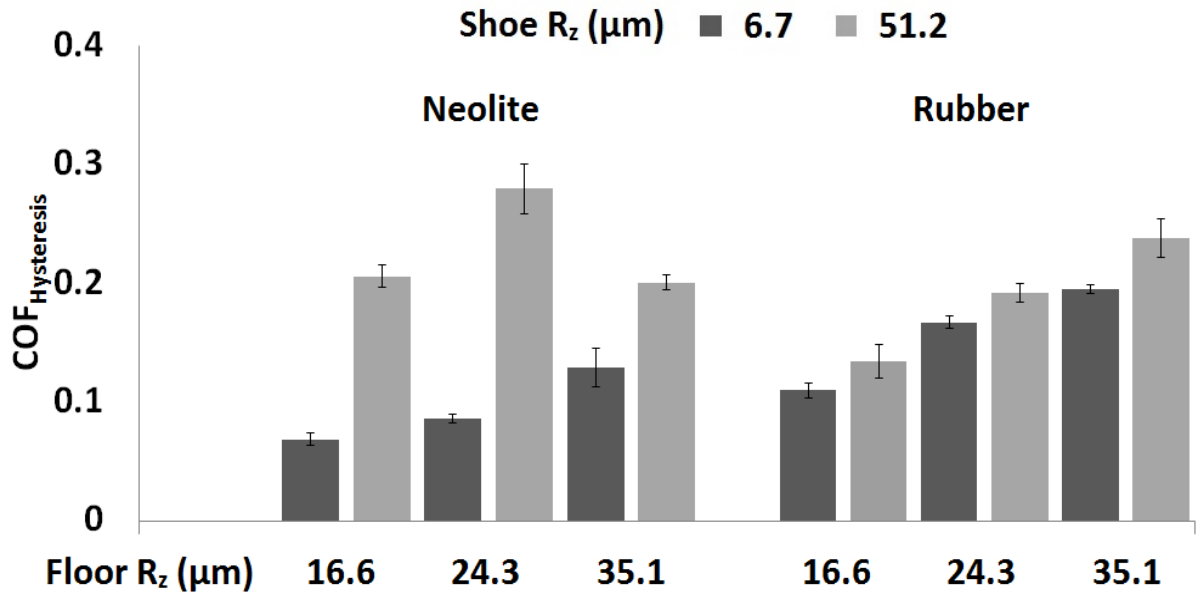


**Figure 3-5.** *$COF_{Hysteresis}$* across different shoe and floor roughness levels averaged across different speeds for Neolite (Left) and rubber (Right). Error bars represent standard deviations across the different speeds.

Sliding speed had a minor and inconsistent effect on hysteresis friction depending on the shoe material, shoe roughness and floor roughness (Figure 3-6). The mean decrease in hysteresis coefficient of friction was 8% (range of -24 to 31%) with increasing sliding speed from 0.1 to 1 m/s.

**a)**

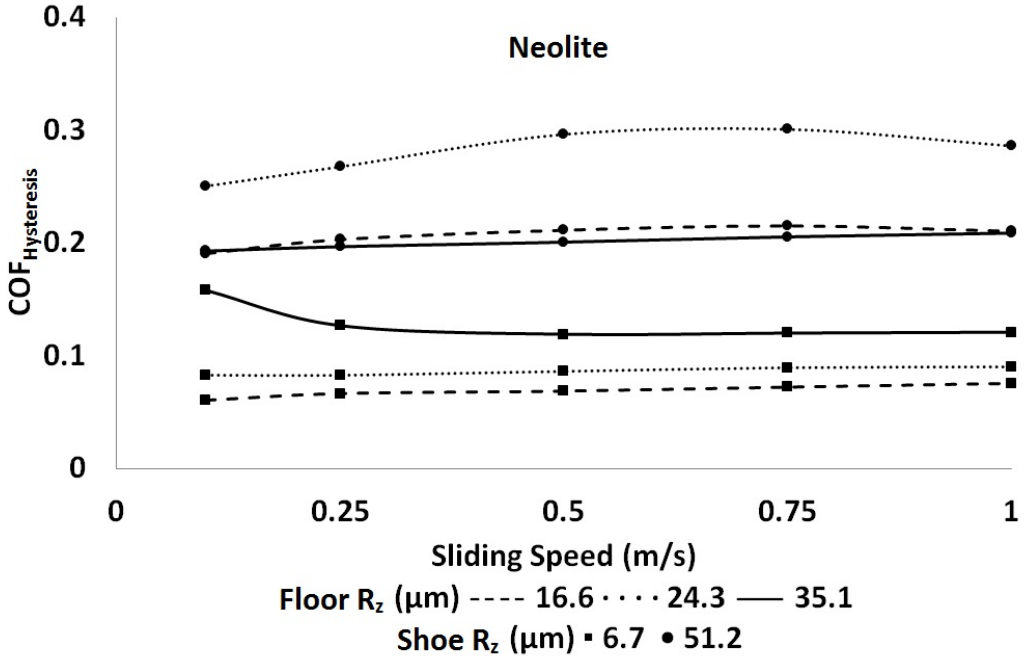


**b)**

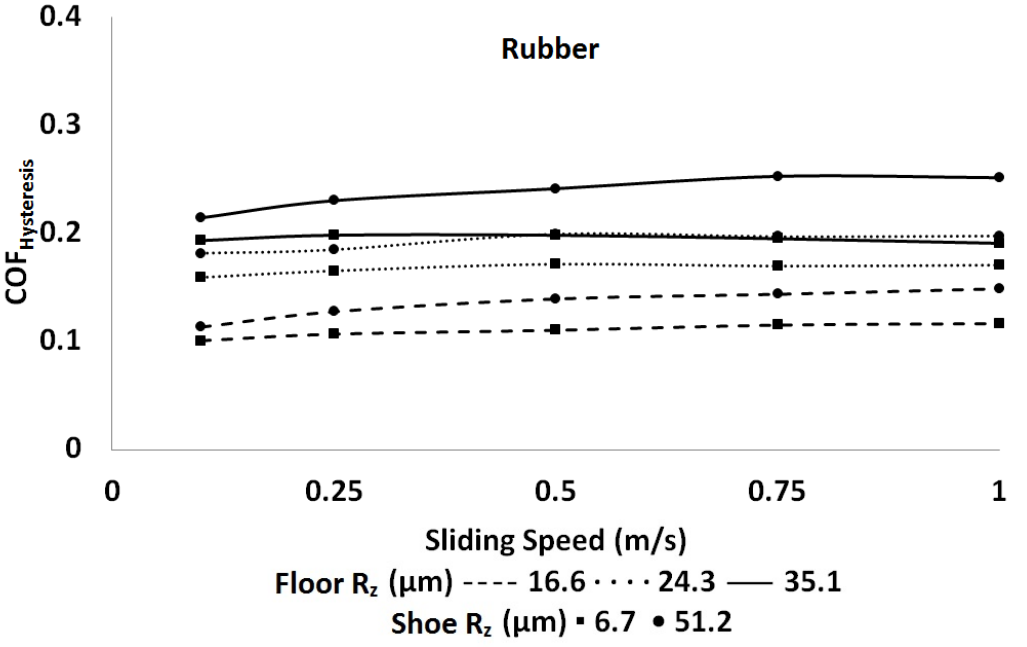


**Figure 3-6.** Effect of speed on $COF_{Hysteresis}$ for Neolite (a) and rubber (b) for the different combinations of shoe-floor roughness.

### 3.4.2 Adhesion

The model indicated that increasing sliding speed led to a reduction in the real contact area, indicating that the adhesion coefficient of friction was dependent on sliding speed. With increasing sliding speed from 0.1 m/s to 1 m/s, a decrease in the ratio of real contact area to normal force was observed in rubber and majority of Neolite simulations (Figure 3-7). The ratio of real contact area to normal force decreased an average of 19% (range of -28 to 54%) with increasing sliding speed for Neolite and decreased an average of 35% (range of 29 to 40%) for the rubber material.

a)

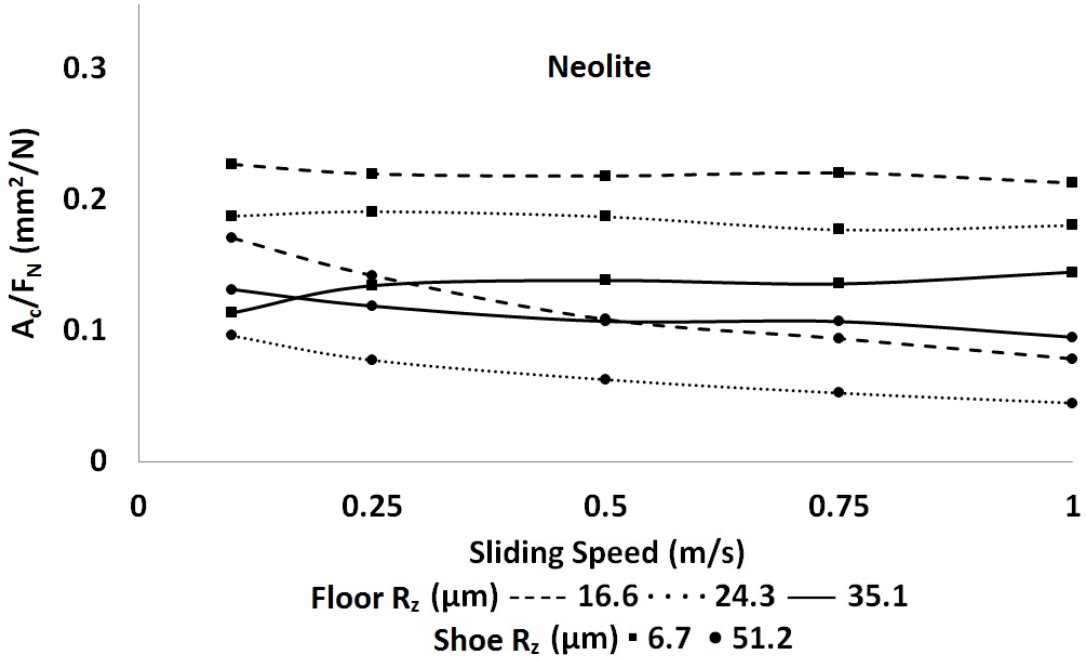


b)

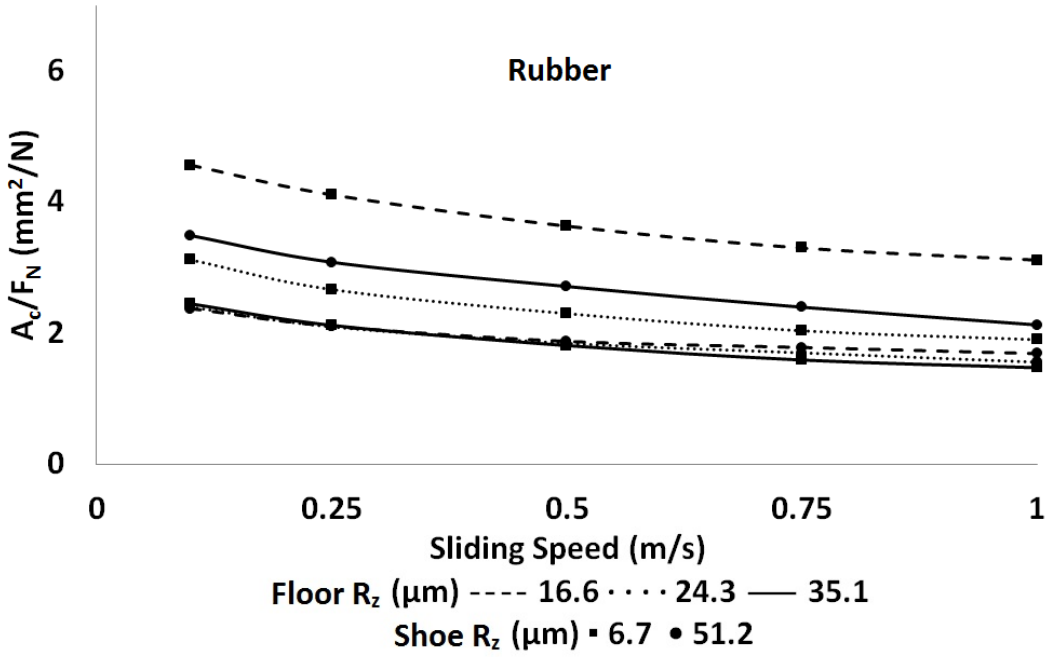


**Figure 3-7.** Effect of speed on the ratio of real contact area to normal force ($A_c/F_N$) for Neolite (a) and rubber (b) across different combinations of shoe-floor roughness.

Increasing shoe or floor roughness reduced the contact area indicating that increased roughness leads to a reduction in adhesion friction in majority of the simulations (Figure 3-8). The ratio of real contact area to normal force decreased an average of 41% (range of 16 to 64%) with increasing Neolite shoe roughness and decreased an average of 7% (range of -46 to 48%) with increasing rubber shoe roughness. Increasing floor roughness caused an average decrease of 5% (range of -67 to 44%) in the ratio of real contact area to normal force in the Neolite material and an average decrease of 4% (range of -43 to 36%) in the rubber material. Increasing floor roughness caused a decrease in the ratio of real contact area to normal force for the low shoe roughness but caused an increase for the high shoe roughness.

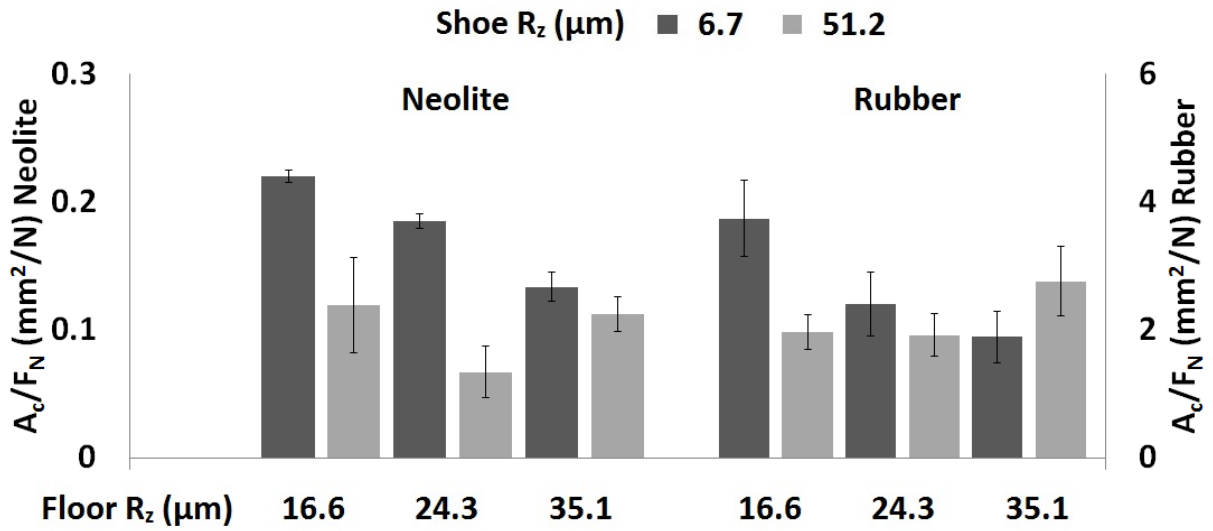


**Figure 3-8.** Effects of shoe and floor roughness on the ratio of real contact area to normal force ($A_c/F_N$) averaged across different speeds for Neolite (Left) and rubber (Right). Error bars represent the standard deviations across the different testing speeds.

### 3.4.3 Experimental validation of model

The hysteresis coefficient of friction magnitudes and the effects of shoe material and floor roughness on hysteresis friction were consistent between the model and the experimental studies (Figure 3-9). Both the experiments and the model demonstrated hysteresis coefficient of friction values ranging from approximately 0.1 to 0.3. Increasing floor roughness led to larger hysteresis friction values both experimentally and in the model. Also, the increase in hysteresis friction between the rougher and softer rubber material in reference to the smooth and hard Neolite was consistent between the model and experiments. Overall, hysteresis coefficient of friction from the model demonstrated a better agreement with the experimental results in the case of the smooth Neolite (Figure 3-9. Left). The predicted effect of sliding speed on hysteresis coefficient of friction differed from the experimental results. The model predicted a fairly constant hysteresis friction with increasing speed while the experimental studies demonstrated a substantial decrease in hysteresis friction with increasing sliding speeds.

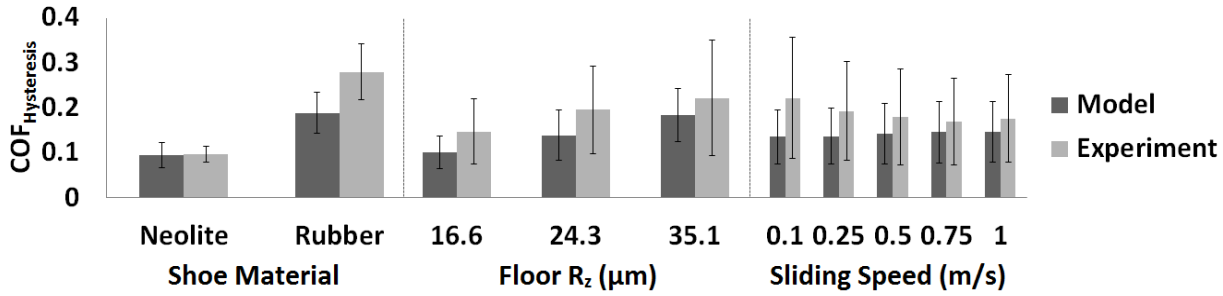


**Figure 3-9.** Comparison between model and experiment in $COF_{Hysteresis}$: for the two shoe materials averaged across different speeds and floors (Left); for the three floor roughness levels averaged across different speeds and shoe materials (Middle); and for the different sliding speeds averaged across different floor roughness levels and shoe materials (Right). Error bars represent standard deviations across the averaged parameters.

The model and experiments were more consistent in reproducing the effects of speed on adhesion for the rubber material than for the Neolite material (Figure 3-10). The model was not effective in reproducing the effects of floor roughness on adhesion friction (Figure 3-10). The model predicted a decreasing trend with increasing floor roughness for the Neolite material whereas experiments showed that it was relatively constant. Also, the model predicted an increasing trend with increasing floor roughness for the rubber material whereas the experiments demonstrated a decreasing trend. Both the model and experiments demonstrated a decay trend in adhesion friction as sliding speed increased for rubber material. This effect was less present for the Neolite models. The reduction in adhesion friction due to increasing sliding speed from 0.25 to 1 m/s was 37% and 41% for Neolite and rubber in the experiments, respectively, while the model predicted a reduction of 2% and 27%, respectively. Therefore, the trend between speed

and adhesion friction was similar between the model and experiments but the model underestimated the magnitude of the adhesion reduction with increasing sliding speed.

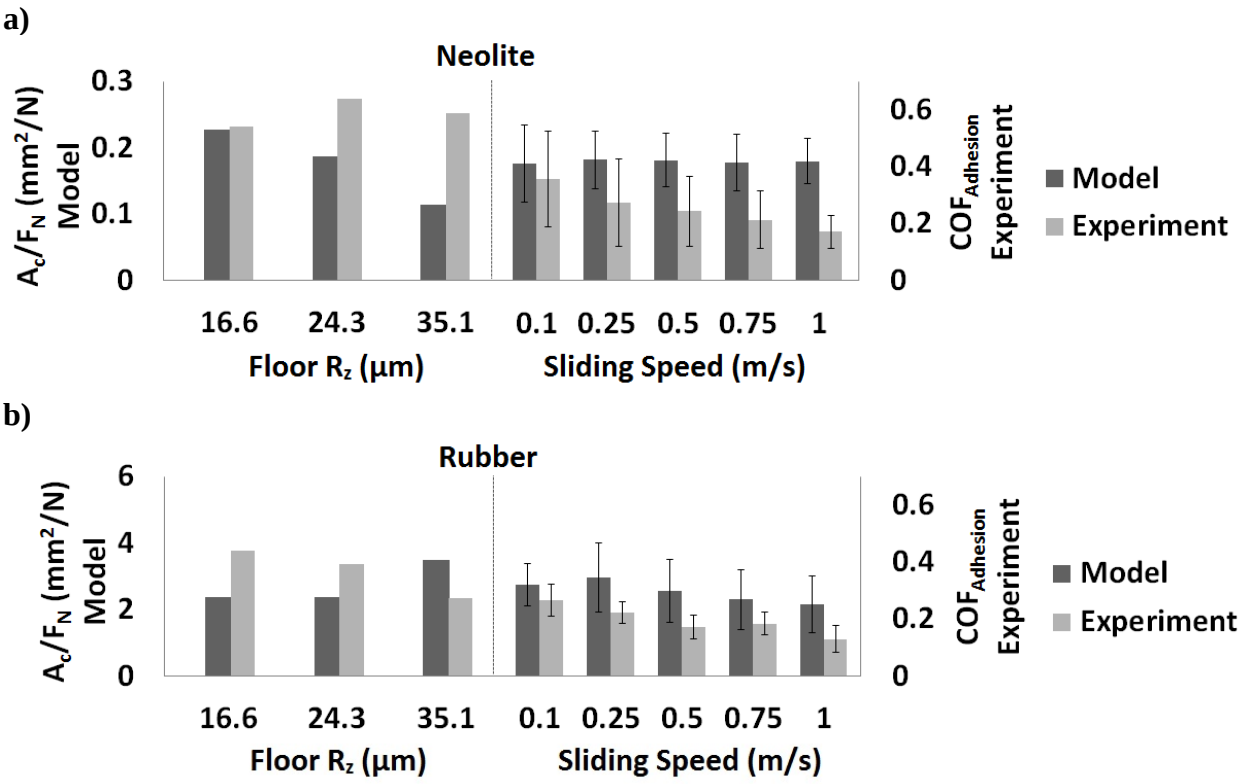


**Figure 3-10.** Comparison between the ratio of real contact area for the model and adhesion friction from the experiments for Neolite (a) and rubber (b) for: different floor roughness levels averaged across sliding speeds (Left) and different sliding speeds averaged across floor roughness levels (Right). Error bars represent the standard deviations across the averaged parameter.

## 3.5 DISCUSSION

The finite element model developed in this paper successfully predicted several trends in hysteresis, partially predicted speed trends for adhesion friction and produced hysteresis

coefficient of friction values similar to those observed experimentally. The model was based on shoe and floor roughness levels, shoe material properties and shoe sliding speeds that are relevant to slipping. Thus, this effort represents a successful step towards the utilization of finite element modeling in evaluating the relationship between shoe and floor design and coefficient of friction.

The finite element model reproduced several experimental trends including the effects of shoe material and floor roughness on hysteresis friction and the effects of speed on adhesion friction. Increased floor roughness resulted in elevated hysteresis coefficient of friction for both materials. Also, the net effect of a softer yet rougher shoe led to an increase in hysteresis friction. The overall magnitude of the predicted hysteresis coefficient of friction values were similar to those measured experimentally. Predicted trends in adhesion friction with floor roughness did not agree with those in the measured friction for either material. Increased sliding speed led to a lower ratio of real contact area to normal force, which was consistent with the experimental data but the model underestimated the magnitude of this reduction compared to experimental results.

The predicted effects of shoe and floor roughness on adhesion and hysteresis friction are consistent with the previous modeling studies and tribological theory. The model predicted a consistent positive correlation between roughness of the shoe or floor material and hysteresis friction. Typically, higher levels of roughness will result in higher deformation in contacting asperities [54, 77, 78], which results in additional energy loss in the viscoelastic material as it was observed in the finite element model of Bui and Ponthot [93], experimental study of [54] and theoretical studies of [77, 78]. The model demonstrated an 80% increase in hysteresis coefficient of friction with increasing floor roughness across the shoe materials. This increase is larger than the increase in hysteresis coefficient of friction due to roughness reported by other

researchers as 33% [53] and 48% [19]. It should be noted that those studies used a narrower range of roughness and different shoe materials which might explain the smaller increase in hysteresis with respect to increasing floor roughness in those studies. The model predicted a lower adhesion friction with increasing shoe/floor roughness due to a reduction in the real contact area. The decrease in the ratio of real contact area to normal force with increasing shoe/floor roughness suggests that increased asperity height reduces the amount that the soft shoe material conforms around the floor surface asperities in agreement with tribological theory [51] and experimental research [19]. There existed a 50% reduction and 31% increase in the ratio of real contact area to normal force with increasing floor roughness for rubber and Neolite, respectively. These effects were not consistent with the effects observed in [53] where 10-30% increase is reported but agree with the findings of [19] that reports a 28% reduction in force of adhesion with increasing floor roughness. Given that the effect of floor roughness on real contact area was reversed for the high shoe roughness (i.e., an increase in real contact area was observed between the medium and high roughness flooring), a likely different explanation is needed for high roughness shoe materials. When shoe roughness is high, increasing floor roughness can cause an interlocking effect between the shoe and floor asperities where the floor geometry conforms with the shoe asperities and leads to a higher area of contact [59]. Thus, an interesting interaction exists between shoe roughness and floor roughness for adhesion friction. This effect may disappear in the model if a distribution of asperity heights were used instead of a constant asperity height, which may reduce this interlocking effect.

The model predictions for the effects of sliding speed on adhesion are largely supported by tribological theory. The model, in agreement with the experimental studies on wet adhesion, demonstrated a reduction in real contact area with increasing sliding speed. At higher sliding

velocities, asperities of the soft shoe surface will have less time to viscoelastically conform around the harder floor asperities to form adhesional bonds, which reduces the real contact area and decreases adhesion [41]. The model indicated a 25-35% reduction in the ratio of real contact area to normal force with increasing sliding speed. This finding is generally in agreement with that findings of [18, 53] where they report a 28-60% reduction in lubricated friction with increasing sliding speed for a shoe material.

Results of the simulations indicated that speed does not have a dramatic effect on the hysteresis friction, while the experimental studies indicate that increasing sliding speed consistently reduced the hysteresis coefficient of friction. The lack of agreement between the simulations and experimental results may be due to limitations in the experimental studies to isolate hysteresis from hydrodynamic effects. Those experiments used a high viscosity oil to block adhesion and isolate hysteresis friction, which may have increased hydrodynamic pressures and reduce interaction by causing a separation between the surfaces [22, 26]. To conclusively test the ability of the model in simulating the effects of speed on hysteresis friction, novel experiments that isolate hysteresis friction without viscous fluid would need to be developed. Alternatively, the model developed in this paper would need to simulate the hydrodynamic effects of the fluid [16].

One strength of the model is its ability to evaluate the net change in hysteresis friction across shoe materials that have different material properties and roughness. Nosonovsky et al. [94] explained that materials self-organize to different steady-state roughness values dependent on their material properties and the counter surface that is causing the wear. Previous work that has attempted to describe the effects of shoe material properties on shoe-floor friction has led to conclusions that softer shoe materials lead to larger lubricated or hysteresis friction [15, 19, 58,

95, 96]. The model used in this study reveals that the increased hysteresis friction for softer shoe materials is likely due to the fact that softer materials typically have higher roughness [25, 58, 94, 96]. Thus, the increased lubricated friction that has been observed for soft shoes is likely caused by the increased roughness of soft materials and not by their hardness. The model used in this study was able to successfully determine that the soft yet rougher shoe material had a net increase in the hysteresis friction when compared to the hard but smoother material. Therefore, this model may have benefits in identifying shoe materials with high hysteresis friction by considering both their material properties and steady-state roughness. This contribution is significant considering that hysteresis is the dominant friction mechanism relevant to shoe-floor-contaminant friction in boundary lubrication regime [53].

Future enhancements to the model may improve its ability to reproduce experimental trends. For example, the relationship between the hysteresis friction and sliding speed may be improved be incorporating a hybrid model capable of considering the effects of both fluid and solid. The fluid component of this model would need to capture the hydrodynamic effects on the separation and deformation of the shoe material similar to [16].

Also, using statistical models for describing asperity distribution of the contacting surfaces might improve the model's predictive capabilities [77, 97]. Future versions of this model should also aim at using various shapes for describing surface asperities and examine its effect on the predicted friction [83]. This first generation of the microscopic model of model of shoe-floor-contaminant friction provided reasonable agreement in trends of the hysteresis and adhesion friction with the experimental results using the simplifying assumption of sawtooth profile. The model could be used as a basic framework for more advanced models of complex multi-factorial shoe-floor-contaminant friction by also considering the macroscopic features of

shoes such as tread. Lastly, more research is needed to quantify interfacial shear stresses for different combinations of shoe materials, floor materials and contaminants in order for the model to predict adhesion coefficient of friction values.

The ultimate goal of these models is to assist in improving shoe and floor design to reduce slips and fall injuries. Our findings suggest that shoe roughness, floor roughness and material properties have a dramatic impact on hysteresis friction, while shoe roughness, floor roughness and sliding speed have an impact on adhesion friction. Thus, controlling these parameters can be useful in designing slip-resistant shoe and flooring surfaces. As these models continually develop, more conditions and parameters that impact friction can be incorporated and more sophisticated designs can be done, leading to the ultimate goal of reduced injuries due to slip accidents.

# 4.0 PREDICTIVE MULTISCALE COMPUTATIONAL MODEL OF SHOE-FLOOR COEFFICIENT OF FRICTION

## 4.1 ABSTRACT

Understanding the frictional interactions between the shoe and floor during walking is critical to prevention of slips and falls, particularly when contaminants are present. A multiscale finite element model of shoe-floor-contaminant friction was developed that takes into account the surface and material characteristics of the shoe and flooring in microscopic and macroscopic scales. The model calculates shoe-floor coefficient of friction (COF) in boundary lubrication regime where effects of adhesion friction and hydrodynamic pressures are negligible. The validity of model outputs was assessed by comparing model predictions to the experimental results from mechanical COF testing. The multiscale model estimates were linearly related to the experimental results ($p<0.0001$). The model predicted 73% of variability in experimentally-measured shoe-floor-contaminant COF. The results demonstrate the potential of multiscale finite element modeling in aiding slip-resistant shoe and flooring design and reducing slip and fall injuries.

**Keywords:** Slips and falls; Shoe-floor friction; Coefficient of friction; Finite element modeling

## 4.2 INTRODUCTION

Slips and falls are among the primary causes of injuries. According to the Centers for Disease Control and Prevention, falls were the leading cause of non-fatal injuries between 2001 and 2014 and are responsible for an annual financial burden of $180 billion in the United States [3, 98]. More than 50% of falls are initiated by slipping accidents in occupational settings [5].

Frictional characteristics of the shoe-floor interface impact the likelihood of slips and falls [6, 7, 37]. The probability of slips has been predicted with the available coefficient of friction (ACOF) and the required coefficient of friction (RCOF) [6, 7, 33, 37]. RCOF is measured during gait using force plates on dry surfaces [38]. ACOF is typically measured using a mechanical device that quantifies the ratio of friction to normal forces between the shoe and flooring [6-8, 33]. Physics-based computational models of frictional behavior of the shoe-floor-lubricant complex have recently been developed to predict ACOF [16, 99]. These models have advantages in that: 1. they can help explain the underlying friction mechanisms pertinent to shoe-floor friction, and 2. they can be used to predict and optimize ACOF of hypothetical shoe-floor designs (i.e., they can be used as a design tool).

Shoe-floor friction is influenced by microscopic and macroscopic features of the shoe and flooring. Relevant factors affecting ACOF on the microscopic scale include shoe and flooring surface topography, contact pressure, and outsole material properties [16, 99, 100]. Relevant factors on the macroscopic scale include shoe tread design features such as geometry, tread depth, width and orientation [12-14], material hardness [15, 101], sliding speed and shoe-floor contact angle [46, 102, 103]. Physics-based modeling of the shoe-floor interface has the potential to elucidate how these various features contribute to friction mechanisms.

Contaminants, particularly liquids, play an important role in slipping accidents and can impact friction. Fluid can reduce ACOF by either becoming pressurized, causing a separation of the contacting surfaces (hydrodynamic lubrication) or by reducing adhesion friction without causing a separation (boundary lubrication). While some studies have utilized solely hydrodynamic theory to explain ACOF of lubricated surfaces [13, 50], research by our group suggests that dangerously low ACOF values can occur even without hydrodynamic effects [18, 19, 53, 99]. Shoes with at least some tread are demonstrated to operate in boundary lubrication [22, 26] suggesting that boundary lubrication is relevant to slipping. In boundary lubrication, hysteresis deformation of the shoe sole material is the major mechanism contributing to friction [19, 53, 99]. Hysteresis friction originates from viscoelastic deformation of the surface asperities [61]. Therefore, modeling hysteresis at the shoe-floor interface is relevant to predicting friction on liquid-contaminated surfaces.

An opportunity exists to use finite element modeling to simulate and predict shoe-floor COF. Finite element modeling has been demonstrated to be effective in modeling the impact of microscopic shoe and floor features on COF [99]. Furthermore, multiscale computational models have been developed for tires that take into account surface features in both microscopic and macroscopic levels to determine hysteresis COF [31, 32]. However, multiscale computational methods have not yet been applied to investigate shoe COF. This study addresses this knowledge gap by applying multiscale computational modeling techniques to actual shoe geometries to predict whole shoe-floor COF.

The purpose of this study is to develop and quantify the predictive ability of a multiscale finite element model for shoe-floor COF. The predictive ability of the multiscale computational model as well as each of its components (microscopic and macroscopic) to predict experimental

ACOF are assessed to evaluate the validity of the model. The scope of this model is boundary lubrication regime where adhesion and hydrodynamic pressure effects are negligible.

## 4.3 METHODS

### 4.3.1 Multiscale model

A computational model was developed that included a microscopic and macroscopic finite element model. The microscopic model simulated the interaction between shoe and floor surface asperities to predict the frictional shear stress due to hysteresis as a function of contact pressure [56, 78, 104]. The macroscopic model simulated shoe heel to floor contact to determine the contact pressure distribution across the outsole surface (Figure 4-1). Contact pressure values from the macroscopic model were then combined with the microscopic model to predict the hysteresis COF. Explicit finite element software (LS-Dyna® Livermore Software Technology Corporation, Livermore, California, USA) was used for simulations.

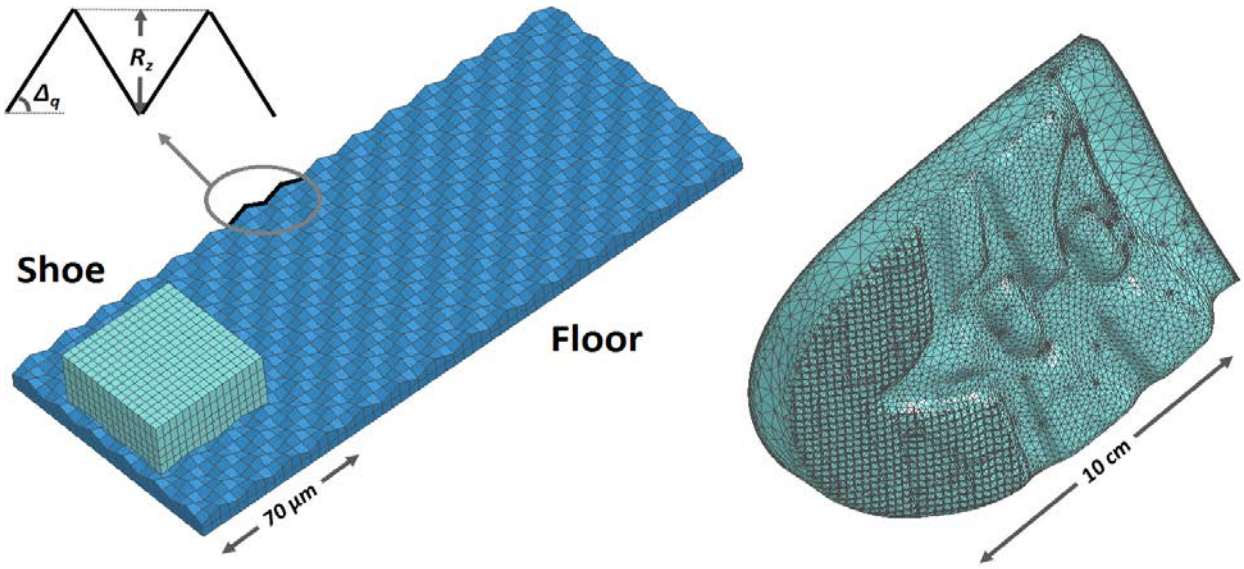


**Figure 4-1.** Representative microscopic (Left. S1-Vinyl) and macroscopic (Right. S6) finite element models. Flooring is not shown in the macroscopic model. A magnified representation of surface asperities is shown in the top left corner.

#### 4.3.1.1 Microscopic model

The microscopic model simulated contact between a rough viscoelastic shoe material and a rough rigid floor. A five-term exponentially decaying function was applied to the shoe, which described the time-dependent behavior of the shear modulus ($G(t)$) (Equation 4-1.) [99]. Flooring was modeled as rigid because it is orders of magnitude harder than the shoe [17, 99]. Roughness parameters including the peak-to-valley distance roughness ($R_z$) and root mean square slope ($\Delta_q$), were incorporated into the models that were consistent with shoes and floors tested in the experimental measurements (See section 4.3.2). Specifically, the peak-to-valley distance ($R_z$) was used to define the vertical distance between peak and valley nodes. Root mean square slope ($\Delta_q$) was used to define the slope of the asperities, which affected the spacing between the asperities (Figure 4-1. Left) [99].

$$G(t) = \sum_{m=1}^{5} G_m e^{-t/\tau_m} \quad , \quad \tau_m = 10^{-(m-1)}\tau_1 \qquad \text{Equation 4-1.}$$

Boundary conditions for the microscopic models included: 1. constraints on the translational and the rotational degrees of freedom at the bottom surface of the floor nodes. 2. Constraints on the translational degrees of freedom at the top surface of the shoe nodes. 3. Contact pressure was controlled using the vertical displacement boundary conditions that were applied at the top surface of the shoe nodes; higher contact pressures were achieved by applying more downward vertical displacement. 4. Velocity boundary conditions consistent with experiments (Section 4.3.2) were applied to the nodes at the top surface of the shoes. The microscopic model geometries were meshed using eight node hexahedral elements. These elements are well suited for simulating extreme deformations of soft materials [82]. Mesh settings that were previously examined for the finite element models of chapter 3.0 (Section 3.3.1) were used for the microscopic models.

#### 4.3.1.2 Macroscopic model

Macroscopic models were either created based on non-contact 3D laser scans (FaroArm®, Faro Technologies, Lake Mary, Florida, USA) of the shoes or CAD models developed based on the measured shoe geometries (ANSYS DesignModeler®, ANSYS Inc., Canonsburg, Pennsylvania, USA). For shoes with repeated pattern geometries, CAD models were developed. For shoes with irregular tread patterns, laser scans were collected, processed to repair surface irregularities (Geomagics®, 3D Systems Corporation, Rock Hill, South Carolina, USA), and tread surface texturing was added to the surface based on the texture's shape, size and orientation

(ANSYS DesignModeler®). Since viscoelastic effects were accounted for in the microscopic models, a linear elastic material based on durometer readings was used for the shoes in macroscopic models (Section 4.3.1.1).

Displacements and rotations of the nodes at the bottom surface of the flooring and the top surface of the shoe in the macroscopic models were constrained similar to the microscopic models. The shoe was slid against the flooring at a normal force of 250 N and a horizontal speed of 0.3 m/s. The vertical velocity was 0.3 m/s until the desired vertical force was reached (Section 4.3.1.2). Shoe-floor angles consistent with experimental measurements were used in macroscopic models (Section 4.3.1.2). Macroscopic models were meshed using tetrahedral elements that are recommended for simulating complex geometries [82]. Flooring was modeled as a rigid material similar to microscopic simulations [17, 99]. Mesh refinement was applied to the elements of the contact region of the shoe. Mesh size for the macroscopic models was determined based on a tradeoff between the convergence in the normal force and the computational cost.

#### 4.3.1.3 Analysis of model data

Frictional shear stress due to hysteresis ($\sigma_f$) was calculated as the ratio of the average hysteresis force to the nominal area (Equation 4-2.). Average contact pressure in the microscopic models was calculated by dividing the average normal force by the area of the shoe interface in the horizontal plane (i.e., nominal area). Between 16 and 21 contact pressures were evaluated using the model for each shoe-floor combination. A piecewise polynomial fit ($f(p)$) [32, 64] was used (MATLAB®, Mathworks, Natick, Massachusetts, USA) to interpolate the shear stress between the discrete levels of contact pressure simulated in microscopic models (Figure 4-2 and Equation 4-3.). Friction forces for the macroscopic models were calculated based on the predicted shear stresses and areas of the contact elements. These friction forces were summed

across the contact elements to calculate the net friction force (Equation 4-4.). Normal force was calculated based on the contact pressure and the area of elements (Equation 4-5.). Whole-shoe COF was the ratio of friction force to normal force (Equation 4-6.). A preliminary analysis of the modeling data and experimental data (described in section 4.3.2) revealed that the relationship between friction force and normal force was linear with a y-intercept of approximately 0 indicating that this definition of whole-shoe COF is relevant even though Amontons' laws are not broadly applicable to polymers [105].

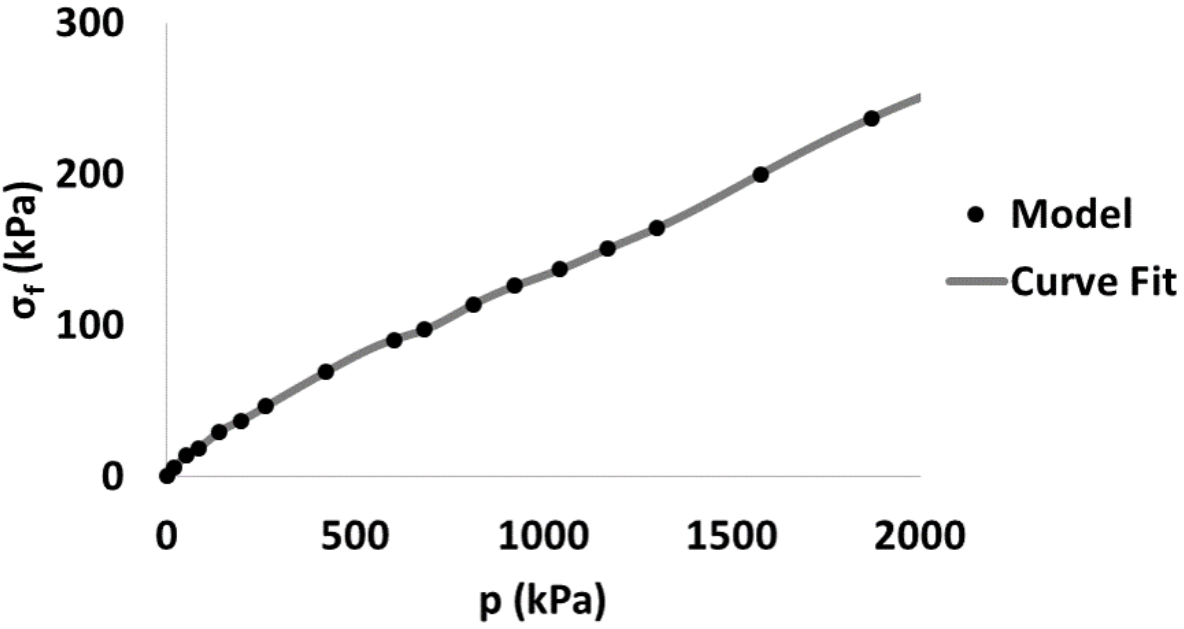


**Figure 4-2.** Representative plot of the frictional shear stress, $\sigma_f$, as a function of contact pressure. The gray line indicates the piecewise polynomial curve fit.

$$\sigma_f = \frac{F_{Hysteresis}}{A_{Micro}}$$ Equation 4-3.

$$\sigma_f(p) = f(p)$$ Equation 4-2.

$$F_{Friction} = \sum f(p_i)A_i$$ Equation 4-4.

$$F_{Normal} = \sum p_i A_i$$ Equation 4-5.

$$COF = \frac{F_{Friction}}{F_{Normal}}$$ Equation 4-6.

#### 4.3.1.4 Multiscale computational modeling of shoe-floor hysteresis friction: An alternative approach for calculating shoe-floor-contaminant coefficient of friction

In this section, an alternative method for analyzing the data from multiscale model to the one that was introduced in section 4.3.1 is presented. This method is based on the premise that it will make it possible that the COF for whole shoe can estimated with the assumption that the entire shoe geometry is at a certain contact pressure level. Later on in this dissertation (Chapter 5.0 ), this approach is used to investigate the effect of shoe design factors and biomechanical parameters on the COF.

In this alternative framework, instead of utilizing the frictional shear stress ($\sigma_f$), COF at the microscopic scale ($COF_{Micro}$) was calculated as the ratio of average hysteresis force to the average normal force during the time period where horizontal sliding was occurring (Equation 4-7.)[99]. Average contact pressure in the microscopic models was calculated by dividing the average normal force by the nominal area of the shoe interface. Between 15 and 19 contact

pressures were evaluated using the model for each shoe-floor combination. The resulting relationship between contact pressure and $COF_{Micro}$ was described with an exponential decay function for each shoe-floor combination (Figure 4-3 & Equation 4-8.). Based on this exponential decay function and the simulated contact pressure in the macroscopic model, the COF in each of the shoe outsole contact elements was determined. Friction forces were calculated based on the $COF_{Micro}(p)$, contact pressures and contact areas of the contact elements [101]. These friction forces were summed across the contact elements to calculate the whole shoe friction force (Equation 4-9.). Normal force was calculated based on the contact pressure and area of elements (Equation 4-5.). Whole shoe COF was the ratio of whole shoe friction force to whole shoe normal force (Equation 4-6.).

$$COF_{Micro} = \frac{F_{Hysteresis}}{F_N}$$ Equation 4-8.

$$COF_{Micro}(p) = COF_{\infty} + (COF_0 - COF_{\infty})e^{-\beta p}$$ Equation 4-7.

$$F_{Friction} = \sum COF_{Micro}(p_i)p_i A_i$$ Equation 4-9.

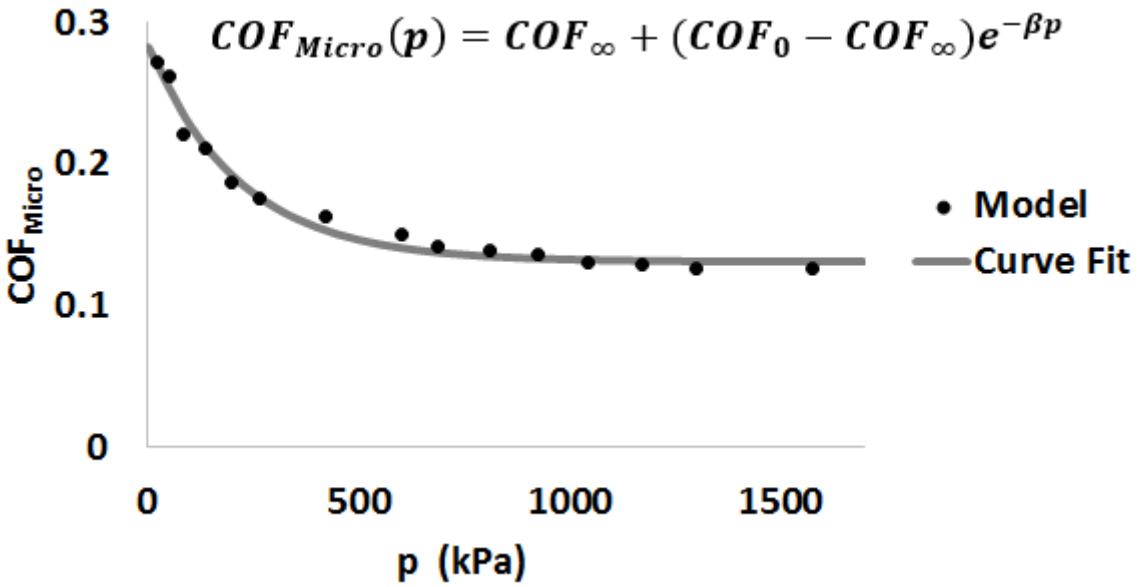


**Figure 4-3.** Representative plot of $COF_{Micro}$ as a function of contact pressure. The gray line indicates the exponential curve fit.

The exponential decay curve (Equation 4-8.) for relating $COF_{Micro}$ values to contact pressure fit the data for all shoe-floor combinations ($R^2$ between 0.96 and 0.99 for all shoe materials and across the two floorings) (Figure 4-4 & Table 4-1). $COF_{Micro}$ was generally higher for the ceramic flooring (higher roughness) compared to the vinyl flooring (lower roughness) (Figure 4-4). $COF_{Micro}$ values ranged between 0.11-0.28 for the vinyl flooring (Figure 4-4. Left

& Table 4-1. Left) and between 0.14-0.36 for the ceramic flooring (Figure 4-4. Right & Table 4-1. Right).

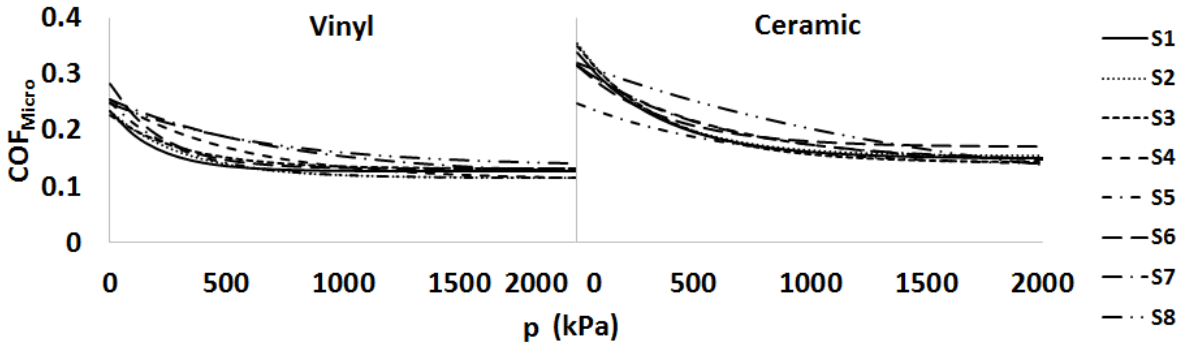


**Figure 4-4.** $COF_{Micro}$ as a function of contact pressure for different shoes when modeled against vinyl (Left) and ceramic (Right) flooring.

**Table 4-1.** Curve fit parameters for Equation 4-8., describing the $COF_{Micro}$ as a function of contact pressure.

| Shoe | Floor | $COF_0$ | $COF_\infty$ | $\beta(1/kPa)$ | Floor | $COF_0$ | $COF_\infty$ | $\beta(1/kPa)$ |
|---|---|---|---|---|---|---|---|---|
| **S1** | **Vinyl** | 0.233 | 0.125 | 0.00489 | **Ceramic** | 0.338 | 0.149 | 0.00276 |
| **S2** | **Vinyl** | 0.232 | 0.114 | 0.00319 | **Ceramic** | 0.353 | 0.153 | 0.003 |
| **S3** | **Vinyl** | 0.226 | 0.131 | 0.00313 | **Ceramic** | 0.349 | 0.141 | 0.00262 |
| **S4** | **Vinyl** | 0.253 | 0.111 | 0.00182 | **Ceramic** | 0.315 | 0.142 | 0.00166 |
| **S5** | **Vinyl** | 0.25 | 0.114 | 0.00325 | **Ceramic** | 0.349 | 0.128 | 0.0018 |
| **S6** | **Vinyl** | 0.282 | 0.131 | 0.00456 | **Ceramic** | 0.314 | 0.17 | 0.00268 |
| **S7** | **Vinyl** | 0.254 | 0.117 | 0.00133 | **Ceramic** | 0.313 | 0.144 | 0.00175 |
| **S8** | **Vinyl** | 0.248 | 0.135 | 0.0015 | **Ceramic** | 0.32 | 0.058 | 0.00059 |

### 4.3.2 Experimental validation

Model results were compared to experimentally-measured ACOFs for eight different shoes (S1-S8) and two different floorings. Three shoes (work boots) had the same geometry but varying material properties (S6-S8). The remaining five shoes had different tread patterns,

material properties and roughness levels (S1-S5). The two floorings included a vinyl composite tile and a high roughness ceramic tile. The high roughness of the ceramic tile was achieved by sand blasting using an aluminum oxide abrasive [53, 106]. Surface characteristics of the shoes and floorings were quantified with a stylus profilometer (Taylor-Hobson Surtronic S100®, Leicester, UK). Specifically, roughness parameters were measured with a sampling length of 1.6 mm and a cut-off length of 0.8 mm and averaged across eight measurements at different orientations (Table 4-2). The ceramic flooring ($R_z$ = 35.6 µm; $\Delta_q$ = 35.4°) had a higher roughness than the vinyl flooring ($R_z$ = 9.1 µm; $\Delta_q$ = 27.8°) for both parameters.

**Table 4-2.** Roughness and material parameters for the modeled shoes.

| Shoe | $R_z$ (µm) | $\Delta_q$(°) | $G_m$(kPa) | | | | | $\tau_1$(s) |
|---|---|---|---|---|---|---|---|---|
| | | | $G_1$ | $G_2$ | $G_3$ | $G_4$ | $G_5$ | |
| **S1** | 4.03 | 10.56 | 1891 | 40.65 | 177.6 | 355.7 | 0.01772 | 2041.65 |
| **S2** | 4.81 | 10.59 | 2617 | 46.31 | 75.77 | 396 | 0.2361 | 1431.02 |
| **S3** | 4.67 | 11.5 | 2595 | 45.15 | 240 | 241.7 | 0.04211 | 1999.6 |
| **S4** | 7.04 | 11.87 | 3764 | 53.99 | 17.72 | 160.5 | 0.00489 | 1330.85 |
| **S5** | 6.63 | 12.61 | 2989 | 0.02327 | 400.3 | 0 | 288.5 | 4450.38 |
| **S6** | 9.35 | 13.85 | 2809 | 95.78 | 459.4 | 0.9468 | 595.9 | 1663.89 |
| **S7** | 7.99 | 13.31 | 5046 | 583.7 | 366.9 | 1.648 | 235.6 | 895.26 |
| **S8** | 7.01 | 13.58 | 8744 | 172.5 | 152.3 | 0.2857 | 885.9 | 1033.38 |

Shore A hardness of the shoes were characterized using a durometer (Intercomp®, Minneapolis, Minnesota, USA) [107]. Readings were sampled over 2-minutes at 10s intervals. Hardness measurements were converted to shear moduli (*G(t)*, Equation 4-1.) using methods recommend by Giacomin, et al. [108] and viscoelastic material models were developed (Table 4-2, $R^2$> 0.99 for exponential decay fits). The initial modulus (at *t=0*, Equation 4-1.) was used for modeling the linear elastic shoe material in macroscopic models. Durometer readings were conducted and averaged across nine heel locations for each shoe.

ACOF measurements were performed using a custom-developed robotic slip-tester at a normal force level of 250 N [33, 37, 42]; a sliding speed of 0.3 m/s; and shoe-floor angles of 7±2° [34, 43]. This speed is within the range of 0-1 m/s that is recommended in literature as 'biofidelic testing' [34, 41, 43]. The average ACOF values were calculated for the first 200 milliseconds after reaching a normal force of 250 N [33, 37]. Testing for each shoe-floor combination was repeated over three different days to achieve reliable ACOF values in the presence of potential day to day variability. Five trials were taken for each shoe-floor combination on each day. Shoe-floor angles (Table 4-3) and sliding speeds were verified using reflective markers placed on the shoes that were tracked using a 14-camera motion capture system (Vicon T40S, Oxford, UK). Canola oil was used as a lubricant in all experiments because preliminary results revealed that this lubricant minimized adhesion forces so that the measured friction was primarily due to hysteresis [19, 53, 54, 109-111].

**Table 4-3.** Shoe-floor angles in friction tests (Average(SD)).

| Shoe | Shoe-Floor Angle - Vinyl ($^0$) | Shoe-Floor Angle – Ceramic ($^0$) |
|---|---|---|
| **S1** | 6.43 (1.01) | 6.90 (0.39) |
| **S2** | 6.48 (0.38) | 6.97 (0.13) |
| **S3** | 6.21 (0.96) | 7.53 (0.18) |
| **S4** | 6.05 (0.78) | 5.53 (0.43) |
| **S5** | 7.79 (0.46) | 6.40 (0.34) |
| **S6** | 7.85 (0.49) | 5.40 (0.59) |
| **S7** | 7.32 (0.33) | 7.27 (1.27) |
| **S8** | 7.00 (0.22) | 7.37 (1.32) |

Contact area was measured as an intermediate validation of the macroscopic model. Black ink imprints of shoes on paper [112] were created at the aforementioned angle and force were generated. The contact area was calculated by a custom-developed image processing code that summed the area of black pixels (MATLAB®, Mathworks, Natick, Massachusetts, USA).

### 4.3.3 Statistical analyses

Statistical analyses compared the model to the experimental results. Three linear regression models were created to assess contributions from components of the multiscale model to the experimentally-measured ACOF. The first statistical analysis quantified the impact of COF predicted by the multiscale model on ACOF. The other statistical models quantified the ACOF predicted by 1. the shear stress predicted by the microscopic model at 200 kPa (roughly the average under-shoe contact pressure [113]) and 2. the contact area from the macroscopic model. A linear regression model between the experimentally-measured contact area and the contact area predicted by the model was performed as an intermediate validation of the macroscopic simulations. Goodness of fit was assessed using the $R^2$ values in linear regression models. An *alpha* value of 0.05 was used for all statistical analyses.

## 4.4 RESULTS

The slopes of the piecewise polynomials (Equation 4-3.) for relating σf values to contact pressure (Figure 4-5) were generally higher at lower contact pressures. The shear stress, $\sigma_f$, was generally higher for the ceramic flooring (higher roughness) compared to the vinyl flooring (lower roughness) (Figure 4-5). For example, $\sigma_f$ values at 200 kPa ranged between 34.1-43.6 kPa for the vinyl flooring (Figure 4-5. Left) and between 50.74-59.9 kPa for the ceramic flooring (Figure 4-5. Right).

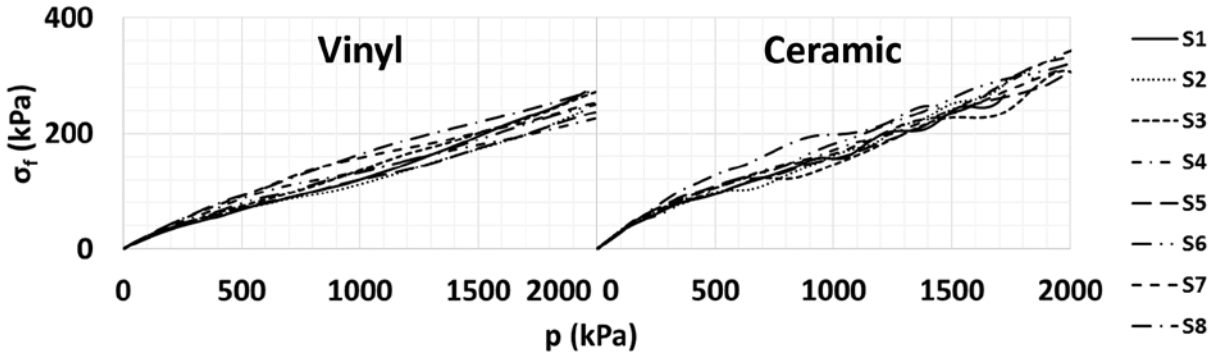


**Figure 4-5.** Frictional shear stress, $\sigma_f$, as a function of contact pressure for different shoes when modeled against vinyl (Left) and ceramic (Right) flooring.

The contact area geometry in the simulations were similar to the experimental contact geometries (Figure 4-6). A strong correlation existed between the predicted and measured contact areas ($R^2$=0.82; $p$=0.002) (Figure 4-7). Similar magnitudes were observed in the model-predicted contact areas (range of 1.44-9.29 $cm^2$) and the experimentally-measured contact areas (range of 2.02-11.83 $cm^2$).

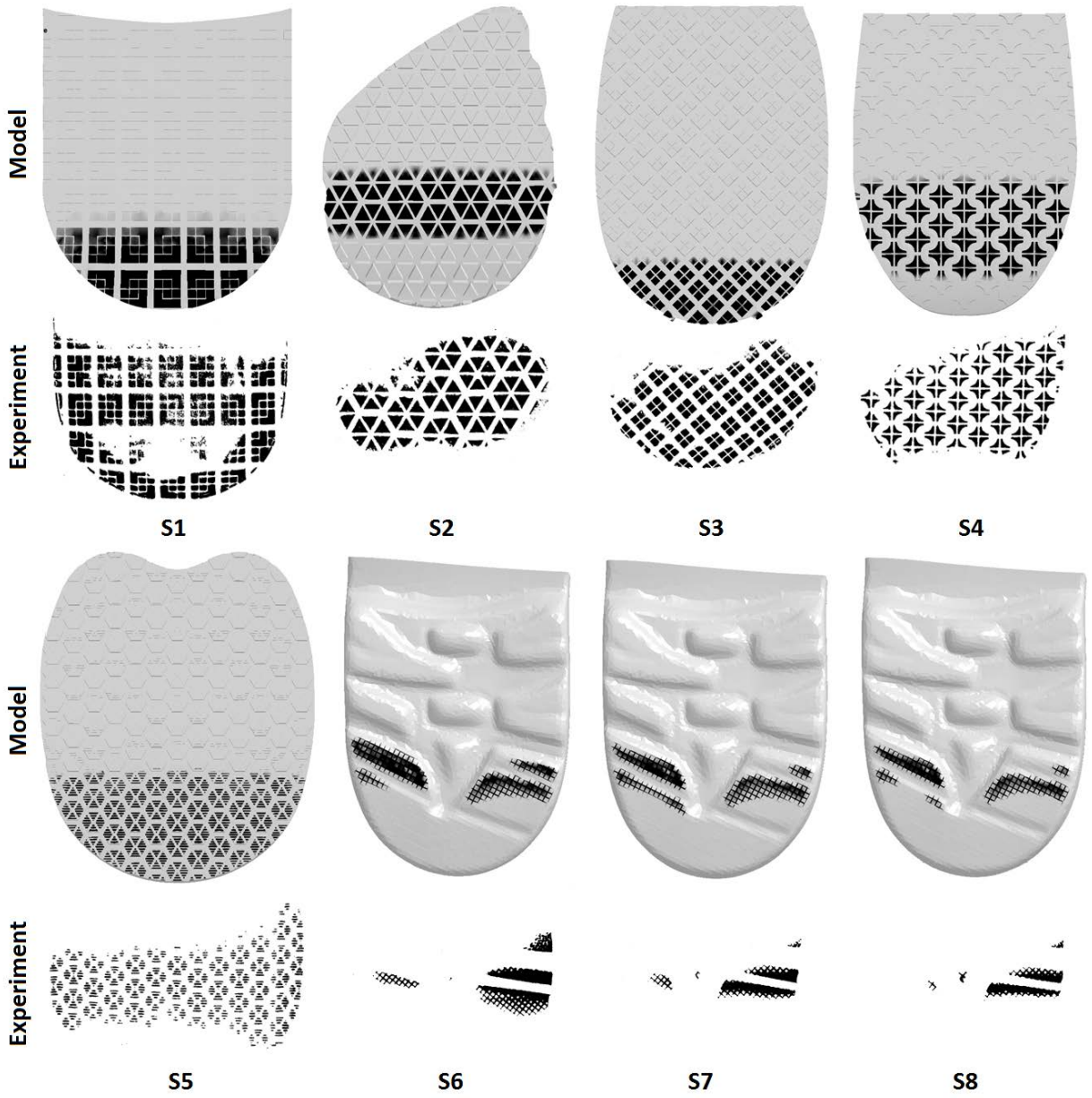


**Figure 4-6.** Predicted macroscopic contact area and experimentally-measured contact area using the ink imprints. For the model, gray indicates no contact and black indicates contact. For the experiment, white indicates no contact and black indicates contact.

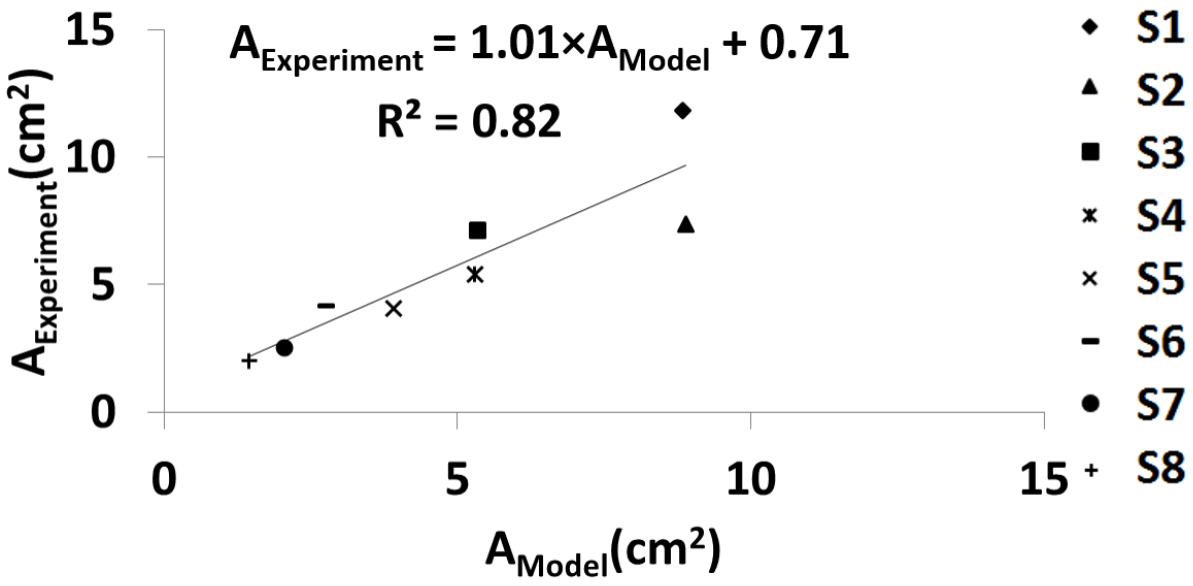


**Figure 4-7.** Experimentally-measured contact area versus contact area predicted by the macroscopic model.

The multiscale model predictions of COF ($COF_{Model}$) were correlated to the measured COF (ACOF) ($p$<0.001, $r$=+0.86) and predicted 73% of the variance (Figure 4-8). The magnitudes of the model predictions were lower than the experimental results. $COF_{Model}$ had a narrower range (0.13-0.26) than the ACOF (range of 0.05-0.87). The slope of this regression line was 5.7. The shear stress of the microscopic model, predicted only 23%of the variation in ACOF ($p$=0.059, $r$=+0.48). The contact area from the macroscopic model explained 34% of the variation in ACOF ($p$=0.017, $r$=+0.58).

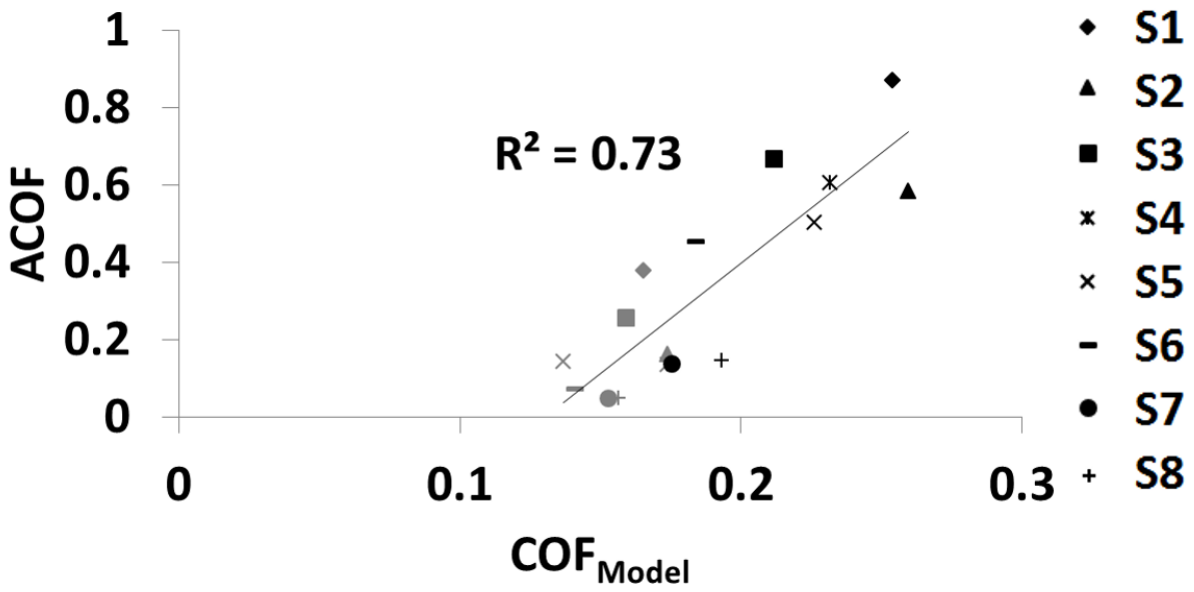


**Figure 4-8.** Experimentally-measured ACOF versus COF predicted by the multiscale model. Marker colors represent floorings: Vinyl (Gray) and ceramic (Black).

## 4.5 DISCUSSION

The presented multiscale modeling predicted most of the variability for the experimentally-measured ACOF and contact area. Parameters from the microscale and macroscale components were much less predictive of the ACOF. This demonstrates the important contributions of each scale to successfully predict the whole shoe-floor ACOF.

The model predicted that shoe designs which lead to lower contact pressures will result in higher COFs and therefore lower the slip risk. This finding is consistent with computational modeling studies on rubber [32] and experimental findings of Grönqvist [113] that reported lower COFs at higher contact pressures. The model also suggests that higher contact areas between shoe and flooring will result in higher COFs and lower fall risk in agreement with

previous research [41, 112-114]. The microscopic model was sensitive to changes in floor roughness, consistent with experimental [72, 73] and modeling studies [16, 99]. This increase in COF for rougher floor surfaces is due to the larger viscoelastic deformation and energy loss [54, 77] in shoe material when it is subjected to floorings with higher asperity heights (high roughness floorings).

The outcomes of this research can be particularly useful in designing shoes by focusing on the design characteristics that increase hysteresis COF. According to the model, a high COF on contaminated surfaces in boundary lubrication can be achieved by more distributed contact pressures. For example, the multiscale modeling framework can explain the effects of tread texturing on COF. Overall, shoes with harder outsoles (S7 and S8) and texturing (S5-S8) demonstrated lower COFs compared to the other shoes. To demonstrate the impact of texture, another simulation was performed on S6 with the texturing removed (S6'). When tread texturing was removed (Figure 4-9. Top), a lower average contact pressure (S6') was observed (Figure 4-9. Bottom). An increase in COF was observed on vinyl and ceramic flooring from 0.14 and 0.19 to 0.16 and 0.21, respectively. Based on the regression equation (Figure 4-8) these changes in $COF_{Model}$ would be expected to increase ACOF on vinyl and ceramic floorings by 0.12 and 0.17, respectively. This finding is consistent with some experimental literature that suggests the use of surface texturing for reducing friction in boundary lubrication [115, 116] and with the shoe design recommendations that suggest that tread texturing would not always cause an improvement in footwear slip-resistance [114, 117]. However, it should be noted that texturing can also lead to an increase in wet COF by preventing hydroplaning [118]. This study utilized treaded shoes which have been shown to operate in boundary lubrication [22, 26]. Thus, the

surface texturing might have been unnecessary for fluid drainage, which may explain why an increase in COF was not observed.

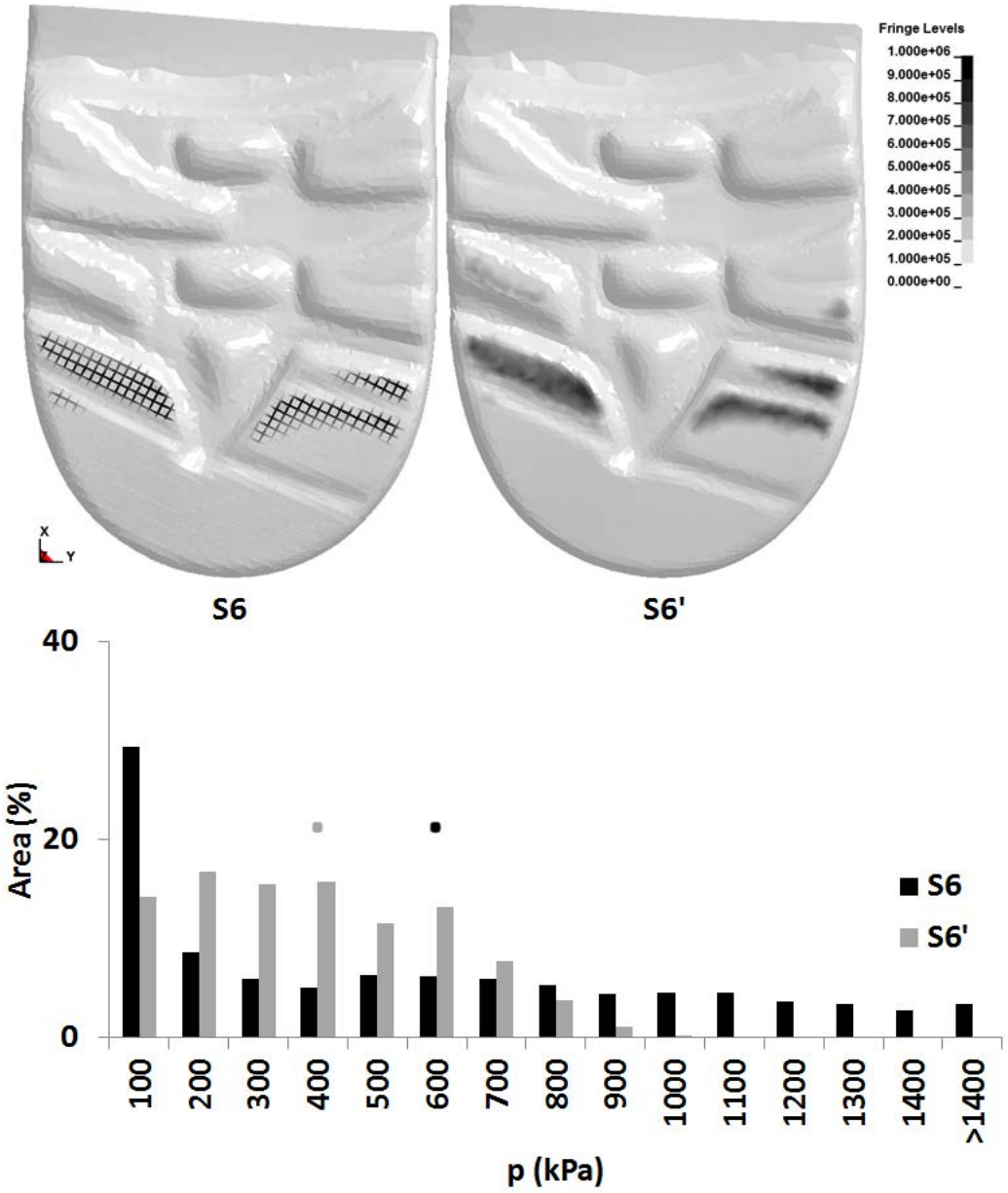


**Figure 4-9.** Top: Contact pressure distribution in a textured shoe (S6) versus the same shoe after removing the texture (S6'). Bottom: Histogram of contact pressure distribution over the areas of a textured (S6-black) versus non-textured (S6'-gray) shoes. Circles indicate average contact pressures.

Significant differences were observed between the COF magnitudes of the model predictions and the experimental data. However, these differences appear to scale linearly. The differences in COF magnitude could be due to the modeling simplifications that deviate from the actual physics. For example, the model only considers hysteresis friction forces originating from the microscopic scale. However, hysteresis deformation and hysteresis friction can occur at multiple length scales from the nanometer scale to the millimeter scale. These forces are additive [32, 78, 110] and therefore increasing the number of scales used in the multiscale modeling would likely lead to larger overall predictions of hysteresis forces and hysteresis COF, especially for rough surfaces where the scale effect would be magnified. This improvement is likely to alleviate the disagreement between the model and experiment, particularly for high roughness floorings where currently a larger disagreement was observed between the model and experiment. Another simplifying assumption in the model is the uniform asperity heights. Real surfaces have a distribution of asperity heights, which causes the largest asperities to come into contact at lower contact pressures followed by asperities of lower heights coming into contact at higher contact pressures [97]. Because microscopic hysteresis friction is dependent on asperity height [99], using probabilistic asperity height distributions for shoe and floor topography is likely to alter the frictional shear stress lines (Figure 4-5) by changing the slope of those lines.

A *post-hoc* analysis on the regression model of Figure 4-8 revealed a root mean square difference of 0.13 when comparing the model predictions with the experimental results. In order to further contextualize this difference and its effects on the accuracy of predicting slips and falls, this value was used to calculate the odds ratio using the existing logistic regression model of [40] that predicts the probability of slips given the ACOF as the input (For the testing conditions that were modeled in this study, i.e. 250 N normal loading, 0.3 m/s, and 7° angle).

The logistic regression indicates that an increase of 0.13 will lead to a slipping odds ratio of 0.35 due to this difference. Thus, modeling efforts alone may be insufficient for predicting slips and expected improvements in friction for new designs should be confirmed experimentally. This finding should be considered when one is making predictive conclusions of the probability of slips using just the computational model of this study.

Notably, this study suggests that modeling on multiple scales improves the ability of the model to estimate shoe-floor COF. The current model using simple 2-scale approach was able to capture much of the variability observed experimentally. While further refinements and potentially additional scales may increase the predictive capability, the present model might be sufficient when used along with a scaling factor (e.g. slope of the fit line in Figure 4-8) to predict ACOF. As this model is extended to more shoe and flooring designs, it should become clearer whether more complexity or the scaling factor provides the best predictions.

Future improvements to the model may include more sophisticated material characterization and modeling adhesion forces and fluid pressures. For example, viscoelastic stress-relaxation testing similar to our previous work [99], can be included. The current shoe-floor friction model did not consider the contributions due to adhesion. Thus, these findings may not apply to conditions where adhesion forces are substantial (dry or wet conditions with lower viscosity fluids). Future versions of this model may also include the impacts of the interfacial wear of the shoe outsole [119] to predict COF in several stages of shoe life. Furthermore, the modeling introduced in this paper only examined the shoe-floor friction in one subset of testing conditions relevant to slip-testing. Future versions should examine the effect of different shoe-floor angles on the contact area and COF [103] since it is expected that different shoe-floor angles lead to changes in contact area, COF and therefore slip risk [46, 103].

The long-term goal of these computational models is to reduce slip and fall accidents by improving shoe and floor designs. Findings of the multiscale model presented here suggest that floor roughness, shoe contact area, and shoe tread design influence shoe-floor COF in lubricated conditions. These findings can be applied to optimize shoe and flooring designs to improve their slip-resistance performance and achieve the ultimate goal of reducing slips and falls accidents.

# 5.0 APPLICATIONS OF THE MULISCALE MODEL OF SHOE-FLOOR FRICTION IN SHOE DESIGN AND CONSIDERING HUMAN FACTORS

## 5.1 ABSTRACT

The multiscale computational model of shoe-floor friction developed in chapter 4.0 was applied to understand the impact of specific shoe design features on the predicted COF. Furthermore, a sensitivity analysis was also performed to analyze the impact of gait parameters (i.e. normal load and shoe-floor contact angle) in order to quantify human factor contributions to shoe-floor tribology. Findings indicate an increase in COF for softer shoes, lower normal loads and lower shoe-floor angles; a finding that is consistent with the available literature. Results also demonstrate a difference in frictional response between flat and beveled shoes. COF of flat and beveled shoes demonstrated more sensitivity to shoe-floor angle and normal load, respectively; a finding that should be considered when designing for slip-resistance.

**Keywords:** Coefficient of friction; Finite element modeling; Normal load; Shoe-floor contact angle; Shoe hardness; Flat shoe; Beveled shoe.

## 5.2 INTRODUCTION

Research presented in chapter 4.0 of this dissertation demonstrated the capability of computational modeling in predicting the available friction of shoes on contaminated surfaces. Specifically, a multiscale finite element model of shoe-floor friction was developed that calculates the hysteresis coefficient of friction (COF) based on the microscopic and macroscopic features of the shoe and flooring such as surface roughness, shoe material properties, shoe-floor contact angle, shoe sliding velocity, normal loading, and whole shoe geometry. This chapter builds on this multiscale model by applying the model to shoe design parameters such as material hardness and beveling of the heel of the shoe and considering human factors such as normal loading and shoe-floor contact angle. Furthermore, some human slipping research is presented to support the validity of the model.

Shoe design parameters can influence the available COF between the shoe and flooring. Several studies have investigated the effects of certain design parameters on the slipping risk and the available friction between the shoe and flooring such as shoe tread depth, width, and orientation [12-14], shoe outsole material hardness [15, 120] and beveling (or curving) of the shoe [121]. It is postulated that softer shoes result in less risk of slips and falls [13, 14] and that beveled shoes demonstrate a lower slip risk [121]. However, the mechanism behind the effect of shoe hardness and the differences in slip-resistance among flat and beveled shoes are not thoroughly understood. This chapter fills knowledge gap by applying the multiscale modeling framework of shoe-floor friction to these shoe design parameters.

Furthermore, several studies have focused their attention to the effects of human factors such as shoe-floor angle and normal loading on the slipping risk. Within this context, normal loading is relevant to understanding the effect of a person’s weight on the available COF.

Typically, higher shoe floor angles are reported to result in higher risk of slips and falls [46] and human subjects with a higher body weight are known to be at a higher risk of fall [47-49]. Yet, no study has used computational modeling to systematically examine the effect of kinetics (force and angle) on the COF at the shoe-floor-contaminant complex. Multiscale model of shoe-floor-contaminant friction may represent an opportunity to isolate the impacts of these parameters on hysteresis friction from other human factors. Thus, this chapter utilizes the computational modeling model of shoe-floor friction to evaluate the above-mentioned effects.

The purpose of this chapter is to apply the multiscale model of shoe-floor friction (Chapter 5.0 ) to examine the impact of shoe design features (i.e. shoe material hardness and beveling of the heel) on COF and to conduct a sensitivity analysis on the frictional response of shoes to shoe-floor angle and normal load. The alternative approach for analyzing the data from the multiscale model, introduced in section 4.3.1.4 is used for this purpose.

## 5.3 METHODS AND RESULTS

Presentation of the three different analyses is organized as follows: 1. Subsection 5.3.1 investigates the impact of shoe hardness on COF. 2. Subsection 5.3.2 conducts a sensitivity analysis on the effects of shoe-floor angle and normal load on COF. 3. Subsection 5.3.3 expands on the findings of subsection 5.3.2 and further investigates the differences in COF response of flat and beveled shoes to normal load. Details of the modeling methods used in this section are similar to the methods from chapter 4.0 unless mentioned otherwise.

### 5.3.1 Effect of shoe hardness using the multiscale model of shoe-floor friction

#### 5.3.1.1 Methods

The multiscale model of shoe-floor friction (Section 4.3.1.4) was applied to model the friction between three different shoes against a vinyl flooring [101]. The three shoes had the same geometry (Figure 5-1). These were the shoes S6-8 in chapter 4.0 except that their texture was removed for this analysis. The shoes had similar roughness and the major difference between them was their hardness (Table 5-1). This way, hardness of the outsole was the only factor that could affect the frictional response of the shoes. Hardness of the shoes was collected using the methods introduced by Giacomin and Mix [108] and examined in section 4.3.2. and was converted to viscoelastic material constants that were used to describe the viscoelastic behavior of the three shoe materials using a three-parameter viscoelastic model [100] for material properties (Equation 5-1. & Table 5-1).

**Figure 5-1.** The macroscopic shoe geometry (meshed in finite element software) recreated from the 3D scans of the actual shoe.

**Table 5-1.** Roughness and material properties used for the shoes.

| Shoe Hardness | Shore A | $R_z$ (μm) | $\Delta_q$ (°) | $G_0$ (MPa) | $G_\infty$ (MPa) | $\gamma$ ($s^{-1}$) | E (MPa) |
|---|---|---|---|---|---|---|---|
| **High** | 85 | 26.6 | 33.6 | 4.39 | 1.84 | 0.022 | 13.18 |
| **Medium** | 76 | 25.2 | 32.5 | 2.48 | 0.99 | 0.017 | 7.44 |
| **Low** | 64 | 24.6 | 33.3 | 1.41 | 0.92 | 0.2 | 4.24 |

$$G(t) = G_\infty + (G_0 - G_\infty)e^{-\gamma t}$$ Equation 5-1.

In order to evaluate slip risk predictions of the modeled shoe outsoles, unexpected slipping experiments were performed. Gait and slip pattern of human subjects were examined when wearing the three modeled shoes to evaluate the slipperiness of the shoe-floor-contaminant combination [37, 40]. A subset of previously published data [37, 40] from 31 subjects that were recruited for the unexpected slipping experiments was used to perform a human validation of the available COF predictions. Healthy individuals between age of 18 and 65 (i.e. those who did not have any neurological or musculoskeletal problems at the time of the experiments that might affect their gait pattern) were asked to participate in human slipping studies.

Gait analysis was performed at a biomechanics motion capture laboratory on a level vinyl flooring surface under dry and contaminated conditions. Glycerol and water solution (50% water and 50% glycerol by volume) was used as the contaminant in the experiment. It has been demonstrated that high-viscosity fluids are able of creating a lubrication film that minimizes adhesion friction so that the friction will be mainly from hysteresis [19, 53, 111]. Subjects were asked to wear one of the three pairs of the modeled boots and reflective markers to track their full body motion were placed on the anatomical landmarks of their body and their shoes. During the experiments, the subjects were fitted with a harness for safety. After 5-7 baseline dry trials, the contaminant was applied to the floor without subject's prior knowledge and an unexpected

slip trial was recorded. Subjects were asked to listen to music between trials to keep them distracted and the lights at the biomechanical testing room were dimmed during testing sessions to minimize anticipation of a slip [22, 37].

#### 5.3.1.2 Data analysis

The COF that was predicted by the model and the COF measured by the robotic slip tester used in chapter 4.0 (Figure 2-3) were compared as the key outcome variables. COF for both the microscopic and macroscopic scale was defined as the ratio of shear force to normal force. Contact area, average and maximum under-shoe contact pressure were also compared across the shoe models.

The marker placed at the inferior-most point of the heel was tracked and used for identifying slip occurrences. Since it was likely that this marker would interfere with subjects' gait pattern or fall off during the trials, it was only put on during the static trial and its location relative to other heel markers were calculated. The occurrence of a slip was identified based on slip distance. The slip distance was calculated from the first local minimum in heel anterior velocity after heel contact to the second local minimum or when the subject's foot slipped off the force plate [37, 46, 122] and a trial was considered as a slip if this slipping distance was greater than 3 cm [37, 123, 124]. Percentage of human subjects that slipped were compared across the three shoes.

#### 5.3.1.3 Results

An exponential decay fit (Equation 4-8.) described the relationship between predicted microscopic COF and contact pressure ($R^2$=0.99) for all three materials (Figure 5-2). The micro-

model revealed that the hardest material experienced the greatest level of hysteresis COF and the medium and low hardness material had similar but less hysteresis COF.

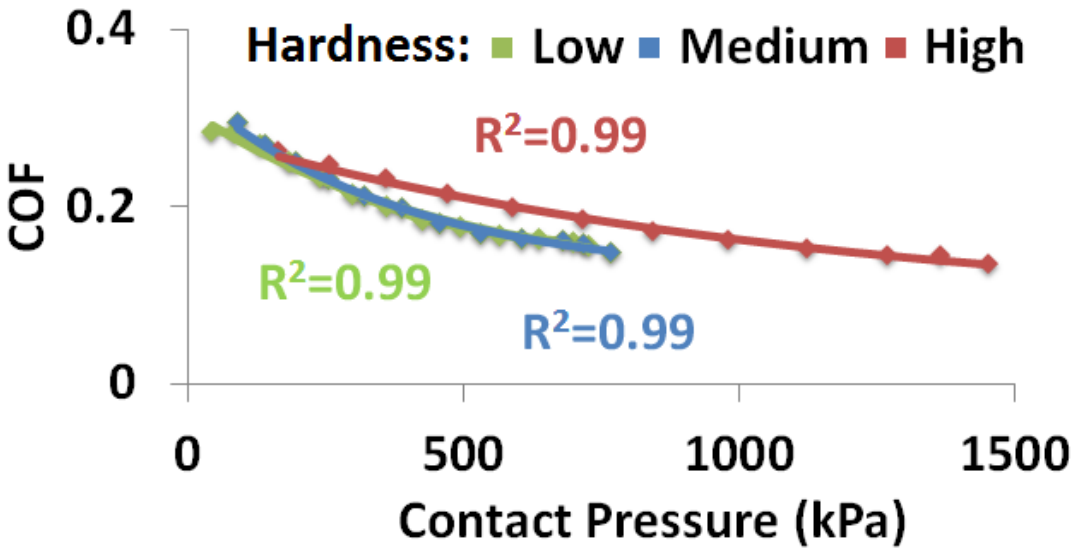


**Figure 5-2.** Curve fitting for the three modeled shoes.

The macro-model revealed that contact pressures were typically on the posterior portion of the shoe (Figure 5-3). Increasing shoe hardness was found to increase the average and peak pressures and reduce contact area (Figure 5-4). Increased contact pressures of the hard shoe led to an overall reduction of hysteresis COF (Figure 5-5) compared to the medium and low hardness shoe. Also, the medium hardness shoe demonstrated a lower COF in comparison to the low hardness shoe because of the reduced contact area and increased contact pressure (Figure 5-4). The model did slightly overestimate hysteresis COF since it predicted COF values around 0.2 whereas experiments found COF values between 0.15 and 0.2 [37].

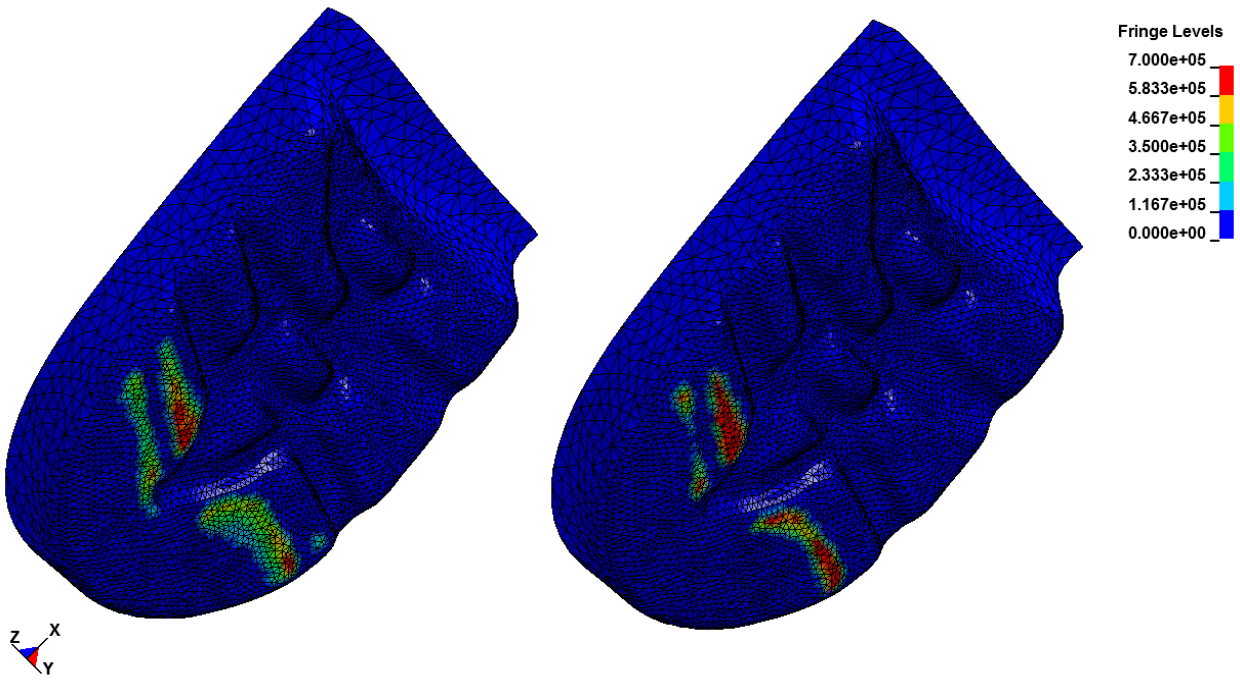


**Figure 5-3.** Contours of under-shoe contact pressure for the shoe with low (Left) and high (Right) hardness.

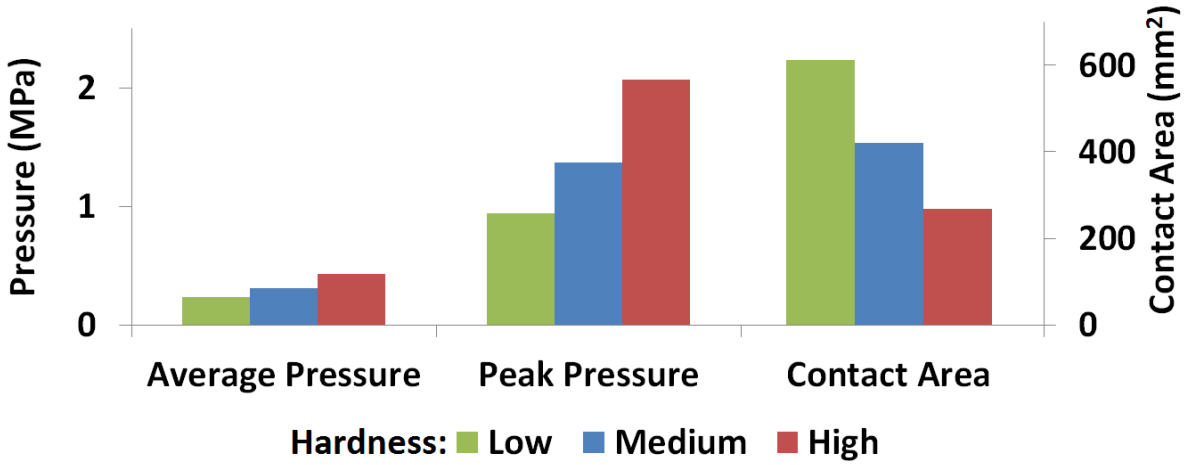


**Figure 5-4.** Contact pressure and contact area across the three modeled shoes.

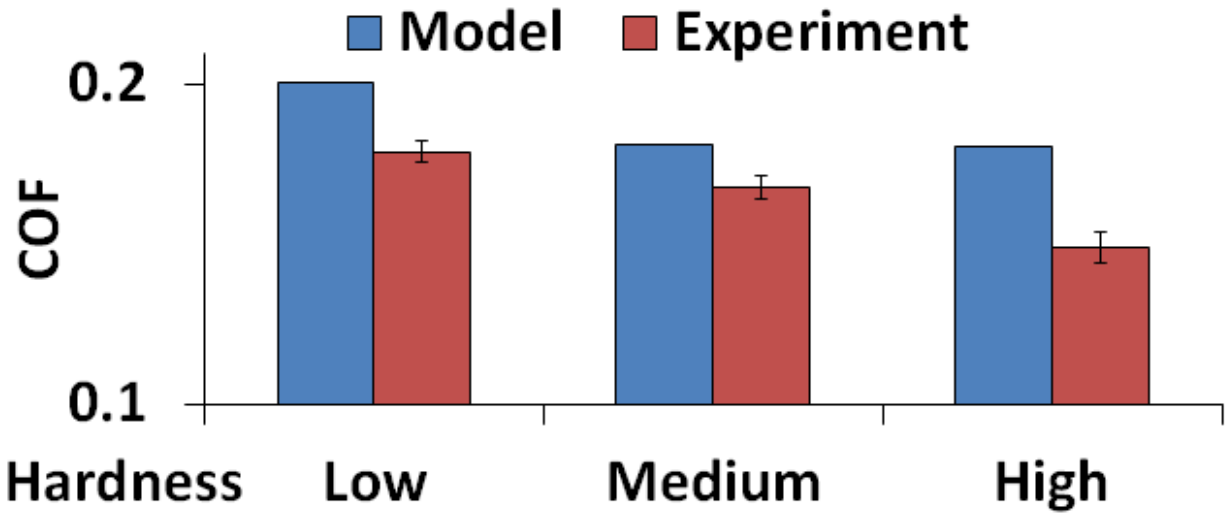


**Figure 5-5.** COF obtained from the models versus experiments.

The results of the unexpected slipping experiment demonstrated that the percentage of human subjects that slipped wearing the softer (Low hardness) shoe was less than those of wearing the medium hardness and harder (High hardness) shoes (Figure 5-6). Also, the percentage of human subjects that slipped wearing the medium hardness shoe was slightly less than the percentage of human subjects that slipped wearing the high hardness shoe.

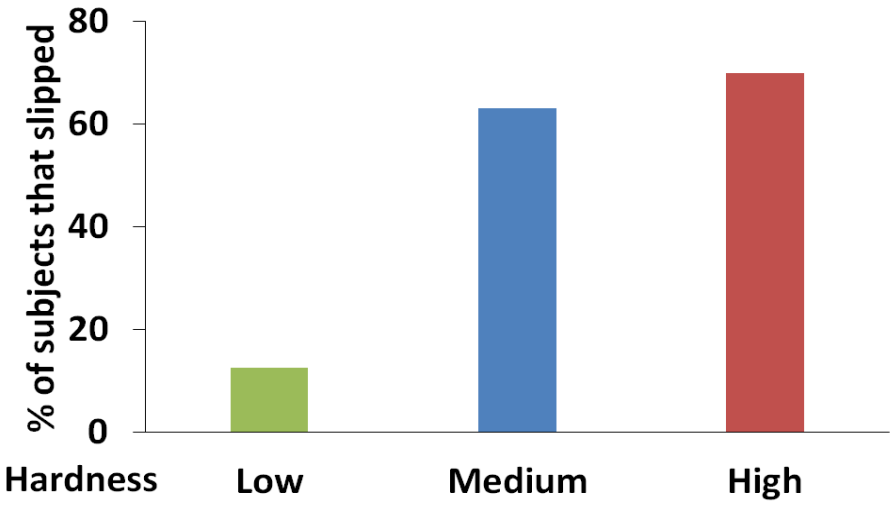


**Figure 5-6.** Percentage of human subjects that slipped in experiments across the shoes.

### 5.3.2 Sensitivity of two footwear designs to normal force and shoe-floor contact angle

#### 5.3.2.1 Methods

The multiscale modeling approach introduced in section 4.3.1.4 was applied to model the frictional response of two shoes (Figure 5-7. S2-3 in chapter 4.0 ) against a vinyl flooring [103]. The two shoes had roughly similar material properties (Table 4-2). One of the shoes had a flat heel and the other shoe had a beveled (curved in the rear) heel style. Multiple simulations across several levels of normal loading (greater than 0 N and smaller than 1100 N) and shoe-floor contact angles (greater than 0 degrees and smaller than 20 degrees) were conducted. These forces and angles are reported to be relevant to slipping accidents (i.e. biofidelic testing conditions) [41]. Predicted COF was the key outcome variable of this analysis.

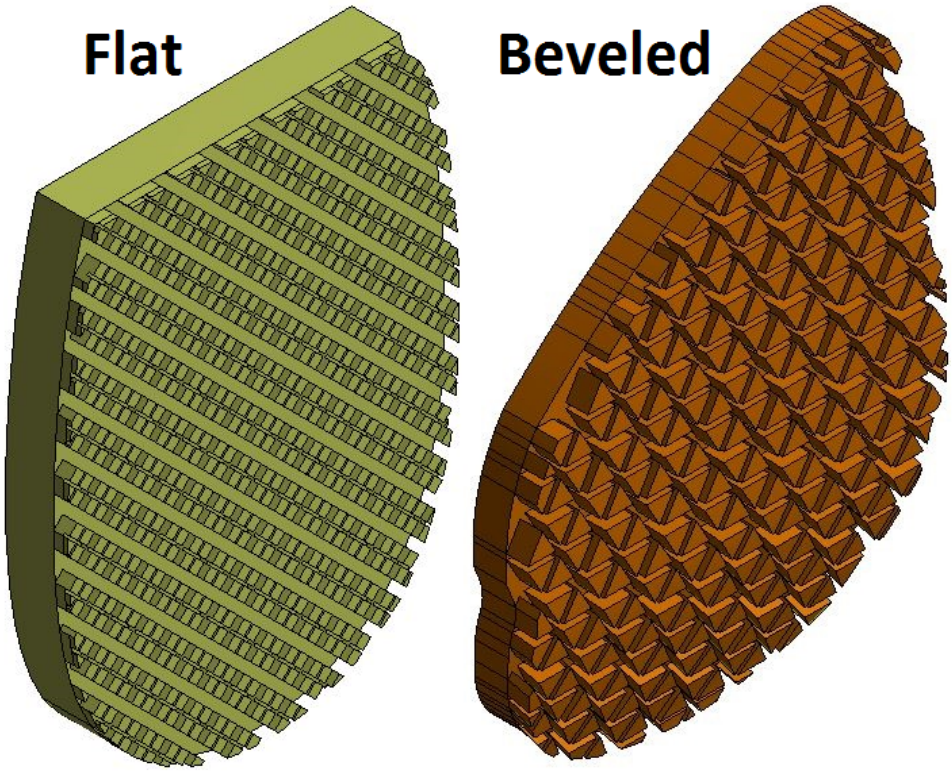


**Figure 5-7.** The two modeled shoes.

#### 5.3.2.2 Results

Overall, COF had higher values in lower normal forces and lower shoe-floor angles for both shoes (Figure 5-8). The COF was more sensitive to an increase in shoe-floor angle than an increase in normal load for the flat shoe (1-30% and 13-34% decrease in COF in response to increase in normal load and shoe-floor angle, respectively). The COF was more sensitive to an increase in normal load than an increase in shoe-floor angle for the beveled shoe (7-39% and 5-18% decrease in COF in response to increase in normal load and shoe-floor angle, respectively). The beveled shoe demonstrated a local minimum followed by a slight increase in COF at higher shoe-floor angles (14-18 degrees). The flat shoe did not experience this type of local minimum (Figure 5-8).

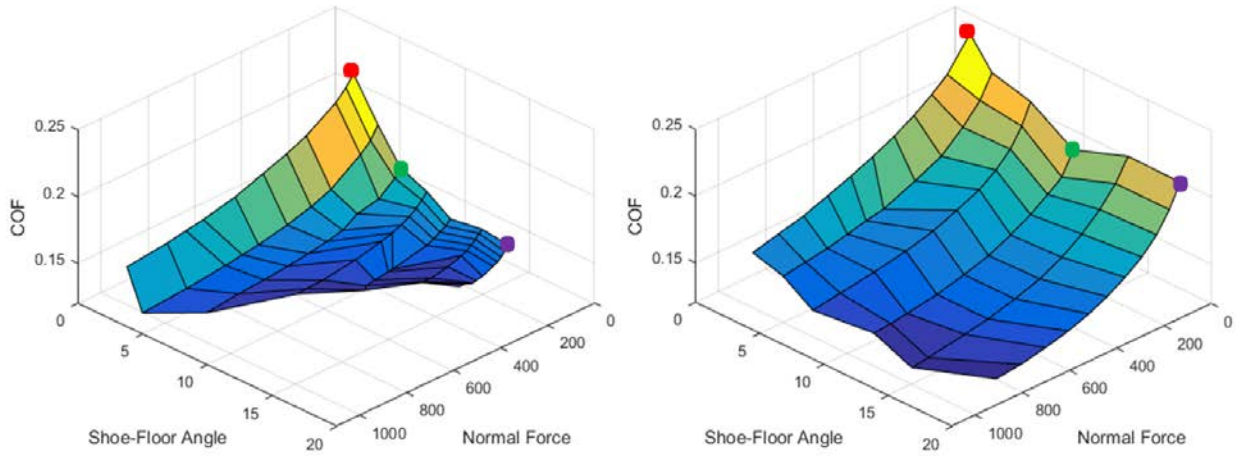


**Figure 5-8.** COF response plot for the flat (Left) and beveled (Right) shoe.

### 5.3.3 Frictional response of multiple slip-resistant beveled and flat shoes to normal loading

This subsection further expands on the findings of subsection 5.3.2 with more slip-resistant designs by focusing solely on the effect of normal load on COF.

#### 5.3.3.1 Methods

The multiscale modeling framework (Section 4.3.1.4) was applied to simulate the friction between four existing shoe designs (S1-4 in chapter 4.0 ) against a vinyl flooring. Four shoes (Figure 5-9) were considered including two flat heel shoes (F1 & F2) and two shoes with beveled heels (B1 & B2). Shore A hardness of the shoes was measured using a durometer (Table 5-2) and was used in models for quantifying material properties of the shoes.

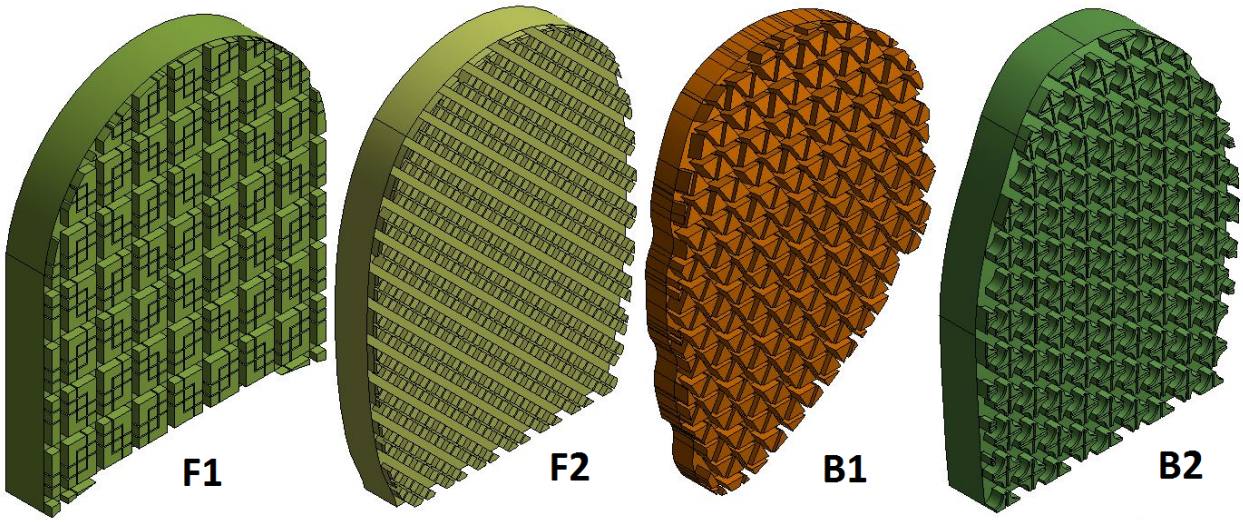


**Figure 5-9.** Geometries of the modeled shoes.

**Table 5-2.** Shore A hardness of the four shoes.

| Shoe | F1 | F2 | B1 | B2 |
|---|---|---|---|---|
| **Shore A Hardness** | 50 | 56 | 56 | 72 |

Simulations for each macroscopic shoe model were conducted over 10-11 normal load levels to generate a relationship between the normal loading and COF as well as contact area ($A_{Model}$). Contact area was chosen because higher contact areas between shoe and floorings are hypothesized to lead to a more distributed under-shoe contact pressure [125, 126] and correlate with a better slip-resistance performance [112, 125, 126].

An exponential decay function (Equation 5-2.) and a power function (Equation 5-3.) were used to describe the variation in macroscopic COF and $A_{Model}$ with respect to the change in normal loading, respectively. In these equations, $\lambda$ and $b$ are coefficients that are determined using curve fitting techniques; $COF_H$ and $COF_L$ represent COF in high and low normal loads, respectively.

$$COF = COF_H + (COF_L - COF_H)e^{-\lambda F_{Normal}} \quad \text{Equation 5-2.}$$

$$A_{Model} = aF_{Normal}{}^{b} \quad \text{Equation 5-3.}$$

#### 5.3.3.2 Results

The computational models indicated that an increase in normal loading led to a decrease in COF (Figure 5-10) and an increase in $A_{Model}$ (Figure 5-11). The exponential decay function (Equation 5-2.) and the power function (Equation 5-3.) successfully described the variation in COF and $A_{Model}$ with respect to the change in normal loading for all the four shoes ($R^2$>0.99).

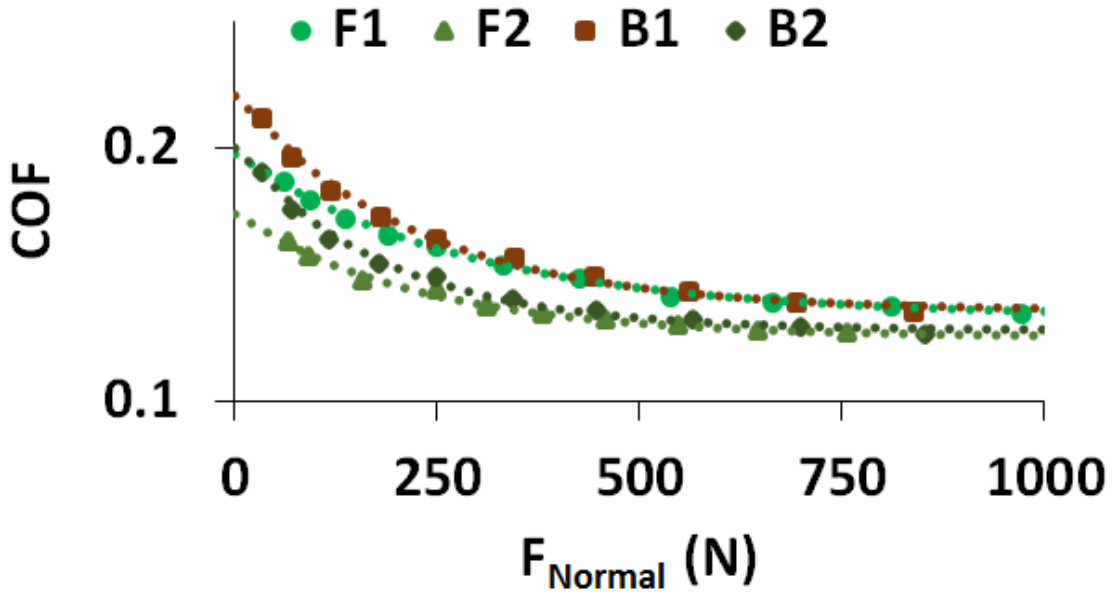


**Figure 5-10.** COF versus normal loading.

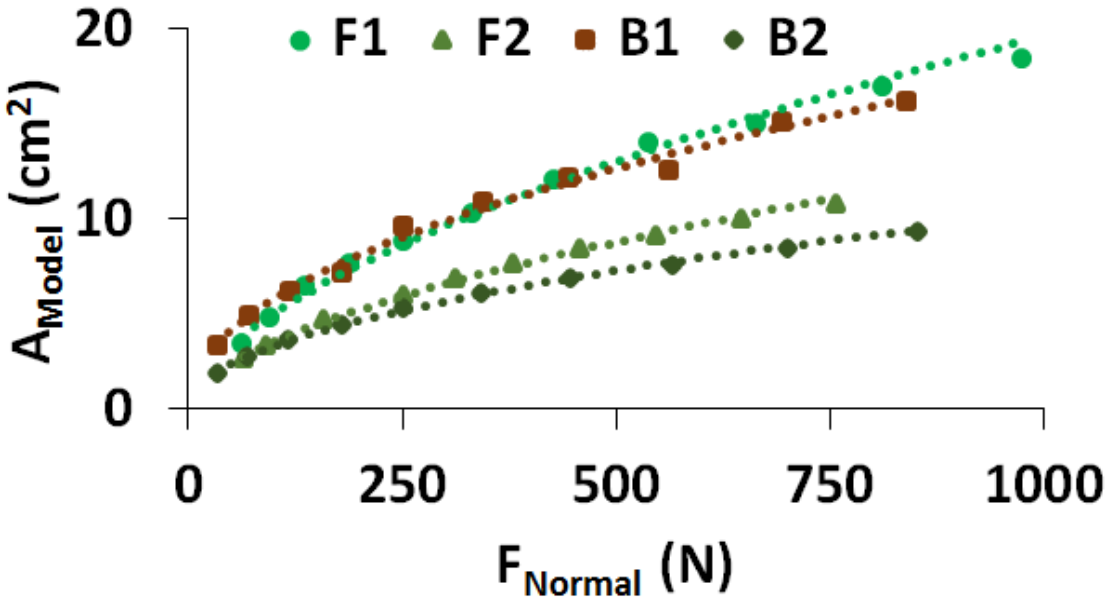


**Figure 5-11.** $A_{Model}$ versus normal loading.

An analysis of the exponential decay coefficients in Equation 5-2. (Table 5-3), revealed that the COF response (Figure 5-10) of flat shoes was less sensitive to normal loading than the

beveled shoes (smaller $\lambda$ in Table 5-3). The contact area, $A_{Model}$, (Figure 5-11) for flat shoes more closely simulated a linear curve compared to the beveled shoes (larger $b$ in Table 5-3). These findings demonstrate a difference in response to normal loading between flat and beveled shoes.

**Table 5-3.** Exponential and power coefficients for different shoes.

| **Shoe** | **F1** | **F2** | **B1** | **B2** |
|---|---|---|---|---|
| $\boldsymbol{\lambda}$ | 0.0035 | 0.0044 | 0.0045 | 0.0054 |
| $\boldsymbol{b}$ | 0.59 | 0.56 | 0.48 | 0.49 |

## 5.4 DISCUSSION

The computational models presented in this chapter demonstrates the feasibility of utilizing the computational model of shoe-floor friction in explaining the impacts of shoe design parameters such as shoe hardness and geometrical curvature of the back of the heel of the shoe and also the effects of kinetic and kinematic parameters of gait such as normal loading and shoe-floor contact angle on shoe-floor COF. Overall, findings of this chapter support the use of the multiscale model as a shoe design tool that can predict slipping risk.

The computational model of subsection 5.3.1 suggests that the mechanism behind increased COF for soft shoe material is increased contact area and reduced contact pressures. This finding is consistent with the measurements of shoe-floor COF and with the slipping risk of unexpected human slips [37]. The decrease in COF with increasing hardness could partially explain the higher percentage of slips in human subjects wearing the harder shoes and it is in agreement with studies that report a lower rate of slips and falls in shoes with lower hardness [15, 120]. It should be noted these differences in COF of the shoes are within the range that

could affect the probability of slips and falls given their proximity to the values of RCOF for level walking in the literature [7, 38]. Thus, this finding indicates the possibility of modeling shoe-floor-contaminant friction in a way that predicts slip risk.

The computational model of subsection 5.3.2 revealed a decrease in COF in response to increase in either the normal load or the shoe-floor contact angle. These findings are consistent with the available literature on the effect of gait kinetics on slipping and could partially explain the higher risk of slips and falls in overweight populations [48, 49] and human subjects with higher shoe-floor angles [46]. It should be noted that overweight human subjects are reported to have a higher RCOF in comparison to the non-obese subjects [127-129]. Therefore, combination of the reduction in COF (observed in the models) and the higher RCOF in overweight people is likely to explain the higher chance of slips and falls in this population given that the difference between ACOF and RCOF predicts the probability of slips and falls [6, 7]. Furthermore, according to the computational model, the beveled shoe demonstrated an increase in COF for higher shoe-floor angles (14-18 degrees) compared to the flat shoe. This effect was due to the higher contact area in the heel of the beveled shoe (Figure 5-12) which leads to a more distributed contact pressure and increases COF [125, 126]. This finding could indicate that a beveled shoe may reduce heel slips, since these angles are relevant to the shoe-floor angles observed in actual human slipping experiments at the event of slip-start [130]. Moreover, a beveled heel led to a more consistent contact area across shoe-floor angles leading to more predictable friction even as a person alters their gait. Thus, this modeling research supports the use of a beveled heel in slip-resistant shoes. However, it should also be noted that changes in shoe-floor angle and normal loading during slipping events [44] are interdependent and not

completely separable from each other. This might limit the applicability of the findings of this model to those effects.

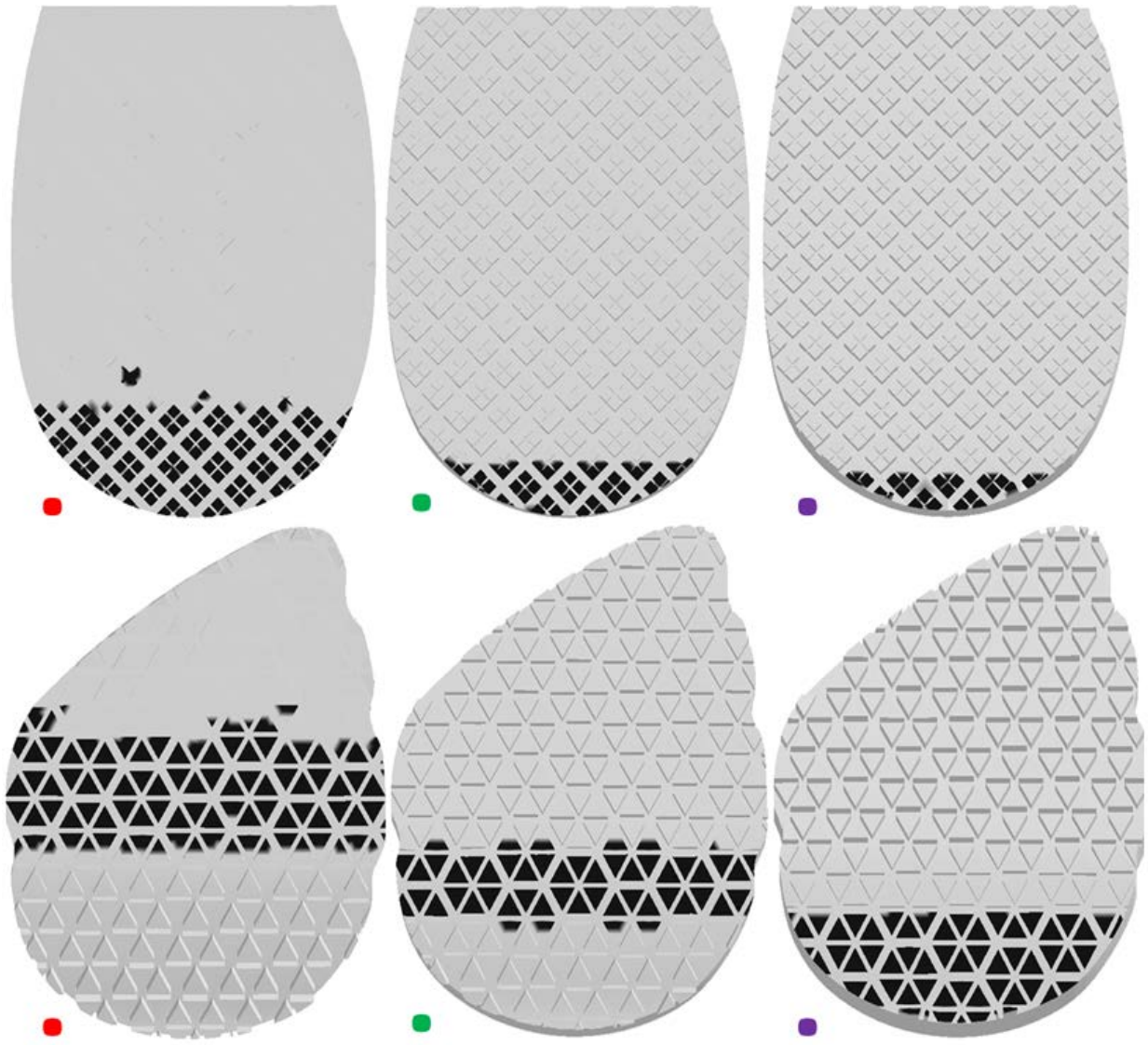

**Figure 5-12.** Contact areas of the flat (Top) and beveled (Bottom) shoe in different shoe-floor angles. Colored dots for each shoe correspond to the colored dots on Figure 5-8.

Findings of the computational models of subsection 5.3.3 can be applied to simulate the effect of a person's weight on slip-resistance performance. These findings suggest that while

certain (beveled) shoes might have superior slip-resistance in lower normal loads, their performance might decay when a heavier person wears those and suggest that slip-resistance performance of flat shoes is less sensitive to a person's weight. Although it should be acknowledged that the range of the normal load that was used for this analysis might not fully represent the body weight of obese people, findings of this section (Similar to subsection 5.3.2) indicate a decrease in COF with increasing normal load, a phenomenon that could be partially responsible for the higher risk of falls in the overweight population [48]. The outcomes of this modeling effort should also be considered when designing slip-resistance experiments for shoes [41], especially for beveled shoes since those shoes demonstrated greater sensitivity to changes in normal loading.

Overall, this chapter provides valuable insights on the effects of shoe design and biomechanical parameters on the frictional response of shoe outsoles and demonstrates applicability of the multiscale model of shoe-floor friction for explaining the differences in slip-resistance behavior of shoes. Future efforts should focus on validating findings of this chapter by conducting COF testing experiments similar to the ones performed in chapter 4.0 .

# 6.0 COMPUTATIONAL MODEL OF SHOE WEAR PROGRESSION

## 6.1 ABSTRACT

Worn shoes increase slip and fall risk. Few research efforts have attempted to predict shoe wear progression. A computational modeling framework is presented that simulates wear progression in footwear outsoles based on finite element analysis and Archard's law. The computational model results were qualitatively and quantitatively compared with results from a shoe wear protocol. Key variables of interest were the size and the shape of the worn region, and the order in which individual tread blocks were worn. Strong correlations existed between the models and experiments for the order of the shoe tread wear ($r_s > 0.74$) and the size of the untreaded area ($R^2 > 0.71$). Findings demonstrate the capability of the computational modeling methodology to provide realistic predictions of shoe wear progression. This model represents a promising first step to developing a model that can guide footwear replacement programs and footwear design with durable slip-resistance.

**Keywords:** Wear; Shoe; Computational modeling; Finite element

## 6.2 INTRODUCTION

Slips and falls continue to be amongst the leading causes of occupational injuries and a serious public health issue. In 2013, the overall annual financial burden of falls to the United States was $180 billion [3] and in 2017, workers' compensation costs due to slips and falls were approximately $18.5 billion [35]. Roughly half of occupational falling accidents are caused by a slipping event [5]. Low available friction between the shoe and flooring increases the risk of slips and subsequent falls [6, 7]. Shoe tread design characteristics such as tread depth, tread width, the size of the region without tread, and the available contact area between shoe and flooring influence the available friction at the shoe-floor interface and therefore affect the risk of slips and falls [13, 14, 41, 131]. These properties change across a shoe's lifetime as tread becomes worn. Specifically, severely worn shoes have been reported to decrease the available friction [23, 26], increase under-shoe fluid pressures [22, 26], and increase the slipping risk in occupational and laboratory settings [22, 27].

Research efforts on elastomer wear have identified that the interfacial contact pressure is an important parameter that influences wear rate [28]. Specifically, the wear equation developed by Archard [28] has been utilized to describe wear of elastomers in applications such as seals and tires [30, 66, 67]. Since Archard's law predicts wear primarily based on contact pressure, wear of the shoe outsoles is likely dependent on shoe tread design and the loading conditions [23].

Previous research has applied computational models with Archard's law to simulate rubber wear in order to predict the life of tires and seals. Typically, these models employ the finite element method to predict the interfacial contact pressure distribution. The geometry is then modified using Archard's law [28] based on the contact pressure distribution to simulate wear. The modeling of contact pressures and updating of the geometry is performed using

iterative methods [29, 30, 66, 67]. To the best knowledge of the authors, these modeling schemes have not been applied to the shoe interface.

Previous research efforts mainly focused on assessing shoe wear and its effects on slips and falls. Slip-resistance performance throughout the life of the shoe has been evaluated using slip-resistance measurement methods at a limited number of time points [23, 26] or without explicitly commenting on the exact degree of wear [27]. Developing a validated computational model of shoe wear progression can be beneficial because it will help characterize the relationship between shoe design properties and its progressive wear. This modeling could then allow for further efforts in order to optimize those properties and guide design improvements that achieve superior slip-resistance similar to wear modeling studies in seals and tires [29, 30, 66]. Furthermore, this method is likely to predict the regions of the shoe in which wear is initiated thus allowing for shoe replacement guidance.

The purpose of this study is to develop a computational model of shoe wear progression using Archard's law and finite element analysis. The validity of the model was assessed by comparing predictions to an experimental shoe wear protocol. Furthermore, this study implicitly examined whether Archard's law is applicable to wear at the shoe contact interface.

## 6.3 METHODS

### 6.3.1 Computational wear model

Modeling of the contact interface was performed in explicit finite element package LS-Dyna® (LSTC, Livermore, California, USA). Efficiency of this software in modeling shoe-floor

contact has been previously demonstrated [126]. The finite element modeling method simulated the contact pressure distribution at the shoe contact interface (Figure 6-1). The output of the finite element model was the nodal contact pressures at the interface. This pressure was used to calculate the nodal wear depths in each iteration by assuming that the wear depth for each node in each wear iteration was proportional to the interfacial contact pressure based on Archard's law [28] (Equation 6-1.). Therefore, the wear process is simulated by moving the respective nodes [29] in a direction perpendicular to the contact interface based on the amount of calculated wear. Specifically, the wear depth at the *i-th* node ($\Delta h_i$), was a function of the wear constant ($k$), the contact pressure at the i-th node ($p_i$), and the sliding distance on the counter-surface ($s$), (Equation 6-1.).

$$\Delta h_i = k p_i s \qquad \text{Equation 6-1.}$$

This study was focused on developing models that predict the locations of the wear as opposed to the overall wear rate. Therefore, $k*s$ in Equation 6-1. was set to a constant value in each wear iteration. Specifically, $k*s$ was set so that the maximum nodal wear depth ($\Delta h_i^{max}$) in each iteration was 0.2 mm. This is equivalent to varying the amount of sliding distance in each wear iteration to achieve a 0.2 mm of wear depth. Preliminary modeling efforts determined that limiting the maximum nodal wear was needed to achieve stability and convergence in wear progression simulations. A custom script (MATLAB®, Mathworks, Natick, Massachusetts, USA) was developed that calculated wear depths across the contact nodes based upon nodal pressures at each iteration, and moved the contact nodes in the finite element software. The amount of wear during the simulation and subsequent deformations that occurred necessitated the use of global remeshing techniques to discretize the shoe geometry throughout the wear

modeling cycles [29]. The global geometry remeshing was performed in meshing software (ANSYS®, ANSYS Inc., Canonsburg, Pennsylvania, USA) when performing the next wear iteration resulted in an error due to a severely deformed finite element mesh.

The computational wear models included heel geometries of five shoes that were also examined experimentally (Section 6.3.2). Computer Aided Design models of the shoes were created in ANSYS DesignModeler® (ANSYS Inc., Canonsburg, Pennsylvania, USA), based on the measurements taken from the shoe outsoles. For shoes with a textured tread, texturing was not included in the CAD models as our preliminary experimental results (Section 6.3.2) revealed that texturing was worn off quickly. Linear elastic material properties in the finite element models for the shoes were obtained using hardness readings of the shoes (Section 6.3.2) based on methods described by Giacomin and Mix [108]. Shoe tread was modeled as a nearly incompressible material with a Poisson's ration of 0.499 [132, 133].

Finite element models were used to simulate contact between the shoe and a smooth, rigid counter-surface. Key parameters were consistent with the experimental wear protocol, including: shoe angles of 2, 7, and 17 degrees, a sliding velocity of 2.4 m/s, a normal force of 40 N, and a lateral tilt angle that was consistent with the experimental wear protocol (Section 6.3.2). Normal force in finite elements models was controlled using the vertical displacement boundary conditions that were applied to nodes at the top surface of the shoe models [126]. The shoe was pressed against the counter-surface until the desired normal force was achieved and then the horizontal sliding velocity boundary condition was applied. Other displacements and rotations of the nodes at the top surface of the shoes were constrained. Shoe models were meshed using tetrahedral elements recommended for simulating rubber-like materials with complex geometries [82]. Mesh size for the shoes were determined based on the following criteria: 1. It provided a

10% accuracy in predictions of the normal loading in the base line iteration of the shoe. 2. All of the shoe elements had element qualities [134] greater than 0.1 in the base line iteration. 3. Mesh refinement was applied only to the elements in the contact region of the shoe to reduce the computational cost without losing accuracy in those regions. 4. The same mesh setting was used for the next iterations of the shoe and when remeshing was needed.

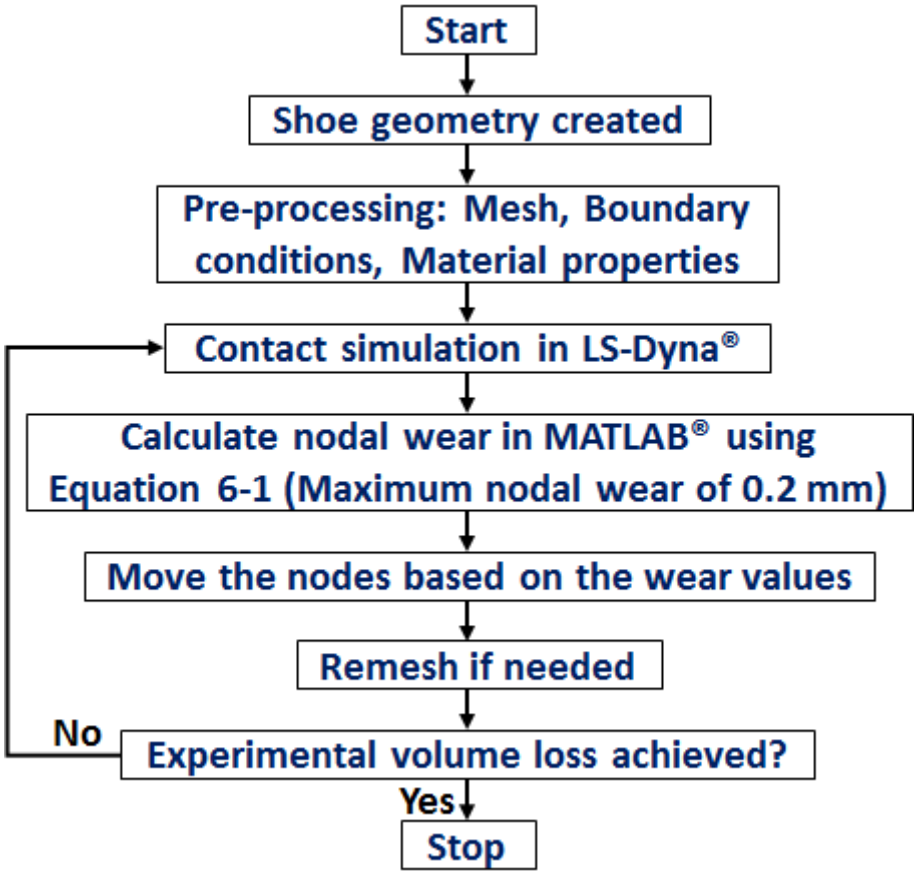


**Figure 6-1.** Flowchart of the iterative scheme for modeling wear.

### 6.3.2 Experimental shoe wear protocol

Five shoes were worn using a custom-developed accelerated wear apparatus. This apparatus utilized a sliding abrasion belt to wear shoes in angles that approximated the shoe

angles of the gait cycle [131]. For each wear trial, the shoe was worn for 20 seconds at three different shoe angles of 2, 7, and 17 degrees at a sliding speed of 2.4 m/s and a normal load of 40 N consistent with the modeling conditions [131] (Section 6.3.1). The wear angles mimic the variation in shoe-floor angles in gait cycle [44, 123] and the abrasion techniques were similar to previous methods for abrasively removing shoe tread and also abrasion resistance measures for footwear [131, 135].

After each wear trial, volume loss of the shoes was measured and imprints of the shoe treads on silicone rubber mold [131] were generated. The cavities in these molds were then filled with water and the mass of the water was weighed to deduce the volume of the water in the tread cavities and subsequently the volume loss between the trials. Material properties were also collected as an input to the finite element models. Shore A hardness of the shoes [107] were characterized using a durometer (Intercomp®, Minneapolis, Minnesota, USA) and were used to calculate linear elastic Young's moduli of the shoe materials [108, 126] for computational models (Section 6.3.1). Durometer readings were conducted on nine various portions of the heel for each shoe and the average was used. Table 6-1 summarizes the elastic moduli values that were derived from the hardness readings.

**Table 6-1.** Elastic modulus of the shoes.

| **Shoe** | **S1** | **S2** | **S3** | **S4** | **S5** |
|---|---|---|---|---|---|
| **Elastic Modulus (MPa)** | 7.5 | 9.36 | 9.27 | 8.2 | 11.01 |

### 6.3.3 Data and statistical analyses

A statistical analysis was performed to evaluate the prediction quality of the model to identify the location of wear. For this statistical analysis, each tread on the actual shoe and model

geometry was coded. Tread blocks on the actual and model geometry of each shoe were ranked based on the order that they became completely worn (Figure 6-2). Agreement between the model and experiments in predicting regional geometrical wear was then assessed using Spearman's rank based regression method that quantified how successful the modeling scheme was in predicting the order of tread wear (Figure 6-3). The rectangular untreaded area in each wear iteration was calculated by finding the largest untreaded length in the anteroposterior (major axis) and mediolateral (minor axis) of the shoes and multiplying the two values [131]. For comparing the model results to the experimental trials, volume loss due to wear in the treaded regions of the shoe was used to pair a specific experimental iteration to a modeling iteration. A second statistical model was then created that compared the rectangular untreaded area in experiments and models after each wear iteration to quantify the accuracy of the model in predicting those areas since this untreaded area has been demonstrated to be a predictor of the change in shoe-floor coefficient of friction due to wear [131].

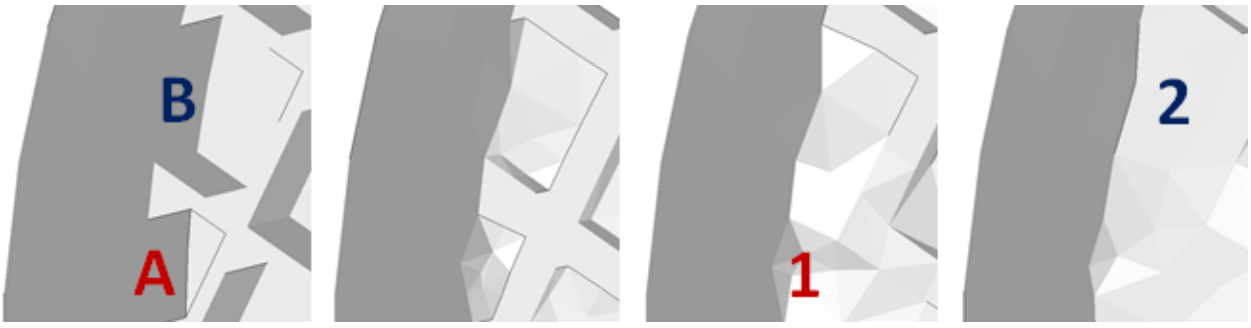


**Figure 6-2.** Coding method that was used to rank the order that tread blocks became completely worn (Left); Letters represent the tread block and numbers represent the wear order. Wear progression of the two tread blocks is displayed in four frames (Left to right); tread A wore down first (1); tread B wore down afterwards (2). This technique was applied to all the treads that wore in the models. The same letters for each shoe were then used in labeling the experimental results.

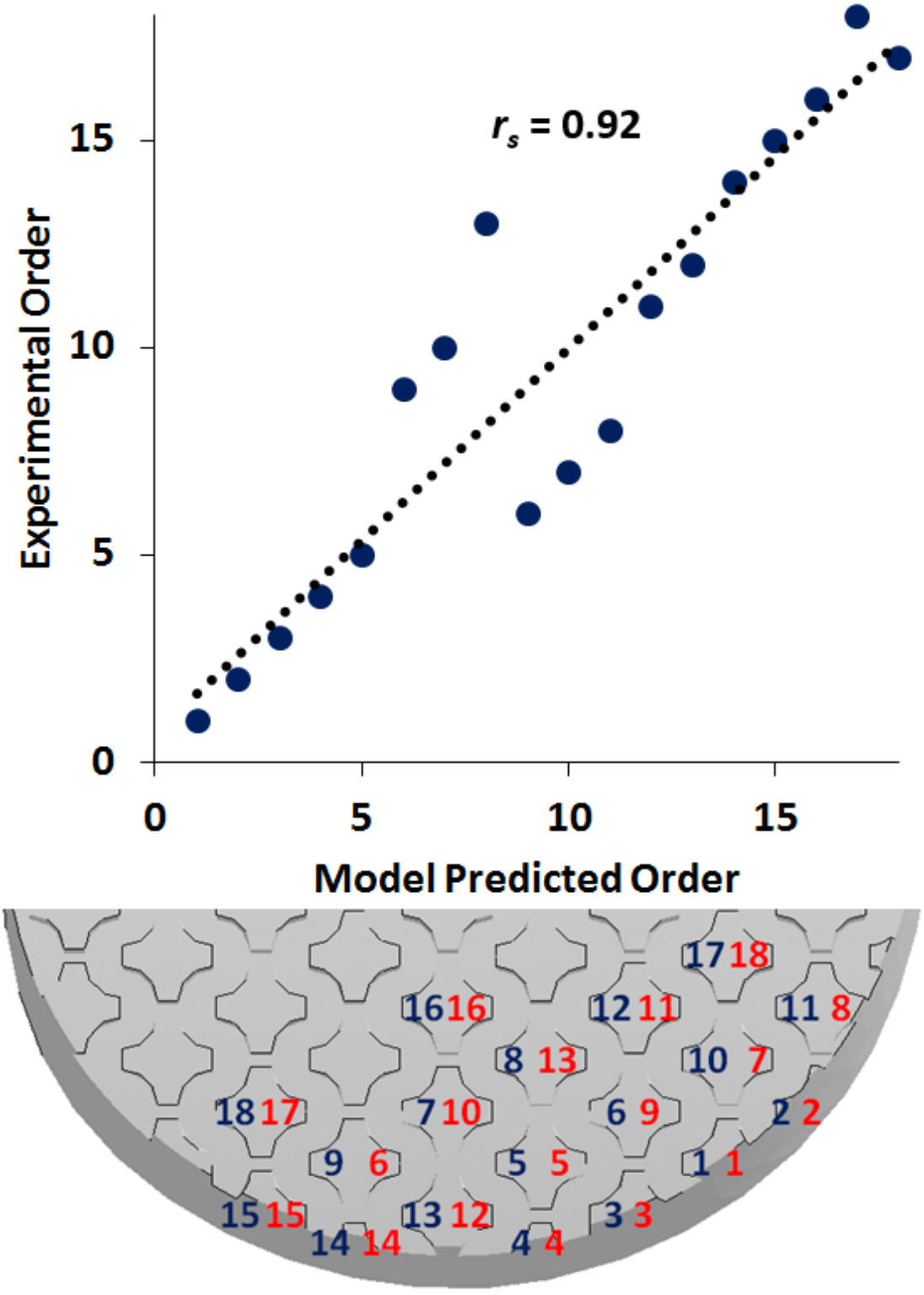


**Figure 6-3.** Bottom: Representative plot demonstrating the order that shoe (S4) tread wore down in the model (Blue) and the experiment (Red). Top: The resulting correlation for this shoe.

## 6.4 RESULTS

Shoes experienced extensive wear in both the experiments and the models (Figure 6-4). Similar regions wore in the models and experiments. For S1, a majority of the wear occurred in the posterior section of the shoe in both the model and the experiment. For S2, a majority of the wear occurred in the lateral and posterior region of the shoe in the model and in the lateral and medial portion of the shoe in the experiment. For S3, wear in the posterior region of the outsole was observed in both the model and the experiment. For S4, wear was dominant in the posterior and medial portions of the shoe in both the model and the experiment. For S5, the model experienced wear mainly in the posterior region of the shoe and the experimental wear trials resulted in wear of the shoe in the medial region. The progression of wear is demonstrated in a video of the shoe models (Figure 6-5).

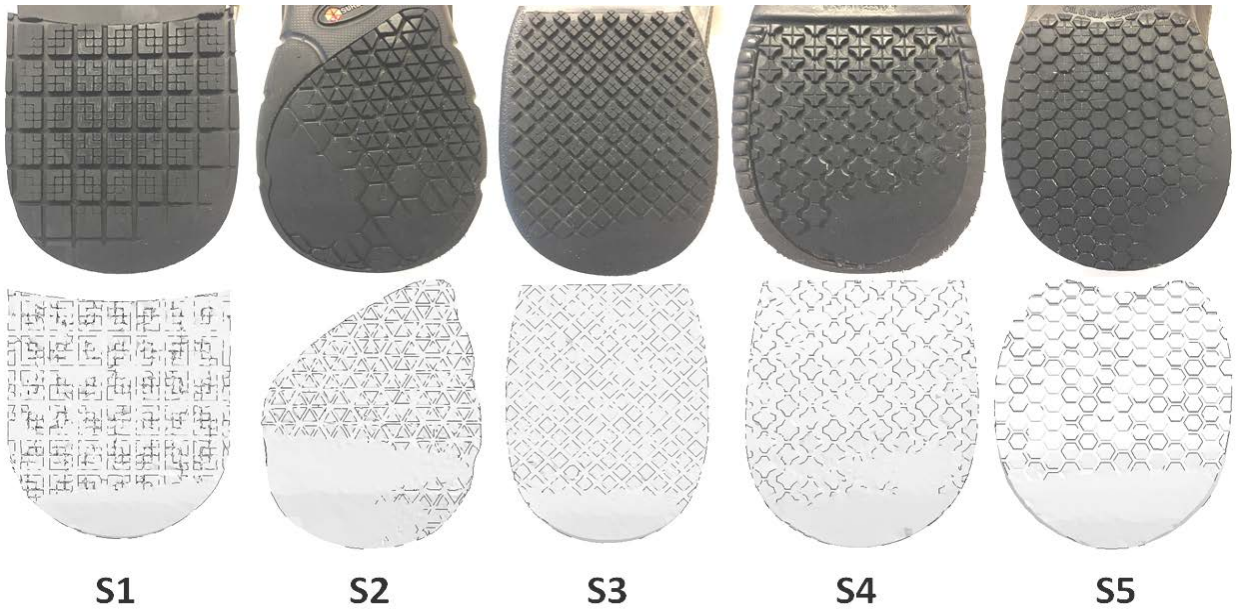


**Figure 6-4.** Pictures of the shoes at the end of the experimental wear protocol (Top) and models of wear of the shoes (Bottom).

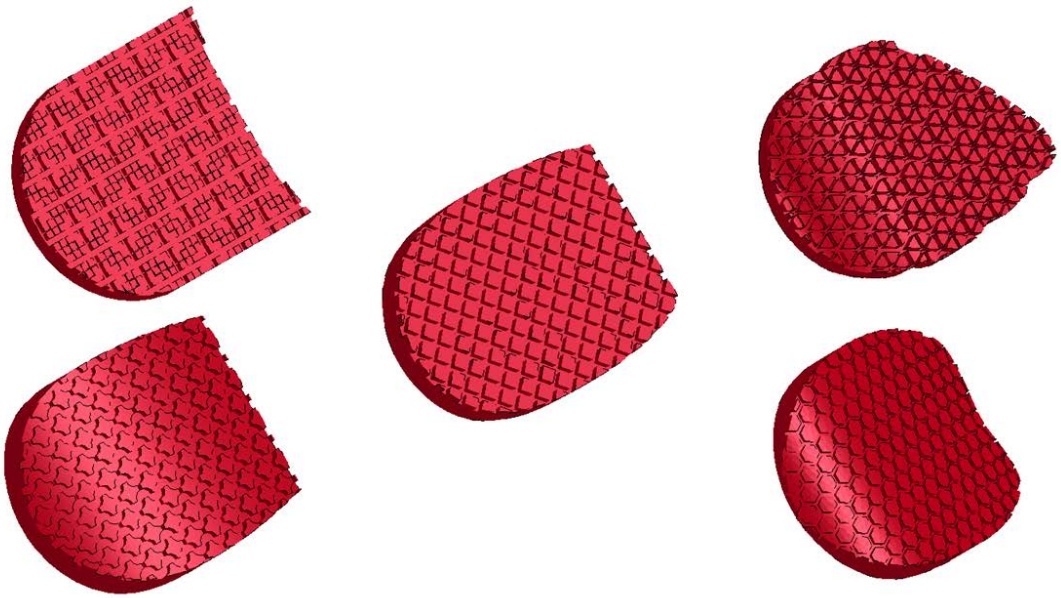

**Figure 6-5.** Video demonstrating wear progression in shoes (Click to open). (S1: Top left, S2: Top right, S3: Middle center, S4: Bottom left, S5: Bottom right.)

Based on the rank correlation analysis of the order that shoe tread blocks became fully worn, a strong, positive, and monotonic correlation existed between the wear model predictions and the accelerated wear experiment (Table 6-2). The strongest and weakest rank order correlations were observed in S1 ($r_s$=0.98) and S5 ($r_s$=0.74), respectively. For all of the shoes except S5, the percentage of the tread blocks that wore down in both the model and experiment was greater than the percentage of the tread blocks that wore down only in the model (Figure 6-6). For all of the shoes, the percentage of the tread blocks that wore down in both the models and experiments was greater than the percentage of the tread blocks that wore down only in the experiments. For S1, a complete agreement in the number of worn tread blocks between the model prediction and experiment results was observed.

**Table 6-2.** Results of the statistical analysis on the order of tread wear.

| Shoe | S1 | S2 | S3 | S4 | S5 |
|---|---|---|---|---|---|
| **Number of tread blocks** | 8 | 10 | 17 | 18 | 15 |
| **Spearman's Rho ($r_s$)** | 0.98 | 0.87 | 0.94 | 0.92 | 0.74 |
| ***t-score*** | 12.06 | 4.99 | 10.67 | 9.39 | 3.97 |
| **(*p-value*)** | (0.000) | (0.001) | (0.000) | (0.000) | (0.002) |

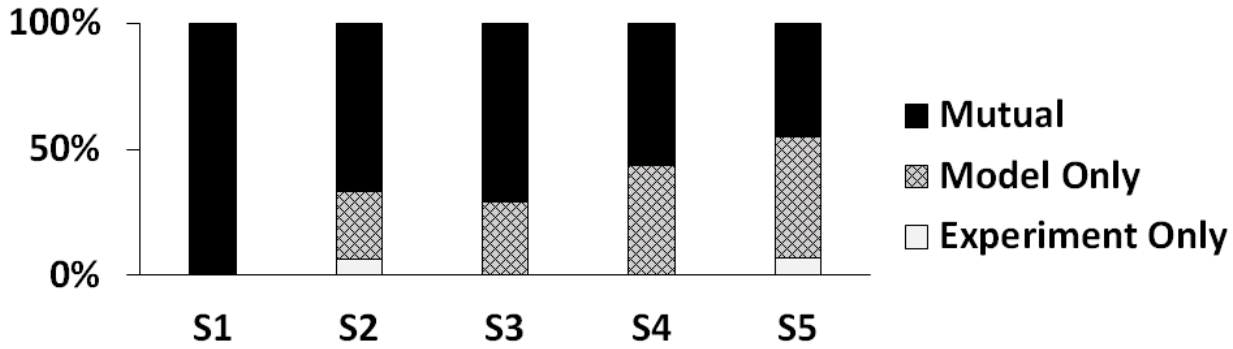


**Figure 6-6.** Percentage of tread blocks that wore down in both models and experiments, only in models and not in models, and only in experiments and not in models.

An untreaded area was observed in the models similar to the experiments. Statistical comparison between the rectangular untreaded areas predicted by the model and observed in the experiments demonstrated strong correlations for all of the five shoes (Figure 6-7). For S1, the slope of the linear correlation was close to one and 83% of the variance was predicted. For S2 and S3, model predictions scaled linearly with the experimental observations and more than 76% of the variance was predicted. Slopes of the correlation lines for S2 and S3 were 1.7 and 2.71, respectively. Shoes S4 and S5 appeared not to be linear and instead a had a parabolic shape describing the relationship between the untreaded area of the models and experiments.

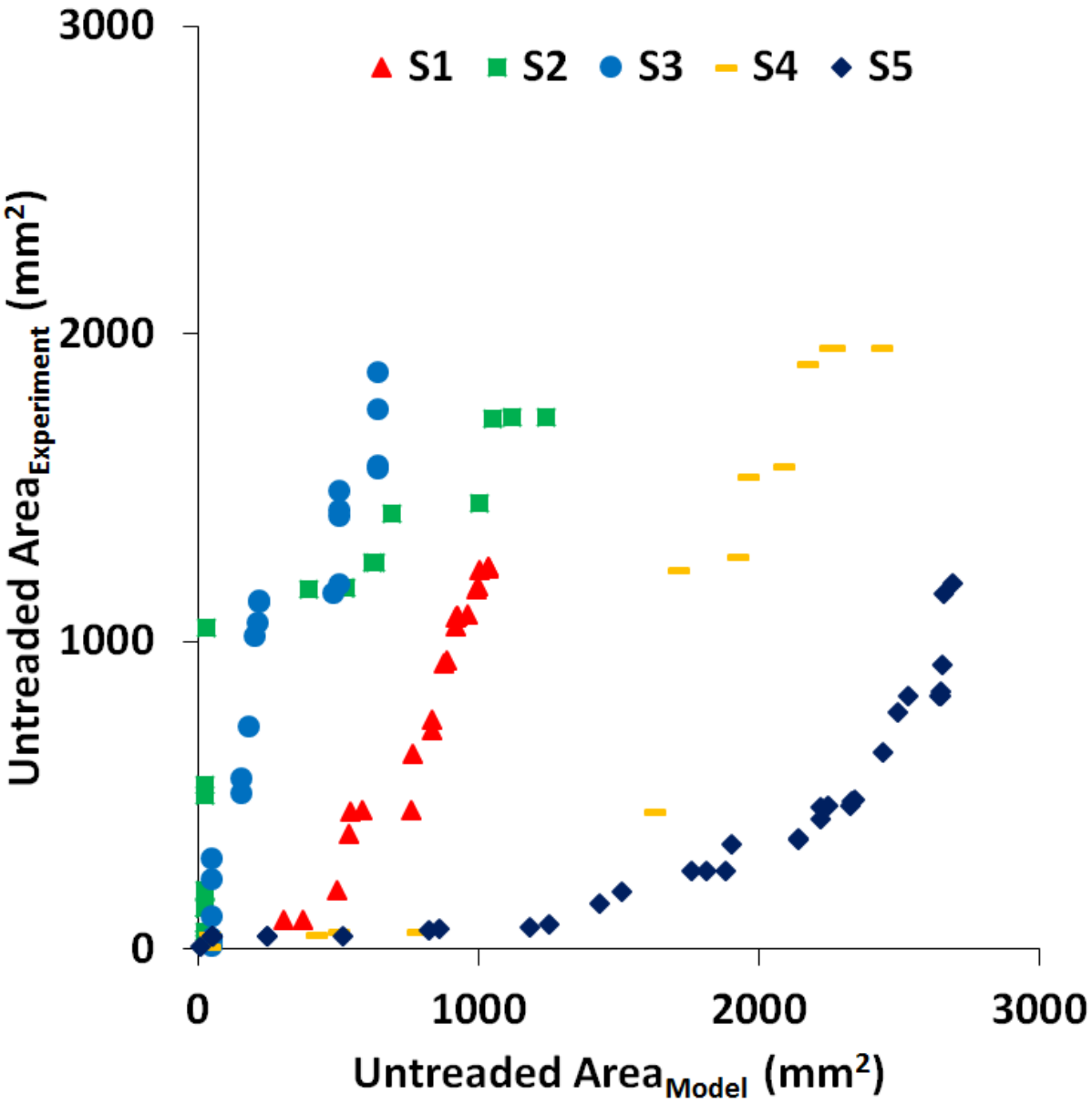


**Figure 6-7.** Comparison of the rectangular untreaded areas predicted by the model versus those observed experimentally.

Further statistical analysis investigated the relationship between the major (anteroposterior) axis of the untreaded areas in the models with the major axis of the untreaded areas in the experiments (Figure 6-8. Left). For S1, S4 and S5, the model was capable of

predicting more than 73% of the variance in experimentally-observed major axis of the untreaded area and the slopes of the linear fits were comparable to unity (i.e. slope of 1.). For S2, the model was successful in predicting the increasing trend in the major axis ($R^2$=0.77) and the areas scaled linearly with a slope of 2.35. For S3, the model predictions of the major axis of the untreaded area were not strongly correlated to those that were observed experimentally ($R^2$=0.27).

A similar analysis was also conducted to investigate the relationship between the minor (mediolateral) axis of the untreaded area in the models and experiments (Figure 6-8. Right). For S1 and S4, the model was capable of predicting more than 75% of the variance in experimentally-observed minor axis of the untreaded area and the slopes of the linear fits were comparable to unity (i.e. slope of 1.). For S2, model predictions of the minor axis of the untreaded area were only moderately correlated to the experimentally-observed ones ($R^2$=0.51). It can be observed that for S2, the untreaded area occurred in the direction of the minor axis in the model, as opposed to the experiments where the majority of wear was observed in the direction of major axis (Figure 6-4; Also, slope of the correlation line for S2 in the direction of major axis was 2.35 (Figure 6-8. Left). For S3, model predictions of the minor axis of the untreaded area strongly correlated with the experimental observations ($R^2$=0.87). For S5, predictions of the model for the minor axis of the untreaded area overestimated those that were observed experimentally by a factor of 3.4 but the correlation was strong ($R^2$=0.74).

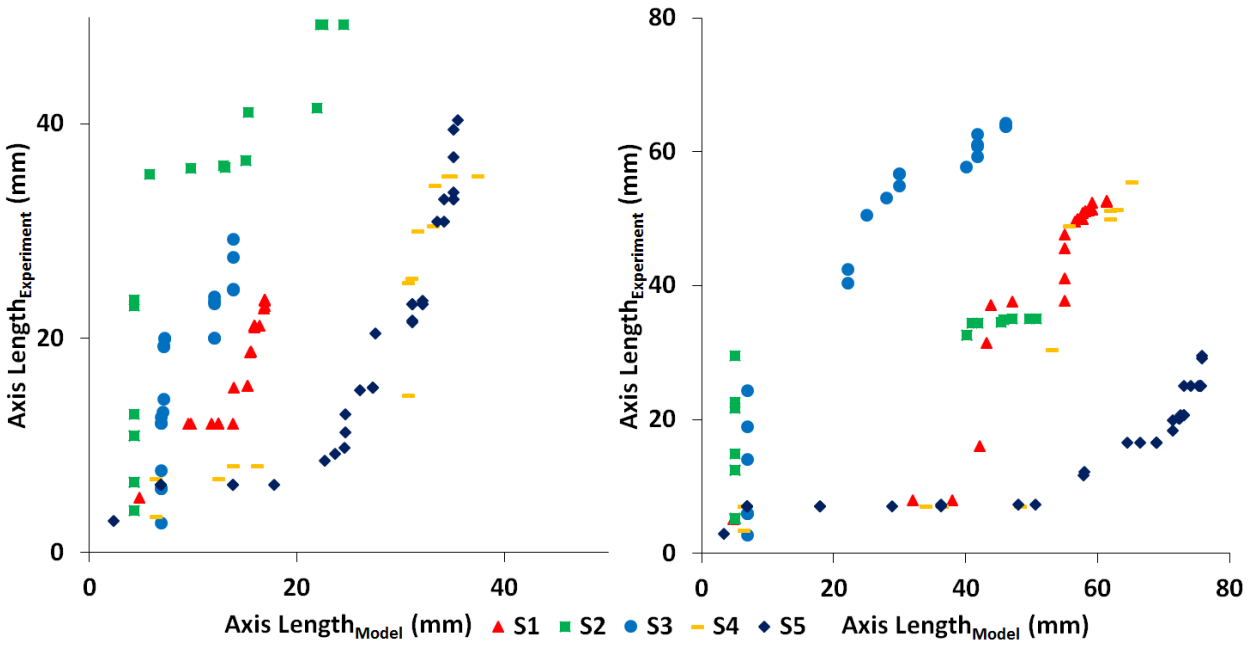


**Figure 6-8.** Comparison of major (Left) and minor (Right) axes of untreaded area predicted by the model versus those observed experimentally.

## 6.5 DISCUSSION

The computational model developed in this paper demonstrates the feasibility of using Archard's law and finite element analysis in predicting shoe wear progression. Qualitative and quantitative agreements between the outcomes of the computational models and the results of the experimental shoe wear protocol were observed. Furthermore, findings of this study support the application and provide the rationale for the application of Archard's law to shoe-floor contact.

The results of this study are consistent with the experimental studies on shoe wear that demonstrate development of wear areas throughout the lifetime of the shoe [23, 27] at the regions of the shoe with higher contact pressures [23, 131, 136]. Findings of this study are also in agreement with the previously developed computational models of wear in other applications

such as disc brakes [69], seals [67] and pin-on-disk friction experiments [137] that use Archard's law for describing the relationship between wear depth and interfacial pressure. Specifically, they demonstrate that wear of the material can be simulated using Archard's law, global remeshing, and finite element analysis [29, 66, 67, 69, 137].

Certain outcomes of the model did not agree with the experimental results, including the shape of the wear region and the order of shoe tread in some of the shoes. One reason could be the assumption of a linear relationship between the contact pressure and wear depth. Previous studies have demonstrated that this phenomenological relationship is described using power-law equations for certain contact interfaces [68, 138]. Assuming the power-law form for the relationship between contact pressure and wear depth would result in a higher difference between the wear depth of the regions with higher and lower contact pressure and lead to a less uniform wear region in model results. The phenomenon of highly localized wear present in the wear experiments (e.g. S2 and S5) is absent in the model (Figure 6-4. The wear models demonstrate a more uniform wear region in comparison to their experimental pairs.). Also, the differences that were observed between the regions of wear development in the models and experiments can be related to the way that the position and angle of the shoes relative to the countersurface was defined in the model (i.e. how the mediolateral and anteroposterior sections of the shoe come into contact with the countersurface at the three different modeled angles). For the current version of the model, these angles were determined using measurement of the shoe tilt against the experimental wear apparatus and utilizing simple trigonometry. For future versions of this wear model, this approach could be improved by matching the two-dimensional location of the center of pressure [139] to achieve more realistic contact regions.

A computational model can be particularly useful in guiding the design of durable slip resistant shoes by applying design modifications within the model (e.g. increasing tread depth in those regions or including more wear-resistant materials in those regions) and observing the results. Furthermore, tread could be designed to spread the contact pressures and wear across a larger region which would increase COF [101, 125, 126] and durability.

The computational model for wear can also be used to describe the "running-in" phenomenon [29, 69] that leads to an increase of COF for slightly worn shoes [119, 131]. An analysis of the contact areas before wearing the shoe and after the initial wear trials demonstrated an increase in contact area of the shoe due to wear both in the models (Figure 6-9) and experiments [131] which led to a more distributed contact pressure (Figure 6-9) over the surface of the shoe [126]. As predicted in previous models [101, 126] and experiments [140], increased contact area and decreased contact pressures led to increased hysteresis friction. This explains the initial increase in shoe-floor coefficient of friction at the early stages of wear [131].

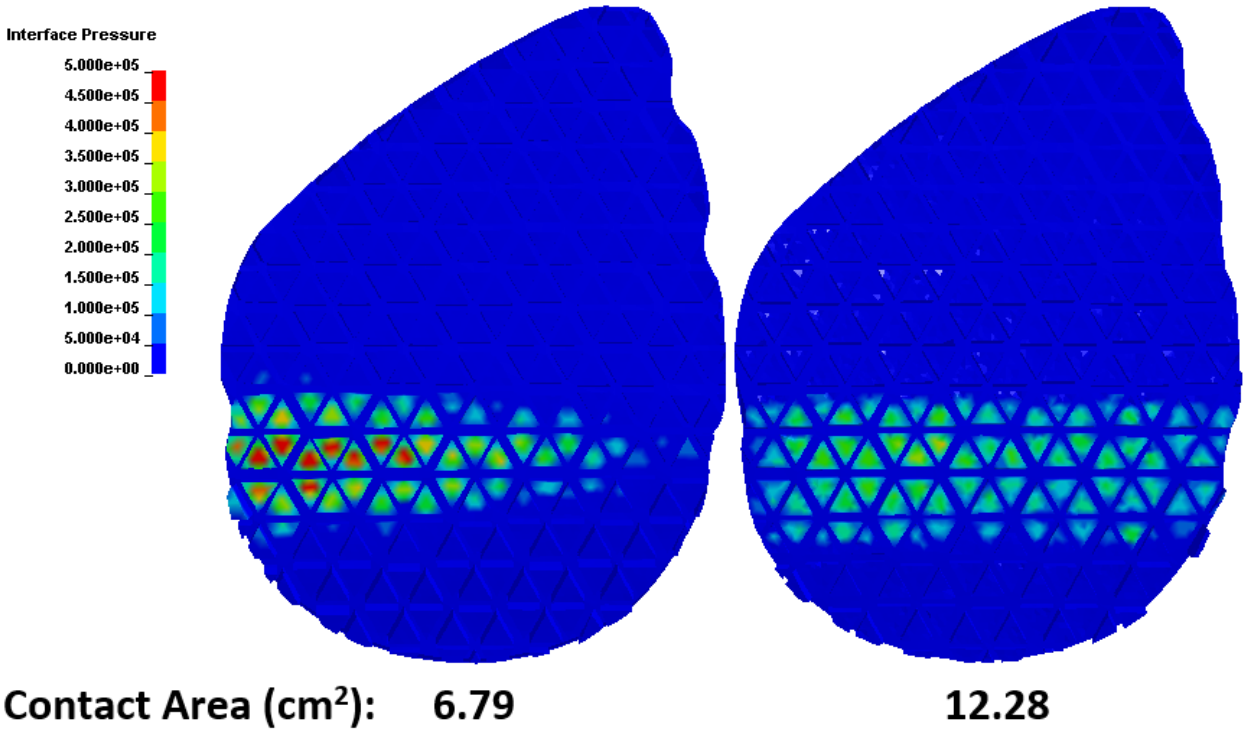


**Figure 6-9.** Under-shoe contact pressure (S2) and contact areas of the shoe at 250 N and 7° shoe angle at the baseline (Left) and after 7 kilometers of simulated wear (Right). Total contact area of the shoe in each case is reported below the shoe.

The computational model for wear demonstrates an important first step toward developing more sophisticated models of the shoe wear progression. The current version of the model can be used to predict the wear progression of the shoe. Future versions of this wear model should advance this framework by using wear constants (*k)* which can be obtained using shoe material wear testing [131]. For the shoes modeled in this is study, wear constants that were calculated using the experimental volume loss, normal force and sliding distance were within the range of 0.002-0.008 $mm^3/(N.m)$. These values are consistent with the wear constants values available in the literature for abrasive wear of elastomers on rough surfaces [141-143]. Future version should also aim at including subject-specific boundary conditions based on each person's

gait parameters. This will allow prospective predictions for different shoes to quantify the duration of usage to reach the point of increased risk of slips and falls [22, 26]. Once these models become available, more reliable predictions on shoe wear and durable slip-resistant designs will become feasible. This result will likely promote the long-term goal of reducing slip and fall injuries.

# 7.0 CONCLUSIONS

## 7.1 SUMMARY

This dissertation aimed to enhance the understanding of slips and falls by applying computational modeling methods that simulate the tribology interaction of the shoe-floor interface. The major contributions of this dissertation are as follows:

- A computational model of the shoe-floor-contaminant complex at the microscopic scale in boundary lubrication was developed and validated. The model predicts the microscopic COF at the shoe-floor-contaminant complex as a function of measurable inputs such as shoe and floor surface topography, shoe material properties, shoe sliding velocity, and contact pressure at the interface. The microscopic model indicated that rougher shoe and floor surfaces lead to an increased hysteresis COF.
- A multiscale computational model of the shoe-floor-contaminant complex in boundary lubrication was developed and validated. The model was demonstrated capable of predicting the whole shoe COF given the inputs of whole shoe geometry (tread), shoe material properties, shoe and floor surface topography, normal loading, shoe-floor contact angle, and shoe sliding velocity. The

multiscale model revealed that shoe designs that lead to a more distributed under-shoe contact pressure result in higher COFs at the interface.

- The multiscale model of shoe-floor-contaminant complex was utilized to assess the hysteresis friction response to shoe design parameters (i.e. shoe hardness and shoe heel's geometrical curvature) and human factors (i.e. shoe-floor contact angle and normal loading). Results demonstrated that softer shoe materials, lower shoe-floor contact angles and lower normal loads result in higher COFs and that flat and beveled shoes respond differently to the changes in normal loading and shoe-floor contact angle.
- A computational model of shoe wear progression was developed and partially validated. The model was capable of predicting the geometrical wear of the outsole given inputs such as shoe material properties, whole shoe geometry, shoe-floor contact angle, and normal loading. Model simulations of the wear of the shoes quantitatively and qualitatively agreed with the experimental wear protocol.

The computational models presented in this dissertation provided predictions that were mostly consistent with the experiments and also the available literature in tribology, biomechanics, and slips and falls research. Thus, this dissertation achieved its purpose of developing predictive computational models for shoe friction and wear. Applications of the computational models introduced in this dissertation include but are not limited to the design of slip-resistant and durable shoes.

The computational models introduced in this dissertation provide an enhanced understanding of the friction and wear of the shoes and demonstrate the possibility of deploying computer models in the process of designing slip-resistant and durable shoes. The outcomes of

this dissertation also have a broader potential to improve quality of life by reducing the number of slip and fall accidents that are caused by insufficient shoe-floor friction and/or worn shoes. Furthermore, these models represent a predictive and evaluative tool that can be used by the following groups:

- Engineers, designers, ergonomists and shoe and flooring manufacturers because it will help them identify the critical shoe characteristics for slip/wear-resistance and will aid them in the development of optimized designs in order to achieve superior friction and wear performance.
- Future researchers in the field of slips and falls, biomechanics, and ergonomics because it will provide them with an improved understanding of the mechanisms behind the effects of biomechanical and design factors such as shoe-floor angle, normal loading, shoe hardness and shoe beveling on the friction at shoe-floor-contaminant complex.
- Researchers in tribology and computational modeling because it represents novel research methodologies in those fields that can be used in other tribological and finite element modeling applications.

Overall, the computational models presented in this dissertation represent the first generation of predictive models with regard to shoe and flooring as it relates to slip-resistance and durability. Through the computational models presented in this dissertation, it became possible to quantify the effects of several shoe and flooring design factors and human-related parameters on the frictional behavior of the complex and identify the critical factors in design and material selection for footwear. Specifically, the computational model of shoe-floor-contaminant friction (Chapters 3.0 -5.0 ) identified contact area of the shoe [125, 126, 144]

followed by flooring roughness [125, 145, 146], shoe material hardness [101, 145], beveling of the shoe [103], and shoe roughness [99, 146] as the key design parameters that influence shoe-floor friction. Furthermore, the computational models identified human factors such as normal loading [103, 147], shoe-floor contact angle [103] and sliding velocity [99] as the parameters that affect friction at the interface.

The remainder of this chapter will be dedicated to identifying how the future research can continue the line of modeling methods introduced in this dissertation. Specifically, the challenges that were met during the research that is presented earlier in this dissertation will be discussed and recommendations for future research to improve the computational models presented in this dissertation and to overcome those challenges will be presented.

## 7.2 FUTURE DIRECTIONS

It is acknowledged that while the research presented in this dissertation accomplished its specific aims which was the development and validation of the first generation of the computational models for shoe friction and wear, further work on improving the predictive features of the models can enhance the quality and ability to provide realistic predictions. Thus, this section discusses the improvements that are recommended for the computational models and validation experiments that were introduced earlier and devises suggestions for future research that enhance the predictive outcomes of these models. Also, recommendations on including the other relevant tribology mechanisms that were neglected in the modeling efforts of this dissertation are presented. Each subsection is dedicated to the respective model of its title. Emphasis is placed on the topics that were not in detail discussed earlier in this dissertation.

### 7.2.1 Friction model

The multiscale model of shoe-floor-contaminant presented in chapters 4.0 and 5.0 of this dissertation was a successful effort in predicting COF for treaded shoes in boundary lubrication regime. However, there exist several features of the model that can be improved in order to make it a more comprehensive model that could be applicable to different shoe designs and different lubrication regimes. The following discusses some of these features:

1. The multiscale model of shoe-floor-contaminant simulates the hysteresis friction interactions in boundary lubrication regime where the effects of hydrodynamic pressure and adhesional contributions are negligible. The assumption of negligible hydrodynamic pressures is particularly true for shoes that have sufficient amount of tread [22, 26]. The assumption of insignificant adhesional effects holds true when a high viscosity contaminant is present on the flooring [53]. However, for a comprehensive model of shoe-floor-contaminant friction that includes the situations relevant to actual slipping accidents these contributions should be considered:
    a. The most recent modeling effort on multiscale modeling of rubber friction suggests that adhesion effects (however small) are still present at contaminated interfaces [148]. Wagner et al. [148] introduce a hybrid methodology (i.e. based on friction experiments and using computational models) to estimate the adhesional force ($F_{Adhesion}$) using the multiscale modeling schemes similar to the one used in chapter 4.0 of this dissertation. In this proposed method, true shearing stress ($\sigma_s$) and real contact area ($A_c$) in Equation 2-2. are estimated using curve fitting to

experimental data and finite element method, respectively. The reader is referred to this work [148] for further information on implementing this multiscale modeling scheme to estimate force of adhesion.

b. Hydrodynamic pressures in non-fully treaded shoes are believed to originate from wedge and squeeze term effects described by Reynolds equation [22, 26, 41, 131]. Wedge effect is associated with the geometry of the shoe while squeeze term is due to transient effects [41]. Modeling squeeze film and including it in a hybrid model for shoe-floor-contaminant seems to be currently too complex given its temporal nature [17] and the quasi-dynamic nature of the current version of the multiscale model. However, as the first step toward including the hydrodynamic effects, the next generation of shoe-floor-contaminant model should aim at simulating wedge effect and use the equation developed by Proctor and Coleman [71] (Equation 7-1.) to estimate fluid film thickness and the subsequent fluid force. Equation 7-1. (with the assumption of a square untreaded area) calculates fluid film thickness ($h$), as a function of fluid viscosity ($\mu$), length of the untreaded area ($l$), sliding velocity ($v$) and normal force ($F_{Normal}$). Once the fluid film thickness is calculated, the force generated by the fluid ($F_{Fluid}$) can be estimated by integrating the resulting shear stress due to the fluid film over the untreaded area [16, 22, 41].

$$h = \sqrt{\frac{0.066\mu l^3 v}{F_{Normal}}} \qquad \text{Equation 7-1.}$$

Once the adhesional (*a*) and hydrodynamic (*b*) forces are calculated, force of friction for the whole shoe can be estimated considering the effects that each of these components generate (Equation 7-2.). In Equation 7-2. $F_{Hysteresis}$ is equivalent to the force of friction calculated using the multiscale modeling method of chapter 4.0 (Equation 4-4.). Finally, whole shoe COF is calculated as the division of frictional force by normal force (Equation 4-6.). It should be noted that the different terms in Equation 7-2. are not independent from each other and affect one another. For example, an increase in fluid film thickness will increase the fluid force and also will lead to separation of the shoe and floor surfaces which will in turn cause a significant drop in friction force of adhesion and hysteresis.

$$F_{Friction} = F_{Hysteresis} + F_{Adhesion} + F_{Fluid} \qquad \text{Equation 7-2.}$$

2. The current version of the multiscale model uses a uniform distribution of surface microscopic asperities to describe the surfaces of shoe and flooring in microscopic scale. Due to this simplifying assumption, all of the peaks of the surface of the shoe model come into contact with the flooring at the same time and stay in contact with the flooring for the same duration of time. However, research on real surfaces has indicated that surface asperities follow a probabilistic distribution [97]. Recent imaging investigation on shoe and floor surfaces in the laboratory (Figure 7-1) confirms this finding. Including real surfaces in the next version of the multiscale model will likely result in different frictional shear stress curves (Figure 4-5) for real shoe samples since it affects the

number of the contacting asperities at a time and also the time that asperities are in contact (Both spatial and temporal effects [99]). The next version of the multiscale model should aim at digitizing images from the actual scans of the shoe and flooring surfaces and implementing those in the finite element analyses for the microscopic model. As this modeling approach develops, experiments that aim to validate the finding of the models need to also be pursued. For example, the effect of contact pressure on COF should be experimentally investigated by conducting pin-on-disk friction testing experiments [18, 19, 53] on the shoe and floor samples that are scanned and models in several normal loadings.

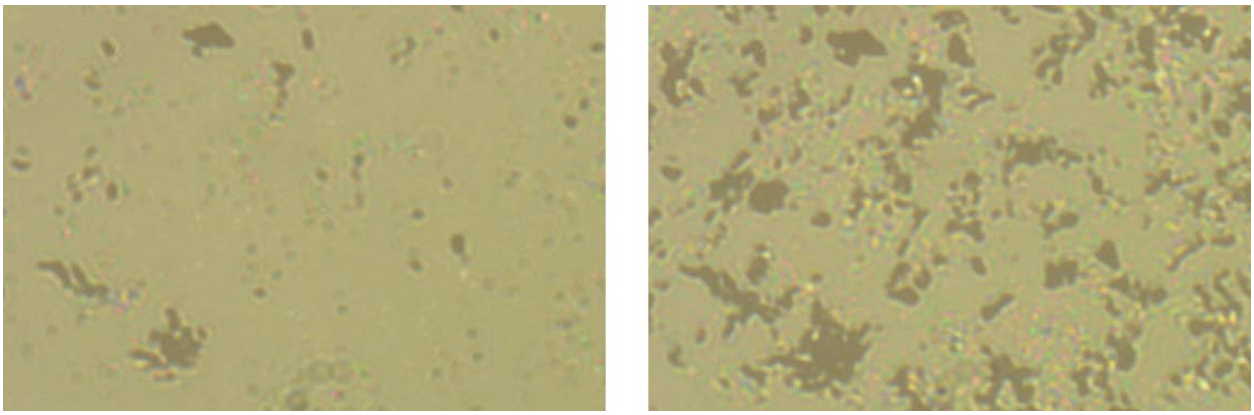

**Figure 7-1.** Development of the contact impression of shoe sample on glass with increasing normal load, captured using surface microscopy (Left. Load of 5 grams on the sample; Right. Load of 80 grams on the sample). Darker areas indicate asperities of the shoe that have come into contact with the glass at the specified load (Courtesy of Jacobs Laboratory, University of Pittsburgh)

### 7.2.2 Wear model

The computational model that was presented in chapter 6.0 of this dissertation was effective in predicting the location of the wear. While this first version represents a significant step in modeling wear of the shoes, several improvements should be made to the model in order to make it more efficient and useful in engineering and ergonomic applications:

1. Current version of the computational wear model lacks the feature that allows for inputting the experimental wear constant ($k$) because it focuses on predicting the location of the wear rather than the duration of shoe usage. Therefore, the model will not be capable of precisely predicting the time it takes for shoes to wear down without matching the model results to the experiments. Next generation of this model should focus on adding the above-mentioned feature to the model. Once the wear constants can be added to model, experimental testing of several shoes on various floorings (with different roughnesses) [131] should be conducted in order to determine the wear constants that correspond to each shoe-floor interface. Once such a database is created, it will become possible for the user to input parameters such as elastic modulus of the shoe and roughness of the flooring (to estimate $k$) and the duration of usage of the shoe (to estimate $s$ in Equation 6-1.) in order to simulate the amount of wear and get the worn geometry of the shoe as the model output.
2. In the current version of the wear model, different sections of the iterative wear modeling process (Figure 6-1) are performed in different software packages; Contact modeling is performed in LS-Dyna®, meshing (when needed) is conducted in ANSYS®, and generating the commands that move the contact

nodes due to wear is performed in MATLAB®. This process increases the computational and processing time that takes to model wear given the inherent differences that exists among those packages. Future versions of the wear model should focus on building one single platform which is capable of performing the iterative process of modeling wear in order to make the wear model more time-efficient.

3. Once the improvements that were recommended for the multiscale model in subsection 7.2.1 are implemented, that model can be used along with the wear model to estimate COF at the shoe-floor-contaminant complex and its changes across a shoe's life. Specifically, the multiscale modeling approach can be applied after each wear iteration to calculate shoe-floor-contaminant COF at those points. Experimental methods that are used for measuring under-shoe fluid pressure [26] should be utilized to determine the governing friction and lubrication regime after each wear iteration. Depending on the governing friction and lubrication mechanisms (i.e. (only hysteresis)/(hysteresis + adhesion)/(hysteresis + hydrodynamic pressures)/(hysteresis + hydrodynamic pressures + adhesion)) and the multiscale modeling scheme relevant to those (Equation 7-2.) should be used for modeling the respective scenario. This will lead to the development of an extensive computational model of shoe friction and wear.

## 7.3 CONCLUDING REMARKS

This dissertation accomplished its purpose of adding to the understanding of slips and falls by developing predictive computational models of friction and wear of the shoes. Microscopic and macroscopic contributions to the friction at shoe-floor-contaminant complex were investigated via finite element modeling. Effects of shoe design and human factors on shoe-floor-contaminant friction were examined. Additionally, a computational methodology was developed and applied to modeling wear of the shoes. The models developed in this dissertation offer a significant tool to engineers, designers, ergonomists, biomechanists and slips and falls researchers that can be used for predicting and evaluating the slip-resistance and durability of the existing and future shoe designs. While improvement in some aspects of the models seem necessary, these models not only enhance the understanding of tribology of shoe-floor-contaminant but also contribute to the final goal of reducing slip and fall accidents.

## BIBLIOGRAPHY


1. *Nonfatal Occupational Injuries and Illnesses Requiring Days Away From Work, 2015*. 2017 [cited 2018 02.02.2018].

2. *National Census of Fatal Occupational Injuries in 2016*. 2017 [cited 2018 02.02.2018].

3. Florence, C., et al., *Estimated Lifetime Medical and Work Loss Costs of Fatal and Nonfatal Injuries, United States 2013.* MMWR Morb Mortal Wkly Rep, 2015. **64**: p. 1074-82.

4. Institute, L.M.R., *Liberty Mutual Workplace Safety Index*. 2012.

5. Courtney, T.K., et al., *Occupational slip, trip, and fall-related injuries–can the contribution of slipperiness be isolated?* Ergonomics, 2001. **44**(13): p. 1118-1137.

6. Burnfield, J.M. and C.M. Powers, *Prediction of slips: an evaluation of utilized coefficient of friction and available slip resistance.* Ergonomics, 2006. **49**(10): p. 982-995.

7. Hanson, J.P., M.S. Redfern, and M. Mazumdar, *Predicting slips and falls considering required and available friction.* Ergonomics, 1999. **42**(12): p. 1619-1633.

8. Chang, W.-R., et al., *The role of friction in the measurement of slipperiness, Part 2: Survey of friction measurement devices.* Ergonomics, 2001. **44**(13): p. 1233-1261.

9. Powers, C.M., et al., *Assessment of Walkway Tribometer Readings in Evaluating Slip Resistance: A Gait-Based Approach.* Journal of forensic sciences, 2007. **52**(2): p. 400-405.

10. Iraqi, A., *Comparison of Interfacial Fluid Pressures Generated Across Common Shoe-Floor Friction Testing Apparatuses.* 2013.

11. Siegmund, G.P., et al., *The effect of subject awareness and prior slip experience on tribometer-based predictions of slip probability.* Gait & posture, 2006. **24**(1): p. 110-119.

12. Blanchette, M.G. and C.M. Powers, *The influence of footwear tread groove parameters on available friction.* Applied ergonomics, 2015. **50**: p. 237-241.

13. Li, K.W. and C.J. Chen, *The effect of shoe soling tread groove width on the coefficient of friction with different sole materials, floors, and contaminants.* Applied ergonomics, 2004. **35**(6): p. 499-507.

14. Li, K.W., H.H. Wu, and Y.-C. Lin, *The effect of shoe sole tread groove depth on the friction coefficient with different tread groove widths, floors and contaminants.* Applied Ergonomics, 2006. **37**(6): p. 743-748.

15. Tsai, Y.J. and C.M. Powers, *The influence of footwear sole hardness on slip initiation in young adults.* Journal of forensic sciences, 2008. **53**(4): p. 884-888.

16. Beschorner, K., et al., *Modeling mixed-lubrication of a shoe-floor interface applied to a pin-on-disk apparatus.* Tribology Transactions, 2009. **52**(4): p. 560-568.

17. Beschorner, K.E., *Development of a computational model for shoe-floor-contaminant friction*. 2008: ProQuest.

18. Moore, C.T., et al., *Analysis of shoe friction during sliding against floor material: role of fluid contaminant.* Journal of Tribology, 2012. **134**(4): p. 041104.

19. Strobel, C.M., et al., *Analysis of the contribution of adhesion and hysteresis to shoe–floor lubricated friction in the boundary lubrication regime.* Tribology Letters, 2012. **47**(3): p. 341-347.

20. Bentley, T., et al., *Investigating slips, trips and falls in the New Zealand dairy farming sector*. Ergonomics, 2005. **48**(8): p. 1008-1019.

21. Bentley, T.A. and R. Haslam, *Identification of risk factors and countermeasures for slip, trip and fall accidents during the delivery of mail.* Applied ergonomics, 2001. **32**(2): p. 127-134.

22. Beschorner, K.E., et al., *Fluid pressures at the shoe–floor–contaminant interface during slips: Effects of tread & implications on slip severity.* Journal of biomechanics, 2014. **47**(2): p. 458-463.

23. Gronqvist, R., *Mechanisms of friction and assessment of slip resistance of new and used footwear soles on contaminated floors.* Ergonomics, 1995. **38**(2): p. 224-241.

24. Kim, I.-J. *Wear progression of shoe heels during slip resistance measurements*. in *Proceedings of the Human Factors and Ergonomics Society Annual Meeting*. 2000. SAGE Publications.

25. Kim, I.-J., R. Smith, and H. Nagata, *Microscopic observations of the progressive wear on shoe surfaces that affect the slip resistance characteristics.* International Journal of Industrial Ergonomics, 2001. **28**(1): p. 17-29.

26. Singh, G. and K.E. Beschorner, *A Method for Measuring Fluid Pressures in the Shoe–Floor–Fluid Interface: Application to Shoe Tread Evaluation.* IIE Transactions on Occupational Ergonomics and Human Factors, 2014. **2**(2): p. 53-59.

27. Verma, S.K., et al., *Duration of slip-resistant shoe usage and the rate of slipping in limited-service restaurants: results from a prospective and crossover study.* Ergonomics, 2014. **57**(12): p. 1919-1926.

28. Archard, J., *Contact and rubbing of flat surfaces.* Journal of applied physics, 1953. **24**(8): p. 981-988.

29. Békési, N. and K. Váradi, *Wear simulation of a reciprocating seal by global remeshing.* Periodica Polytechnica. Engineering. Mechanical Engineering, 2010. **54**(2): p. 71.

30. Lupker, H., et al., *Numerical prediction of car tire wear.* Tire Science and Technology, 2004. **32**(3): p. 164-186.

31. Wagner, P., et al., *A multiscale contact homogenization approach for hysteresis friction of rubber on rough surfaces.* Book of Abstracts-Extract, 2015: p. 25.

32. Wagner, P., et al., *Multiscale FEM approach for hysteresis friction of rubber on rough surfaces.* Computer Methods in Applied Mechanics and Engineering, 2015. **296**: p. 150-168.

33. Iraqi, A., R. Cham, and K.E. Beschorner, *Assessment of slip-risk using a portable slip simulator.* American Society of Biomechanics. Columbus, OH, 2015.

34. Powers, C.M. and M.G. Blanchette, *Slip Prediction Accuracy and Bias of the SATRA STM 603 Whole Shoe Tester.* Journal of Testing and Evaluation, 2014. **43**(3): p. 491-498.

35. Institute, L.M.R., *Liberty Mutual Workplace Safety Index*. 2017.

36. Redfern, M.S. and B. Bidanda, *Slip resistance of the shoe-floor interface under biomechanically-relevant conditions.* Ergonomics, 1994. **37**(3): p. 511-524.

37. Beschorner, K.E., D.L. Albert, and M.S. Redfern, *Required coefficient of friction during level walking is predictive of slipping.* Gait & Posture, 2016.

38. Chang, W.-R., C.-C. Chang, and S. Matz, *The effect of transverse shear force on the required coefficient of friction for level walking.* Human Factors: The Journal of the Human Factors and Ergonomics Society, 2011. **53**(5): p. 461-473.

39. Perkins, P., *Measurement of slip between the shoe and ground during walking*, in *Walkway surfaces: Measurement of slip resistance*. 1978, ASTM International.

40. Iraqi, A., et al., *Coefficient of friction testing parameters influence the prediction of human slips, in press.* Applied Ergonomics.

41. Chang, W.-R., et al., *The role of friction in the measurement of slipperiness, Part 1: friction mechanisms and definition of test conditions.* Ergonomics, 2001. **44**(13): p. 1217-1232.

42. Aschan, C., et al., *Development and validation of a novel portable slip simulator.* Applied ergonomics, 2005. **36**(5): p. 585-593.

43. ASTM, *Standard Test Method for Measuring the Coefficient of Friction for Evaluation of Slip Performance of Footwear and Test Surfaces/Flooring Using a Whole Shoe Tester*. 2011, ASTM International.

44. Redfern, M.S., et al., *Biomechanics of slips.* Ergonomics, 2001. **44**(13): p. 1138-1166.

45. Beschorner, K. and R. Cham, *Impact of joint torques on heel acceleration at heel contact, a contributor to slips and falls.* Ergonomics, 2008. **51**(12): p. 1799-1813.

46. Moyer, B., et al., *Gait parameters as predictors of slip severity in younger and older adults.* Ergonomics, 2006. **49**(4): p. 329-343.

47. Allin, L.J., et al., *Falls resulting from a laboratory-induced slip occur at a higher rate among individuals who are obese.* Journal of biomechanics, 2016. **49**(5): p. 678-683.

48. Fjeldstad, C., et al., *The influence of obesity on falls and quality of life.* Dynamic Medicine, 2008. **7**(1): p. 4.

49. Madigan, M., N.J. Rosenblatt, and M.D. Grabiner, *Obesity as a factor contributing to falls by older adults.* Current obesity reports, 2014. **3**(3): p. 348-354.

50. Beschorner, K.E., et al., *Effects of slip testing parameters on measured coefficient of friction.* Applied ergonomics, 2007. **38**(6): p. 773-780.

51. Bhushan, B., *Introduction to tribology*. 2013: John Wiley & Sons.

52. Szeri, A.Z., *Fluid film lubrication*. 2010: Cambridge university press.

53. Cowap, M., et al., *Contributions of adhesion and hysteresis to coefficient of friction between shoe and floor surfaces: effects of floor roughness and sliding speed.* Tribology-Materials, Surfaces & Interfaces, 2015. **9**(2): p. 77-84.

54. Grosch, K. *The relation between the friction and visco-elastic properties of rubber*. in *Proceedings of the Royal Society of London A: Mathematical, Physical and Engineering Sciences*. 1963. The Royal Society.

55. Moore, D.F., *The friction of pneumatic tyres.* 1975.

56. Persson, B., *Sliding friction: physical principles and applications*. 2013: Springer Science & Business Media.

57. Pálfi, L., et al., *FE prediction of hysteretic component of rubber friction.* Advances in Tribology, 2012. **2012**.

58. Persson, B., et al., *On the nature of surface roughness with application to contact mechanics, sealing, rubber friction and adhesion.* Journal of Physics: Condensed Matter, 2004. **17**(1): p. R1.

59. Le Gal, A. and M. Klüppel, *Investigation and modelling of rubber stationary friction on rough surfaces.* Journal of Physics: Condensed Matter, 2007. **20**(1): p. 015007.

60. Le Gal, A., X. Yang, and M. Klüppel, *Evaluation of sliding friction and contact mechanics of elastomers based on dynamic-mechanical analysis.* The Journal of chemical physics, 2005. **123**(1): p. 014704.

61. Tabor, D., *Friction, adhesion and boundary lubrication of polymers*, in *Advances in Polymer Friction and Wear*. 1974, Springer. p. 5-30.

62. Kummer, H., *Lubricated friction of rubber discussion.* Rubber Chemistry and Technology, 1968. **41**(4): p. 895-907.

63. Tokura, S. and J. Solutions, *Contact and Sliding Simulation of Rubber Disk on Rigid Surface with Microscopic Roughness.*

64. Wriggers, P. and J. Reinelt, *Multi-scale approach for frictional contact of elastomers on rough rigid surfaces.* Computer Methods in Applied Mechanics and Engineering, 2009. **198**(21): p. 1996-2008.

65. Kim, I.-J. and H. Nagata, *Research on slip resistance measurements—A new challenge.* Industrial health, 2008. **46**(1): p. 66-76.

66. Békési, N., *Modelling Friction and Abrasive Wear of Elastomers*, in *Advanced Elastomers-Technology, Properties and Applications*. 2012, InTech.

67. Békési, N., K. Váradi, and D. Felhős, *Wear simulation of a reciprocating seal.* Journal of Tribology, 2011. **133**(3): p. 031601.

68. Ludema, K., *Mechanism-based modeling of friction and wear.* Wear, 1996. **200**(1-2): p. 1-7.

69. Söderberg, A. and S. Andersson, *Simulation of wear and contact pressure distribution at the pad-to-rotor interface in a disc brake using general purpose finite element analysis software.* Wear, 2009. **267**(12): p. 2243-2251.

70. *Nonfatal Occupational Injuries and Illnesses Requiring Days Away From Work, 2012*. 2013 [cited 2016 10.17.2016].

71. Proctor, T.D. and V. Coleman, *Slipping, tripping and falling accidents in Great Britain—present and future.* Journal of Occupational Accidents, 1988. **9**(4): p. 269-285.

72. Chang, W.-R., *The effect of surface roughness on dynamic friction between neolite and quarry tile.* Safety Science, 1998. **29**(2): p. 89-105.

73. Chang, W.-R., et al., *The role of surface roughness in the measurement of slipperiness.* Ergonomics, 2001. **44**(13): p. 1200-1216.

74. Cheung, J.T.-M., et al., *Current methods in computer-aided engineering for footwear design.* Footwear science, 2009. **1**(1): p. 31-46.

75. Sun, Z., D. Howard, and M. Moatamedi, *Finite element analysis of footwear and ground interaction.* Strain, 2005. **41**(3): p. 113-117.

76. Bowden, F.P., D. Tabor, and F. Palmer, *The friction and lubrication of solids.* American Journal of Physics, 1951. **19**(7): p. 428-429.

77. Heinrich, G., *Hysteresis friction of sliding rubbers on rough and fractal surfaces.* Rubber chemistry and technology, 1997. **70**(1): p. 1-14.

78. Persson, B.N., *Theory of rubber friction and contact mechanics.* The Journal of Chemical Physics, 2001. **115**(8): p. 3840-3861.

79. Bielsa, J., et al., *Application of finite element simulations for data reduction of experimental friction tests on rubber–metal contacts.* Tribology International, 2010. **43**(4): p. 785-795.

80. Gracia, L., et al., *Finite element simulation of the hysteretic behaviour of an industrial rubber. Application to design of rubber components.* Finite Elements in Analysis and Design, 2010. **46**(4): p. 357-368.

81. Liu, F., M. Sutcliffe, and W. Graham, *Modeling of tread block Contact mechanics using linear viscoelastic theory 3.* Tire Science and Technology, 2008. **36**(3): p. 211-226.

82. Erhart, T., *Review of solid element formulations in LS-DYNA.* LS-DYNA Entwicklerforum, 2011.

83. Thompson, M.K., *A multi-scale iterative approach for finite element modeling of thermal contact resistance*. 2007, Massachusetts Institute of Technology.

84. Greenwood, J. and J. Tripp, *The contact of two nominally flat rough surfaces.* Proceedings of the institution of mechanical engineers, 1970. **185**(1): p. 625-633.

85. Schwarzer, N., *Modelling of contact problems of rough surfaces.* 2006.

86. Chang, W.-R., M. Hirvonen, and R. Grönqvist, *The effects of cut-off length on surface roughness parameters and their correlation with transition friction.* Safety science, 2004. **42**(8): p. 755-769.

87. Chang, W.-R., et al., *Linear regression models of floor surface parameters on friction between Neolite and quarry tiles.* Applied ergonomics, 2010. **41**(1): p. 27-33.

88. LS-DYNA®. *KEYWORD USER'S MANUAL. VOLUME II. Material Models. Version 971 R6.1.0. LIVERMORE SOFTWARE TECHNOLOGY*. 2012.

89. Chuckpaiwong, B., et al., *The effect of foot type on in-shoe plantar pressure during walking and running.* Gait & posture, 2008. **28**(3): p. 405-411.

90. Heinrich, G. and M. Klüppel, *Rubber friction, tread deformation and tire traction.* Wear, 2008. **265**(7): p. 1052-1060.

91. Yura, J., et al., *Elastomeric bridge bearings: Recommended test methods*. 2001.

92. Gent, A.N., *Engineering with rubber: how to design rubber components*. 2012: Carl Hanser Verlag GmbH Co KG.

93. Bui, Q. and J.-P. Ponthot, *Estimation of rubber sliding friction from asperity interaction modeling.* Wear, 2002. **252**(1): p. 150-160.

94. Nosonovsky, M. and V. Mortazavi, *Friction-induced vibrations and self-organization: mechanics and non-equilibrium thermodynamics of sliding contact*. 2013: CRC Press.

95. Manning, D. and C. Jones, *The effect of roughness, floor polish, water, oil and ice on underfoot friction:: current safety footwear solings are less slip resistant than microcellular polyurethane.* Applied ergonomics, 2001. **32**(2): p. 185-196.

96. Zhang, S.-W., *Tribology of elastomers*. Vol. 47. 2004: Elsevier.

97. Greenwood, J. and J. Williamson. *Contact of nominally flat surfaces*. in *Proceedings of the Royal Society of London A: Mathematical, Physical and Engineering Sciences*. 1966. The Royal Society.

98. Florence, C., et al., *Estimated lifetime medical and work-loss costs of fatal injuries-United States, 2013.* MMWR: Morbidity and mortality weekly report, 2015. **64**(38): p. 1074-1077.

99. Moghaddam, S.R.M., M.S. Redfern, and K.E. Beschorner, *A Microscopic Finite Element Model of Shoe–Floor Hysteresis and Adhesion Friction.* Tribology Letters, 2015. **59**(3): p. 1-10.

100. Moghaddam, S., *Finite Element Analysis of Contribution of Adhesion and Hysteresis to Shoe-floor Friction.* 2013.

101. Moghaddam, S.R.M. and K.E. Beschorner, *Multiscale Computational Modeling of Shoe-Floor Friction.* American Society of Biomechanics. Columbus, OH, 2015.

102. Moghaddam, S.R.M. and K.E. Beschorner, *Multiscale Shoe-Floor Friction Model Predicts Impact of Shoe-Floor Angle on Utilized Coefficient of Friction During Slipping.* American Society of Biomechanics. Raleigh, NC, 2016.

103. Moghaddam, S.R.M. and K.E. Beschorner. *Sensitivity of a Multiscale Model of Shoe-Floor-Contaminant Friction to Normal Force and Shoe-Floor Contact Angle*. in *2017 STLE Annual Meeting & Exhibition*. 2017.

104. Fortunato, G., et al., *Dependency of Rubber Friction on Normal Force or Load: Theory and Experiment.* Tire Science and Technology, 2017. **45**(1): p. 25-54.

105. Hutchings, I. and P. Shipway, *Tribology: friction and wear of engineering materials*. 2017: Butterworth-Heinemann.

106. Chang, W.-R., et al., *The effect of surface waviness on friction between Neolite and quarry tiles.* Ergonomics, 2004. **47**(8): p. 890-906.

107. ASTM, *D2240, Test Method for Rubber Property–Durometer Hardness*. 2010, ASTM International.

108. Giacomin, A. and A. Mix, *Standardized polymer durometry.* Journal of Testing and evaluation, 2011. **39**(4): p. 1-10.

109. Goda, T. *On the viscoelastic component of rubber friction*. in *VI. InterNatl. Engineering Symposium at Banki, Budapest*. 2016.

110. Kluppel, M. and G. Heinrich, *Rubber friction on self-affine road tracks.* Rubber chemistry and technology, 2000. **73**(4): p. 578-606.

111. Menezes, P.L. and S.V. Kailas, *THE ROLE OF SURFACE TEXTURE ON FRICTION AND TRANSFER LAYER FORMATION–A STUDY OF ALUMINIUM AND STEEL PAIR USING PIN-ON-PLATE SLDIING TESTER.* 2006.

112. Tencer, A.F., et al., *Biomechanical properties of shoes and risk of falls in older adults.* Journal of the american geriatrics society, 2004. **52**(11): p. 1840-1846.

113. Grönqvist, R., *Mechanisms of friction and assessment of slip resistance of new and used footwear soles on contaminated floors.* Ergonomics, 1995. **28**: p. 224-241.

114. Menz, H.B., S. Lord, and A.S. McIntosh, *Slip resistance of casual footwear: implications for falls in older adults.* Gerontology, 2001. **47**(3): p. 145-149.

115. Pettersson, U. and S. Jacobson, *Influence of surface texture on boundary lubricated sliding contacts.* Tribology International, 2003. **36**(11): p. 857-864.

116. Pettersson, U. and S. Jacobson, *Friction and wear properties of micro textured DLC coated surfaces in boundary lubricated sliding.* Tribology letters, 2004. **17**(3): p. 553-559.

117. Wilson, M.P., *Development of SATRA slip test and tread pattern design guidelines*, in *Slips, stumbles, and falls: pedestrian footwear and surfaces*. 1990, ASTM International.

118. Varenberg, M. and S.N. Gorb, *Hexagonal surface micropattern for dry and wet friction.* Advanced Materials, 2009. **21**(4): p. 483-486.

119. Moghaddam, S., A. Iraqi, and K. Beschorner. *Finite Element Model of Wear Progression in Shoe Soles*. in *STLE Tribology Frontiers Conference*. 2014.

120. Tsai, Y.J. and C.M. Powers, *The Influence of Footwear Sole Hardness on Slip Characteristics and Slip-Induced Falls in Young Adults.* Journal of forensic sciences, 2013. **58**(1): p. 46-50.

121. Lloyd, D. and M. Stevenson, *Measurement of slip resistance of shoes on floor surfaces: part 2. effect of a beveled heel.* J Occup Health Saf, 1989. **5**(3): p. 229-35.

122. Lockhart, T.E., J.C. Woldstad, and J.L. Smith, *Effects of age-related gait changes on the biomechanics of slips and falls.* Ergonomics, 2003. **46**(12): p. 1136-1160.

123. Cham, R. and M.S. Redfern, *Changes in gait when anticipating slippery floors.* Gait & posture, 2002. **15**(2): p. 159-171.

124. Leamon, T. and K. Li. *Microslip length and the perception of slipping*. in *23rd International Congress on Occupational Health, Montreal, Canada*. 1990.

125. Moghaddam, S.R.M., A. Acharya, and K.E. Beschorner. *Multi-Scale Finite Element Model for Predicting Hysteresis Coefficient of Friction of Slip-Resistant Shoes*. in *2016 STLE Annual Meeting & Exhibition*. 2016.

126. Moghaddam, S.R.M., et al., *Predictive multiscale computational model of shoe-floor coefficient of friction original article.* Journal of biomechanics, 2017.

127. Arena, S.L., et al., *Required friction during overground walking is lower among obese compared to non-obese older men, but does not differ with obesity among women.* Applied ergonomics, 2017. **62**: p. 77-82.

128. Liu, J. *Effect of Excessive Adiposity on Risk of Slip Initiation and Postural Stability*. in *International Conference on Fall Prevention and Protection, Morgantown, WV*. 2010.

129. Wu, X., T.E. Lockhart, and H.T. Yeoh, *Effects of obesity on slip-induced fall risks among young male adults.* Journal of biomechanics, 2012. **45**(6): p. 1042-1047.

130. Albert, D., B. Moyer, and K.E. Beschorner, *Three-Dimensional Shoe Kinematics During Unexpected Slips: Implications for Shoe–Floor Friction Testing.* IISE Transactions on Occupational Ergonomics and Human Factors, 2017. **5**(1): p. 1-11.

131. Hemler, S.L., D.N. Charbonneau, and K.E. Beschorner. *Effects of Shoe Wear on Slipping–Implications for Shoe Replacement Threshold*. in *Proceedings of the Human*

*Factors and Ergonomics Society Annual Meeting*. 2017. SAGE Publications Sage CA: Los Angeles, CA.

132. Centeno Gil, O.J., *Finite Element Modeling of Rubber Bushing for Crash Simulation-Experimental Tests and Validation.* 2009.

133. Suh, J.B., *Stress analysis of rubber blocks under vertical loading and shear loading*. 2007, University of Akron.

134. Guide, A.M.U.s., *Rel. 14.5.* ANSYS Inc, 2012.

135. ISO/IEC, *ISO 20871:2001 Footwear - Test methods for outsoles - Abrasion resistance*. 2001, ISO/IEC: Geneva, Switzerland.

136. Facey, O., I. Hannah, and D. Rosen, *Shoe wear patterns and pressure distribution under feet and shoes, determined by image analysis.* Journal of the Forensic Science Society, 1992. **32**(1): p. 15-25.

137. Podra, P. and S. Andersson, *Simulating sliding wear with finite element method.* Tribology international, 1999. **32**(2): p. 71-81.

138. Meng, H. and K. Ludema, *Wear models and predictive equations: their form and content.* Wear, 1995. **181**: p. 443-457.

139. Trkov, M., et al. *Shoe-floor interactions during human slip and fall: Modeling and experiments*. in *ASME 2014 Dynamic Systems and Control Conference*. 2014. American Society of Mechanical Engineers.

140. Jones, T., A. Iraqi, and K. Beschorner, *Performance testing of work shoes labeled as slip resistant.* Applied Ergonomics, 2018. **68**: p. 304-312.

141. Békési, N., *Friction and wear of elastomers and sliding seals.* Budapest University of Technology and Economics, Budapest, 2011.

142. Lhymn, C. and Y. Lhymn, *Friction and wear of rubber/epoxy composites.* Journal of materials science, 1989. **24**(4): p. 1252-1256.

143. Padenko, E., et al., *Mechanical and abrasion wear properties of hydrogenated nitrile butadiene rubber of identical hardness filled with carbon black and silica.* Journal of Reinforced Plastics and Composites, 2016. **35**(1): p. 81-91.

144. Acharya, A., S.R.M. Moghaddam, and K.E. Beschorner, *The Effect of Hardness and Contact Area on the Overall Hysteresis COF in a Multi-Scale Computational Model*, in *Biomedical Engineering Society Annual Meeting,*. 2015: Tampa, Fl.

145. Moghaddam, S.R.M., et al., *Predictive Multiscale Computational Model of Shoe-Floor Coefficient of Friction Original Article.* Journal of Biomechanics.

146. Acharya, A., S.R.M. Moghaddam, and K.E. Beschorner, *QUANTIFYING THE SENSTIVITY OF A MULTI-SCALE SHOE-FLOOR FRICTION MODEL AGAINST SHOE AND FLOOR PARAMETERS*, in *Undergraduate Research Reports*. 2016, University of Pittsburgh: Swanson School of Engineering.

147. Moghaddam, S. and K. Beschorner. *Finite Element Model of Shoe-Floor Hysteresis Friction*. in *STLE Tribology Frontiers Conference 2014*. 2014.

148. Wagner, P., et al., *Numerical multiscale modelling and experimental validation of low speed rubber friction on rough road surfaces including hysteretic and adhesive effects.* Tribology International, 2017. **111**: p. 243-253.